INFLUENCE OF VARIOUS PARAMETERS ON SEISMIC-INDUCED PERMANENT DISPLACEMENT OF GEOSYNTHETIC REINFORCED SEGMENTAL RETAINING WALLS

by

Ali Kadayıfçı

B.S. in C.E. Yıldız Teknik University, 2003

Submitted to the Institute for Graduate Studies in
Science and Engineering in partial fulfillment of
the requirements for the degree of
Master of Science

Graduate Program in Civil Engineering

Boğaziçi University

2005

ACKNOWLEDGEMENTS

I owe special thanks to Prof. Dr. Erol Güler for his helpful guidance through out this thesis.

ABSTRACT

INFLUENCE OF VARIOUS PARAMETERS ON SEISMIC-INDUCED PERMANENT DISPLACEMENT OF GEOSYNTHETIC REINFORCED SEGMENTAL RETAINING WALLS

The study on the seismic performance of reinforced soil structures has received much attention following 1995 Kobe Earthquake, and especially with the failures reported during Ji – Ji Earthquake in Taiwan. After 1999 Adapazarı Earthquake, Turkey realized the importance of the earthquakes in many ways especially in structures. The use dry-stacked concrete blocks in geosynthetic reinforced soil retaining wall construction has gained popularity throughout the world and is becoming widespread in Turkey. The facing consisting of block layers provides an aesthetically pleasing, cost-effective alternative, easy to construct and the performance of geosynthetic-reinforced soil structures under seismic loading are reported to be satisfactory, but some suffered from minor cracking and sliding after major earthquakes.

This study is aimed to investigate the influence of reinforcement length, wall height, block width, reinforcement spacing and wall inclination angle on seismic-induced permanent displacements. Permanent displacements associated with three sliding mechanisms are investigated; (1) external sliding along the base of total structure; (2) internal sliding along a reinforcement layer and through the facing column; and (3) block interface shear between facing column units. A pseudo-static method based on Mononobe-Okabe earth pressure theory and NCMA's Segmental Retaining Wall – Seismic Design Manual is used to determine the value of critical acceleration associated with each potential failure mechanism. Newmark's sliding block displacement, and Bathurst and Cai's empirical methods are used for the displacement calculations and 1999 Sakarya Earthquake is taken as Earthquake data. At last, as a verification Valencia Wall permanent displacement after the 1994 Northridge Earthquake is calculated using this calculations and results are compared.

ÖZET

GEOSENTETİK DONATILI İSTİNAT DUVARLARINDA DEPREMDEN OLUŞAN KALICI YER DEĞİŞTİRMELERİN ÇEŞİTLİ PARAMETRELERLE İNCELENMESİ

1995 Kobe ve özellikle Ji – Ji depremindeki hasarlardan sonra donatılı zemin yapılarındaki deprem performansı çok önem kazanmıştır. 1999 Adapazarı depreminden sonra Türkiye'de depremin önemini, özellikle de yapılar konusunda, anlamıştır. Geosentetik donatılı istinat duvarlarında harçsız istiflenmiş beton blokları bütün dünyada popülerlik kazanmış ve Türkiye'de de yayılmaya başlamıştır. Beton bloklardan oluşan cepheler, estetik görünüm, daha düşük maliyetli bir alternatif, inşaa kolaylığı sağlar ve deprem sırasındaki performansının, bazılarının büyük depremlerdeki hafif kırıkları ve kaymaları dışında, tatmin edici sonuçları olduğu görülmüştür.

Bu çalışma, donatı uzunluğunun, duvar yüksekliğinin, blok genişliğinin, donatı aralığının, ve duvar eğiminin etkisinin, depremde oluşan kalıcı yer değiştirmelerine olan etkisini incelemeyi amaçlamıştır. Yer değiştirmelere bağlı üç kayma mekanizması incelenmiştir; (1) Tüm yapının temelinde oluşan dış kayma; (2) Donatı katmanı ve cephe bloğunun birlikte içten kayması ve; (3) Cephe blokları arasındaki içsel kayma. Mononbe-Okabe toprak basıncı teorisinden esinlenmiş pseudo-statik metot ve NCMA'nın Katmanlı İstinat Duvarı – Sismik Tasarım Klavuzu kitabı, kritik ivmeleri kayma mekanizmalarına bağlı olarak bulmak için kullanılmıştır. Newmark'ın kayan blok metodu be Bathurst ve Cai'nin ampirik metodu, deplasman hesabında kullanılmıştır ve 1999 Sakarya Depreminin verileri baz alınmıştır. En sonunda da 1994 Northridge Depreminde, Valencia duvarında oluşan deplasman hesaplanmış ve gerçek deplasmanla karşılaştırılmıştır.

TABLE OF CONTENTS

LIST OF FIGURES

LIST OF TABLES

LIST OF SYMBOLS/ABBREVIATIONS

$a(t)$	ground acceleration with time t (m/s^2)
a_{cs}	minimum peak connection strength (N/m)
a_u	minimum peak interface shear strength (N/m)
B_f	footing width (m)
B'_f	equivalent footing width (m)
c	soil cohesion (N/m^2)
c_f	foundation soil cohesion (N/m^2)) capacity design (dimensionless)
C_{ds}	coefficient of direct sliding (dimesionless)
C_i	coefficient of interaction of anchorage (pullout) capacity design (dimensionless)
e	eccentricity (m)
f_g	ground motion predominant frequency
f_l	wall fundamental frequency
$F_{dtyn\ i}$	dynamic reinforcement load (component) in reinforcement layer i (N/m)
F_i	total reinforcement load in reinforcement layer i (N/m)
$F_{sta\ i}$	static reinforcement load (component) in reinforcement layer i (N/m)
FS_{bc}	factor of safety against bearing capacity failure (dimensionless)
FS_{cs}	factor of safety against connection failure (dimensionless)
FS_{gl}	factor of safety against global stability failure (dimensionless)
FS_{os}	factor of safety against reinforcement tensile over-stress (dimensionless)
FS_{ot}	factor of safety against base overturning (dimensionless)
FS_{otc}	factor of safety against crest toppling (dimensionless)
FS_{oti}	factor of safety against internal overturning for conventional SRW structures (dimensionless)
FS_{otl}	factor of safety against local overtuning for reinforced SRW structures (dimensionless)
FS_{po}	factor of safety against pullout (dimensionless)
FS_{sc}	factor of safety against interface shear failure (dimensionless)
FS_{sl}	factor of safety against base sliding (dimensionless)
FS_{sli}	factor of safety against internal sliding (dimensionless)

g	gravitational constant (m/s^2)
h	height at back of reinforcement soil zone used in external stability calculations (m)
h_{IR}	height from toe of wall to line of action of inertial force P_{IR} (m)
h_{zi}	height of soil at back of reinforced soil zone used in internal sliding calculations (dimensionless)
h_β	height from base of wall to center of gravity of wedge of soil above reinforced soil zone (m)
H	vertical wall height measured at face of wall (m)
H_{emb}	embedment depth of wall (m)
H_f	leveling pad thickness (m)
H_h	hinge height of facing column (m)
H_w	height of facing unit (m)
k_h	horizontal seismic coefficient (dimensionless)
k_h (ext)	value of k_h used for all external stability calculations and internal sliding calculations for reinforced SRW structures (dimensionless)
k_h (int)	value of k_h used for all internal and facing stability calculations for reinforced SRW structures (dimensionless)
k_v	vertical seismic coefficient (dimensionless)
K_A	static earth pressure coefficient calculated using Coulomb earth pressure theory (dimensionless)
K_{AH}	horizontal component of static earth pressure coefficient calculated using Coulomb earth pressure theory (dimensionless)
K_{AE}	dynamic earth pressure coefficient calculated using Mononbe-Okabe (M-O) method (dimensionless)
K_{AEH}	horizontal component of dynamic earth pressure coefficient calculated using Mononbe-Okabe method (dimensionless)
ΔK_{dyn}	dynamic active earth pressure coefficient increment (dimensionless)
ΔK_{dynH}	horizontal component of dynamic active earth pressure coefficient increment (dimensionless)
L_{Ai}	anchorage length of reinforcement layer i (m)
L_g	distance from the toe of a SRW unit to the center of gravity of theunit (including contribution of granular soil infill volumes if applicable)

L_i	total length of reinforcement layer i beginning at face of wall (m)
L_{min}	base width of reinforced soil zone plus facing column ≤ H (m)
L_w	width of facing column (toe to heel dimension of SRW unit) (m)
M_o	driving moment taken about toe of wall (N-m/m)
M_o (z)	driving moment over depth z (N-m/m)
M_r	resisting moment taken about toe of wall (N-m/m)
M_r (z)	resisting moment due to weight of facing column over depth z (N-m/m)
m	ratio of moment arm of dynamic active earth force to wall height (dimensionless)
N	number of reinforcement layers (dimensionless)
N_c, N_γ, N_q	bearing capacity coefficients (dimensionless)
N_h	integer number of standard SRW units comprising hinge height of facing column (dimensionless)
N_w	total number of standard SRW units in facing column (dimensionless)
N_z	integer number of facing units above the target point of rotation at depth z (dimensionless)
P_A	static active earth force (N/m)
P_{AH}	horizontal component of static active earth force (N/m)
P_{AH} (z)	horizontal component of static active earth force acting over depth z (N/m)
P_{AE}	(total) dynamic earth force (N/m)
P_{AEH}	horizontal component of (total) dynamic active earth force (N/m)
P_{AEH} (z)	horizontal component of (total) dynamic active earth force acting over depth z (N/m)
P_{IR}	horizontal inertial force due to the reinforced soil mass used in external stability factor of safety calculations (N/m)
ΔP_{AE}	(total) dynamic earth force (N/m)
ΔP_{dyn}	dynamic earth force increment (N/m)
ΔP_{dynH}	horizontal component of dynamic earth force increment (N/m)
ΔP_{dynH} (z)	horizontal component of dynamic earth force increment acting over depth z (N/m)
ΔP_{IR} (z)	inertia force acting over sliding surface at depth z below crest of wall (N/m)
q_a	applied foundation bearing stress (N/m^2)
q_{ult}	ultimate bearing capacity of the foundation soil (N/m^2)

RF_{CR}	creep reduction factor (dimensionless)
R_S	base sliding resistance at bottom of reinforced soil zone including facing column for reinforced SRW structures (N/m)
R_{SW}	base sliding resistance at bottom of facing column for conventional SRW structures (N/m)
R_S (z)	internal sliding resistance at depth z below the crest of the wall (N/m)
S_i (z)	out-of-balance horizontal shear force transmitted through facing unit interface at depth z below crest of wall (N/m)
S_{vi}	contributory area corresponding to reinforcement layer i (m^2/m)
T_a (dyn)	allowable tensile load for the reinforcement under *seismic* loading (N/m)
T_{ci}	peak connection capacity corresponding to reinforcement layer i
$T_{pull\ i}$	peak anchorage (pullout) capacity corresponding to reinforcement layer i (N/m)
V_u (z)	peak interface shear capacity at interface located at depth z below crest of wall (N/m)
W	weight of active earth wedge behind retaining wall weight of
W_A	weight of static internal failure wedge (AASHTO/FHWA method) (N/m)
W_h	weight of facing column at base of wall using hinge height (N/m)
W_i	total weight of the reinforced soil zone extending from the back weight ofof the facing column to length L_{min} beyond the face of the wall and having constant height H (N/m)
W'i	reduced weight of the reinforced zone extending from the back of the facing column to length 0,5H beyond the face of the wall and having constant height H used to calculate inertial force P_{IR} or P_{IR} (z) (N/m)
W_w	total weight of facing column (N/m)
W_r	total weight of reinforced sol zone (= $W_w + W_i + W_\beta$) (N/m)
W_β	weight of the wedge of soil in the slope above the crest of the wall wall at height H (N/m)
W'_β	reduced weight of the wedge of soil in the slope above the crest of the wall at height H used to calculate inertial force P_{IR} or P_{IR} (z) (N/m)
ΔW_h (z)	weight of the facing column above the sliding surface based on the hinge height taken at sliding surface at depth below crest of wall (N/m)

ΔW_i (z)	weight of reinforced soil with constant height z acting on an internal sliding surface at depth below crest of wall (N/m)
$\Delta W'_i$ (z)	reduced weight of the reinforced zone extending from the back of the facing column to length 0,5H beyond the face of the wall and having constant height z used to calculate inertial force P_{IR} (z) (N/m)
ΔW_w (z)	total weight of the facing column above the sliding surface at depth z below the crest of the wall (N/m)
ΔW_{wi}	weight of the facing falling with the contributory area S_{vi} of the corresponding reinforcement layer I (N/m)
X_h	horizontal distance from the toe of the facing column to the center of gravity of the facing column corresponding to the hinge height weight W_h (m)
X_i	horizontal distance from the toe of the facing column to the center of gravity of the reinforced soil zone corresponding to the weight W_i (m)
X_w	horizontal distance from the toe of the facing column to the center of gravity of the facing column corresponding to the weight W_w (m)
X_β	horizontal distance from the toe of the facing column to the center of gravity of the wedge of soil corresponding to the weight W_β (m)
ΔX_h (z)	horizontal distance from the toe of the internal sliding surface to the center of gravity of the facing column above the sliding surface based on the hinge height weight ΔW_h (z) (m)
y_i	vertical distance from point of rotation on wall face to reinforcement layer I (m)
y_{dyn} (z)	moment arm between the point of rotation at depth z and the centroid of the dynamic earth pressure distribution (m)
z	depth from crest of wall (m)
z_i	depth from crest of wall to reinforcement layer i (m)
z_{idyn}	moment arm between the point of rotation at depth z and the line of action of the dynamic earth force increment (m)
z_{vi}	distance from the crest of the wall to the middle of the contributory area S_{vi} (m)
α_{AE}	orientation of failure plane from horizontal using M-O method (°)
β	backslope angle(°)

δ	mobilized interface friction angle (°)
δ_w	mobilized interface friction angle at the back of wall facing column (°)
ϕ	peak friction angle of soil (°)
ϕ_b	peak friction angle of retained (backfill) soil (°)
ϕ_{cv}	residual (constant volume) friction angle of soil (°)
ϕ_d	peak friction angle of drainage (leveling pad) soil (°)
ϕ_f	peak friction angle of foundation soil (°)
ϕ_r	peak friction angle of reinforced (infill) soil (°)
γ	unit weight of soil (N/m^3)
γ_b	unit weight of retained (backfill) soil (N/m^3)
γ_f	unit weight of foundation soil (N/m^3)
γ_r	unit weight of reinforced (infill) soil (N/m^3)
γ_w	unit weight of SRW units (N/m^3)
λ_{cs}	slope of peak connection strength failure envelope (°)
λ_u	slope of peak interface shear strength failure envelope for SRW units(°)
μ_b	masonry friction reduction factor (dimensionless)
σ_{vi}	average overburden pressure acting over anchorage length L_{Ai} (N/m^2)
θ	seismic inertia angle (°)
ω	wall inclination angle (positive in a clockwise direction from the vertical) (°)

AASHTO	American Association of State Highway and Transportation Officials
DMSRW	Design Manual for Segmental Retaining Walls (Second Edition 1997)
FHWA	Federal Highway Administration
NCMA	National Concrete Masonry Association
MSE	Mechanically Stabilized Earth
M-O	Mononbe-Okabe (pseudo-static earth pressure theory)
SRW	Segmental Retaining Wall

1. INTRODUCTION

The use of segmental retaining walls that include dry-stacked concrete block units as the facia system together with extensible sheets of polymeric materials (geosynthetics) that internally reinforce the retained soils and anchor the facia has gained wide popularity in North America (Bathurst and Simac 1994). These structures have also been reported in Europe, Scandinavia and Australia in recent years (Cazzuffi and Rimaldi 1994; Gourc *et al.* 1990; Knutson 1990; Won 1994). An example of a reinforced segmental retaining wall structure is illustrated in Figure 1.1. The distinguishing feature of these structures is the facing column that is constructed using mortarless modular concrete block units that are stacked to form a wall batter into the retained soils (typically 3° to 15° from vertical). The economic benefits of these systems over conventional reinforced concrete gravity wall structures and mechanically stabilized soil retaining walk that use inextensible (steel) reinforcement) and select backfills have been demonstrated in several of the references cited in an earlier paper by Bathurst and Simac (1994).

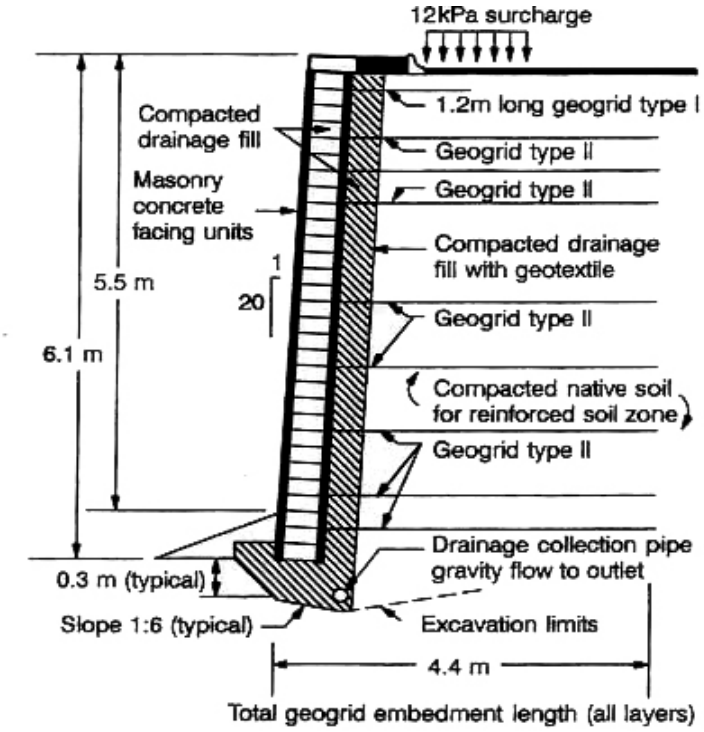

Figure 1.1. Typical geosynthetic-reinforced soil segmental retaining wall cross-section (after Simac *et al.* 1991)

Stability analyses for geosynthetic-reinforced soil walls under static loading conditions (including segmental retaining wall systems) involve separate calculations to establish factors of safely against external modes of failure and internal modes of failure (Figure 1.2). External stability calculations consider the reinforced soil zone and the facing column as a monolithic gravity structure. The evaluation of factors of safety against base sliding, overturning about the toe and foundation bearing capacity is analytically identical to that used for conventional gravity structures. Internal stability analyses for geosynthetic-reinforced soil walls are carried out to ensure that the structural integrity of the geosynthetic-reinforced soil mass is preserved with respect to reinforcement over-stressing and pullout of geosynthetic reinforcement layers from the anchorage zone.

A comprehensive design methodology has been recently proposed by the National Concrete Masonry Association (NCMA) for the static analysis of segmental retaining walls (Simac *et al.* 1993; Bathurst *et al.* 1993). The NCMA guidelines address potential failure mechanisms not found in other geosynthetic-reinforced soil wall systems as illustrated in Figures 1.2 (f), 1.2 (g), 1.2 (h) and 1.2 (i). The dry-stacked (mortarless) concrete blocks are discrete units that transmit shear through concrete keys, interface friction, mechanical connectors, or a combination of these methods. The stacked facing units result in potential failure plants through the facing column and this requires that additional stability calculations be carried out to estimate interface shear forces and to compare these forces with available shear capacity. In addition, the connection between the reinforcement layers and the facia is typically formed by extending the reinforcing layers along the interface between facing units to the front of the wall. The connection detail must also be evaluated for satisfactory design capacity (Bathurst and Simac 1993).

The NCMA method proposes a consistent approach to calculate earth pressures for both external and internal stability calculations that is based on Coulomb earth pressure theory. The advantage of Coulomb earth pressure theory over Rankine theory which has been adopted in earlier guide lines for geosynthetic- reinforced soil walls (AASHTO 1990, 1992: Christopher *et al.* (FHWA) 1989) is that the former explicitly accounts for the influence of wall batter and wall-soil friction on the development of earth pressures and hence is less conservative. A review of the essential features of the Coulomb earth pressure approach as it applies to segmental retaining wall structures and comparisons of the NCMA design methodology with

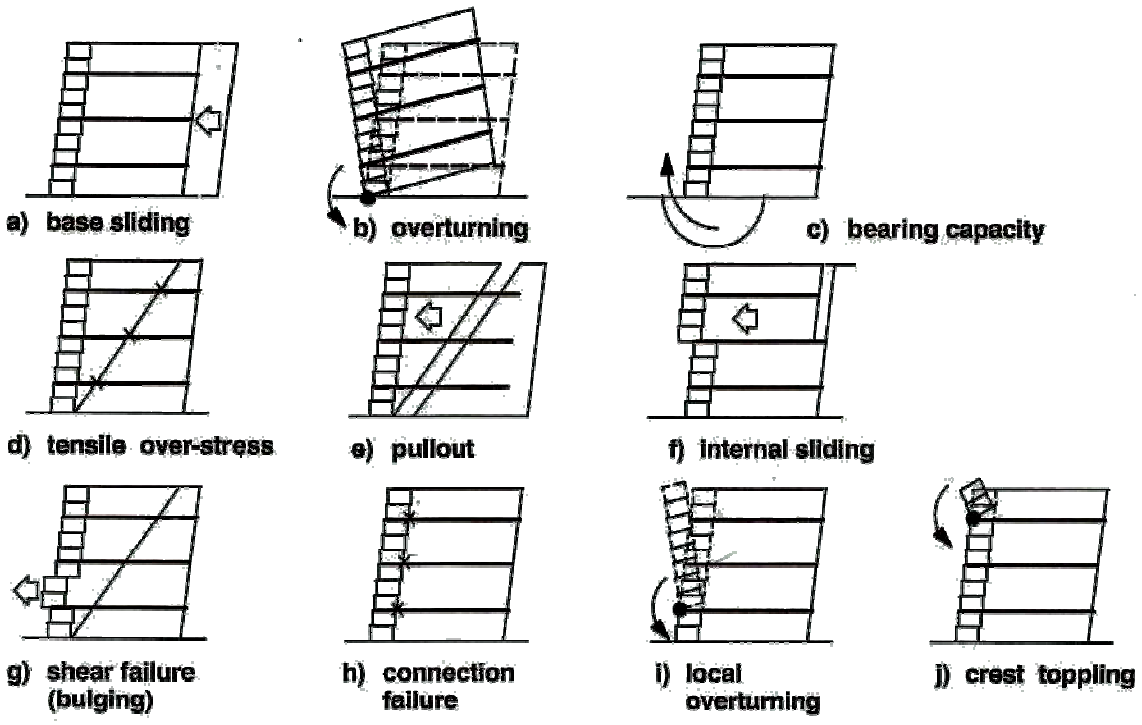

Figure 1.2. Modes of failure for reinforced SRW structures: external (a,b,c); internal (d,e,f); and facing (g,h,i,j) (after Bathurst and Cai 1995)

earlier limit-equilibrium methods of design can be found in the paper by Bathurst *et al.* (1993).

The scope of the NCMA guidelines is currently restricted to design of routine segmental retaining walls under static loading conditions. Questions related to the performance of the discrete facia system and the connections between the facia units and geosynthetic reinforcement layers during a seismic event have been raised (Allen 1993). Nevertheless, the satisfactory performance of a number of geosynthetic-reinforced segmental walls during the Loma Prieta Earthquake of 1989 (Eliahu and Watt 1991; Collin *et al.* 1992) and the Northridge Earthquake of 1994 in California (Sandri 1994) has been qualitatively demonstrated.

This study investigates the influence of reinforcement length, wall height, facing column, reinforcement spacing and wall inclination angle on displacements of

geosynthetic-reinforced segmental retaining walls under dynamic loading due to seismic excitation (earthquake). A pseudo-static rigid body approach that uses the well-known Mononobe-Okabe (M-O) method to calculate dynamic earth forces (Okabe 1924) is outlined in this study. The method is restricted to a limit-equilibrium approach in which factors of safely against collapse or rupture mechanisms are calculated. The M-O method has been used to calculate earth forces for seismic stability analyses of conventional gravity wall structures (Seed and Whitman 1970; Richards and Elms 1979), NCMA's Segmental Retaining Walls – Seismic Design Manual is used to calculate the critical acceleration and Newmark's and Bathurst - Cai's displacement methods are used to calculate the permanent displacements.

2. SEISMIC ANALYSIS APPROACHES

Analytical and numerical approaches for the seismic analysis of reinforced walls, slopes and embankments can be divided into the following categories:

1) pseudo-static methods;
2) displacement methods; and
3) dynamic finite element/finite difference methods.

In this study dynamic finite element/finite difference methods are not addressed.

2.1. Pseudo-static Methods

Pseudo-static methods extend conventional limit-equilibrium methods of analysis including destabilizing body forces that are related to assumed horizontal and vertical components of ground acceleration.

2.1.1. Mononobe-Okabe Earth Pressure Theory

2.1.1.1. Calculation of Earth Dynamic Force: The Mononobe-Okabe method is used to calculate dynamic active earth forces acting on a planar surface that is inclined at an angle, ω, into an unsaturated homogeneous, cohesionless soil mass (Figure 2.1). In Figure 2.1, W refers to the static weight of the active wedge of soil acting behind the wall and W_w refers to the static weight of the facing column. Quantities k_h and k_v are horizontal and vertical seismic coefficients, respectively expressed as fractions of the gravitational constant, g. Horizontal inertial forces are assumed to act outwards ($+k_h$) to be consistent with the notion of active earth pressure conditions. Positive vertical seismic coefficient, $+k_v$, corresponds to a seismic inertial force that acts upward. The total dynamic active earth force, P_{AE}, imparted by the backfill soil is calculated as (Seed and Whitman 1970):

$$P_{AE} = \frac{1}{2}\left(1 \pm k_v\right) K_{AE} \gamma H^2 \qquad (2.1)$$

where: γ = unit weight of the soil; and H = height of the wall. The dynamic earth pressure coefficient, K_{AE}, can be calculated as follows:

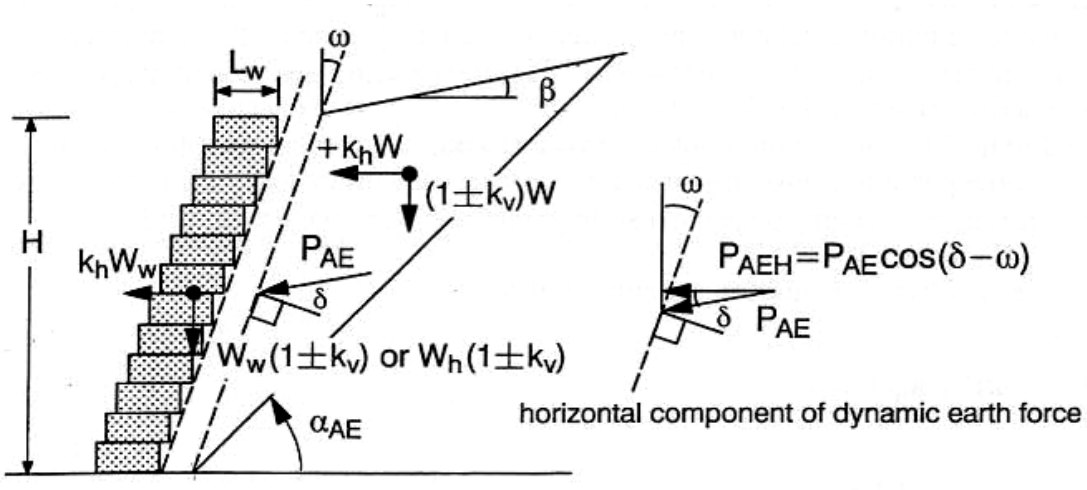

Figure 2.1. Forces and geometry used in pseudo-static seismic analysis.

$$K_{AE} = \frac{\cos^2(\phi + \omega - \theta)}{\cos\theta\cos^2\omega\cos(\delta - \omega + \theta)\left[1 + \sqrt{\frac{\sin(\phi + \delta)\sin(\phi - \beta - \theta)}{\cos(\delta - \omega + \theta)\cos(\omega + \beta)}}\right]^2} \tag{2.2}$$

where: ϕ = peak soil friction angle; ω = total wall inclination (positive in a clockwise direction from the vertical); δ = mobilized interface friction angle assumed to act at the back of the wall; β = backslope angle (from horizontal); and θ = seismic inertia angle given by:

$$\theta = \tan^{-1}\left(\frac{k_h}{1 \pm k_v}\right) \tag{2.3}$$

The seismic inertia angle represents the angle through which the vectoral resultant of the gravity force and the inertial forces (both horizontal and vertical} is rotated from vertical. Equations 2.1 to 2.3 are an exact analytical solution to the classical Coulomb wedge problem that is modified to include the inertial forces k_hW and k_vW. Examination

of the trigonometric terms in Equation 2.2 shows that solutions are only possible for $\theta \leq \phi - \beta$. Hence, the maximum value of horizontal seismic coefficient for which there are solutions to Equation 2.2 is restricted to $k_h \leq (1 \pm k_v)\tan(\phi - \beta)$.

Equations 2.1 and 2.2 can be modified to account for additional loads due to an uniformly distributed surcharge acting behind the wall (Okabe 1924; Motta 1994). However, the influence of any surface distributed surcharge loading on the stability of segmental retaining walls is not evaluated in this thesis. A closed-form solution for the calculation of dynamic earth force for c-ø soils in retaining wall design is reported by Prakash (1981); however, this solution is restricted to the special case of $\beta = 0$ and $k_v=0$. For more complicated wall geometries and cases with surface loadings, trial single failure plane geometries, or two-part wedge failure plane geometries, can be evaluated to find the critical geometry giving the maximum value of P_{AE}. However, while these solutions are more general they do not offer the designer the convenience of the closed-form solutions adopted in the current study.

In the discussions to follow, it is convenient to decompose the total dynamic active earth force, P_{AE}, calculated according to Equations 2.1 and 2.2 into two components representing the static earth force component, P_A, and the incremental dynamic earth force due to inertial seismic effects. ΔP_{dyn} (Seed and Whitman 1970). Hence:

$$P_{AE} = P_A + \Delta P_{dyn} \tag{2.4}$$

or

$$(1 \pm k_v)K_{AE} = K_A + \Delta K_{dyn} \tag{2.5}$$

where: K_A = static active earth pressure coefficient; and ΔK_{dyn} = incremental active earth pressure coefficient. For brevity in the following text, the quantity P_{AE} be called the dynamic earth force.

2.1.1.2. Distribution of Dynamic Lateral Earth Pressure and Point of Application: The position of the dynamic earth force, P_{AE}, acting against gravity retaining walls has been shown to be variable and to depend on the magnitude of ground acceleration. A general range for the point of application of the dynamic force increment (ΔP_{dyn} in Equation 2.4) has been reported to be $\eta H = 0.4H$ to $0.7H$ above the toe of the wall (Seed and Whitman 1970). (η is the distance of the dynamic load increment above the toe of the wall normalized with respect to wall height H). Seed and Whitman suggest that a value of $\eta = 0.6$ is reasonable for practical design purposes and this value is consistent with the results of small-scale shake table tests reported by Ishibashi and Fang (1937). The parameter m in Figure 2.2 denotes the normalized point of application of the dynamic earth force and it is limited to the range of $1/3 \leq m \leq 0.6$. This range compares favorably to measured values of m ranging from 0.3 to 0.5 reported by Ichihara and Matsuzawa (1973) from the results of shake table tests on small-scale gravity wall models. The distributions for static and dynamic increment of active earth pressure illustrated in Figure 2.2 are also identical to those recommended from the design of flexible anchored sheet pile walls (Ebling and Morrison 1993).

2.1.1.3. Orientation of Active Failure Plane: Closed-form solutions for the orientation of the critical planar surface from the horizontal, α_{AE}, have been reported by Okabe (1924) and Zarrabi (1979). These solutions are rewritten as:

$$\alpha_{AE} = \phi - \theta + \tan^{-1}\left[\frac{-A_{AE} + D_{AE}}{E_{AE}}\right] \tag{2.6}$$

where

$$A_{AE} = \tan(\phi - \theta - \beta)$$

$$D_{AE} = \sqrt{A_{AE}\left[A_{AE} + B_{AE}\right]\left[B_{AE}C_{AE} + 1\right]}$$

$$E_{AE} = 1 + \left[C_{AE}\left(A_{AE} + B_{AE}\right)\right]$$

$$B_{AE} = \frac{1}{\tan(\phi - \theta + \omega)}$$

$$C_{AE} = \tan(\delta + \theta - \omega)$$

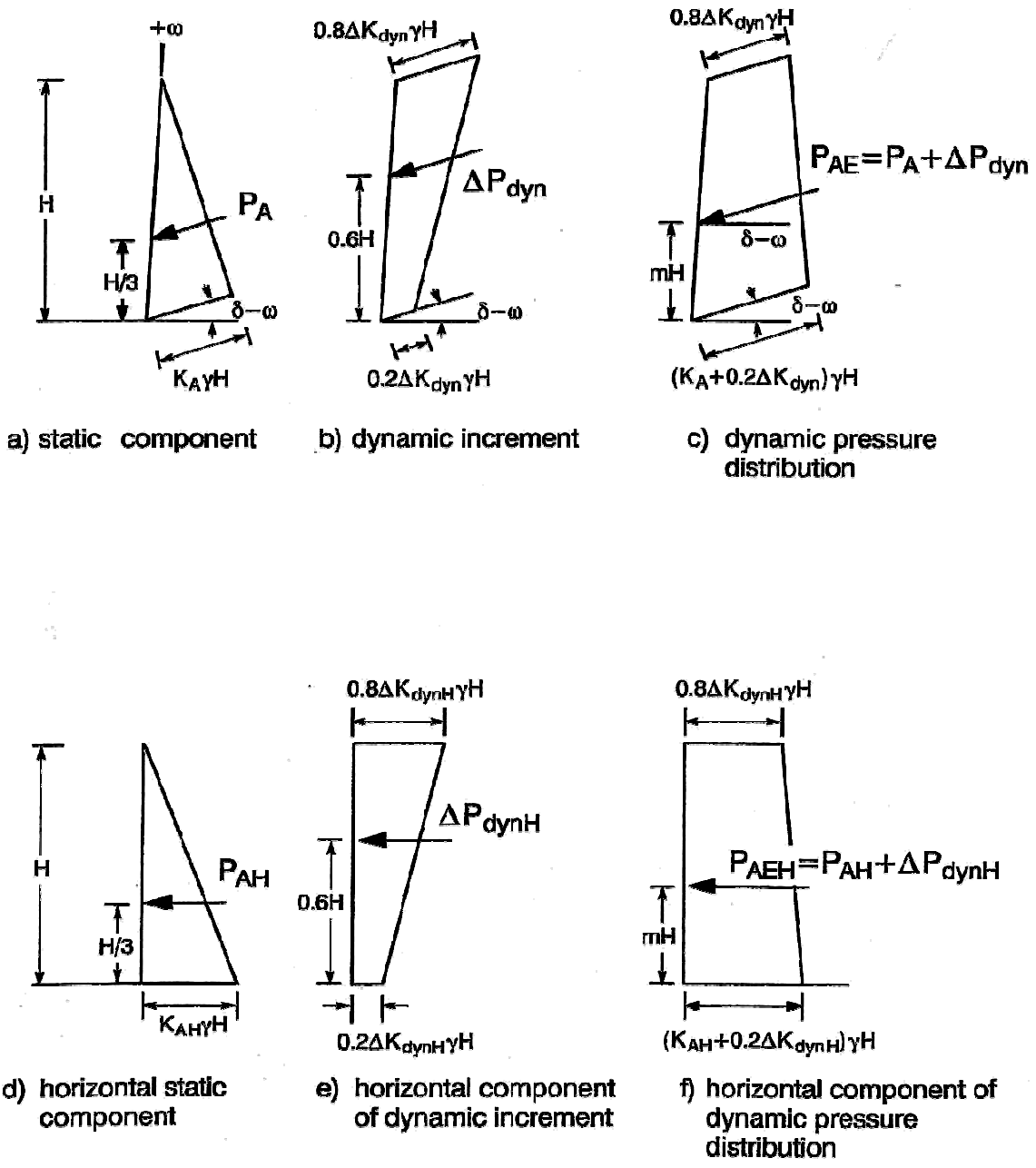

Figure 2.2. Earth pressure distributions due to soil self-weight.

Equation 2.6 can be used to calculate the orientation of the assumed active failure plane within the reinforced soil mass and in the retained soil.

2.1.2. External Stability Calculations for Walls

External stability calculations for factors for safety against base sliding and overturning of geosynthetic reinforced retaining walls are similar to those carried out for conventional gravity structures. For reinforced structures, the gravity mass is taken as the composite mass formed by the reinforced soil zone. For segmental retaining walls the gravity mass includes the facing column since it may comprise a significant part of the gravity mass particularly for low height structures (and hence generates additional inertial forces during a seismic event). The earth pressure distribution shown in Figure 2.2 is used to calculate the destabilizing forces in otherwise conventional expressions for the factor of safety against sliding along the foundation surface and overturning about the toe of the structure. The simplified geometry and body forces assumed in these calculations for the case of segmental retaining walls are illustrated in Figure 2.3. The term W_R in the figure is the weight of the reinforced zone plus the weight of the facing column used to calculate resisting terms in factor of safety expressions for base sliding and overturning. The quantity P_{IR} denotes the horizontal inertial force due to the gravity mass used in external

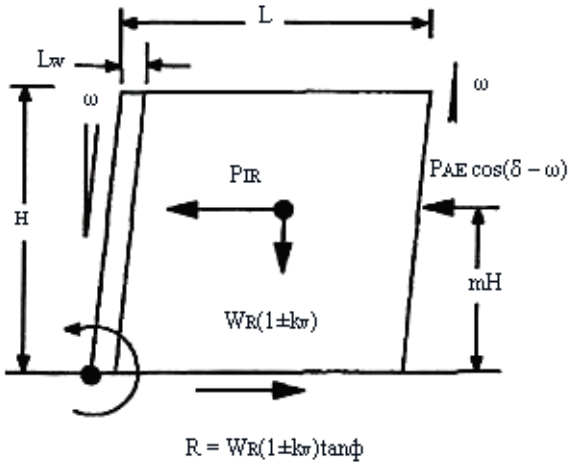

Figure 2.3. Forces and geometry for external stability calculations for base sliding and overturning

stability factor of safety calculations. Different strategies have been proposed in North America to compute $P_{IR} < k_h W_R$ to ensure reasonable designs. The justifications is based on the expectation that horizontal inertial forces induced in the gravity mass and the

retained soil zone will not reach peak values at the same time during a seismic event. Christopher *et al.* (1989) proposed the following expressions for horizontal backfills:

$$P_{IR} = 0.5\eta k_h \gamma H^2 \tag{2.7}$$

where $\eta = 0{,}6$ based on recommendations for reinforced walls that use steel reinforcement strips (Segrestin and Bastick 1988). Cai and Bathurst (1995) proposed an expression that gives similar results for typical L/H ratios for segmental retaining walls:

$$P_{IR} = \eta k_h W_R \tag{2.8}$$

where η = 0.6 AASHTO (1996) interim guidelines propose that P_{IR} be calculated using Equation 2.7 with $\eta = 1$ and the external dynamic active earth force component, ΔP_{dyn}, be reduced by 50%. North American practice is to reduce dynamic static factors of safety against sliding and overturning to 75% of the static factor of safety values in recognition of the transient nature of seismic loading.

Factors of safety are also reduced in Japan (PWRI 1992; GRB 1990; segmental retaining walls Koga and Washida 1992). However, factor of safety calculations for wall base sliding in Japan do not consider any reduction in inertial force, P_{IR} (i.e. Equation 2.8 is used with $\eta = 1$). In order to further reduce conservativeness in the Japanese approach for base sliding, Fukuda *et al.* (1994) have proposed ignoring the dynamic force increment, ΔP_{dyn}, and to restrict seismic loading contributions to the gravity mass term, P_{IR}, only. Overturning criteria for walls are restricted to ensuring that the resultant force acting at the base of the reinforced mass, W_R, falls within L/3 of the base midpoint for walls subject to earthquake. FHWA (1996) guidelines for geosynthetic reinforced walls also omit overturning as a potential failure mode for geosynthetic reinforced soil walls.

2.1.3. Internal Stability Calculations for Walls and Slopes

Pseudo-static/dynamic methods for walls, which involve an assumed distribution of internal earth pressure (e.g. Figure 2.2), require that each reinforcement layer carry a

portion of the integrated earth pressure over a tributary area, S_v, as illustrated in Figure 2.4**.** The magnitude of tensile force must not exceed the allowable design load in the reinforcement based on tensile over-stressing, facing connection strength and pull-out capacity of the layer. In North American practice, factors of safety against these modes of failure are reduced to values that are typically 75% of static values. Figure 2.4 also demonstrates that the inertial force due to the tributary portion of the facing column should be added to the reinforcement forces under seismic loading in the case of segmental walls. An important implication of the assumed earth pressure distribution using the pseudo-static M-O method described earlier, is that the relative proportion of load to be carried by the reinforcement layers closest to the crest of a wait with uniform reinforcement spacing increases with increasing horizontal acceleration. This may require a greater number of layers towards the top of the wall than is required for static load environment. A similar conclusion was reached by Vrymoed (1989) using a tributary area approach that assumes that the

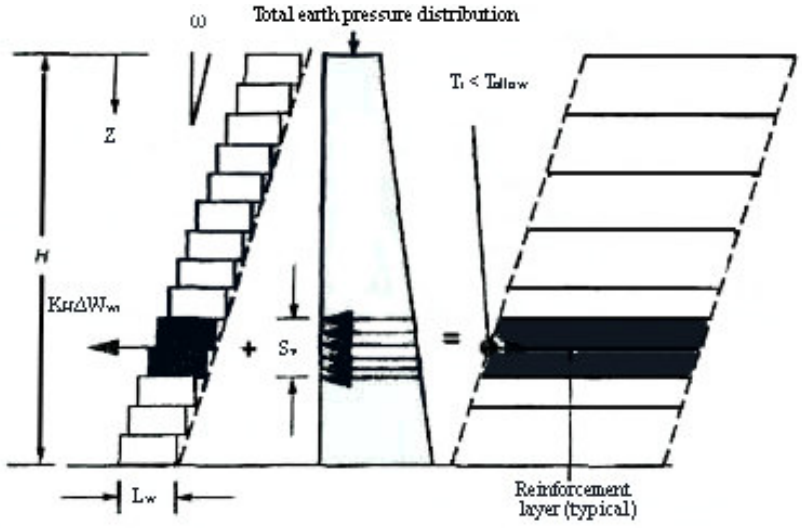

Figure 2.4. Calculations of tensile load, T_i, in a reinforcement layer due to dynamic earth pressure and wall inertia for segmental retaining walls

martial force carried by each reinforcement layer increases linearly with height above the toe of the wall for equally spaced reinforcement layers. Bonaparte *et al.* (1986) applied the tributary area method to walls and slopes but recommended a uniform distribution for the dynamic earth pressure increment (i.e. H_d = 0.5 H in Figure 2.2). Nevertheless, Bonaparte *et al.* (1986) concluded that the combination of higher available reinforcement strength and reduced factors of safety used for seismic loading cases will often result in

no requirement to increase the number of reinforcement layers required for static loading cases. FHWA (1996) guidelines use the procedure shown in Figure 2.5 to assign reinforcement forces for over-stressing and pullout calculations. In this method, the static earth force, P_A, is calculated using Rankine earth pressure theory with a Rankine failure plane ($\alpha = \pi/4 + \phi/2$) for vertical walls, and Coulomb theory with a Coulomb angle according to Equation 2.6 (using $k_h = k_v = 0$ in Equation 2.3) for walls with a facing batter greater than 10°. The dynamic earth force is calculated as $\Delta P_{dyn} = k_h W_A$, where W_A is the weight of the static internal failure wedge. The distribution of the dynamic tensile reinforcement load increment, ΔT_{dyn}, is weighted based on total anchorage length in the resistance zone according to:

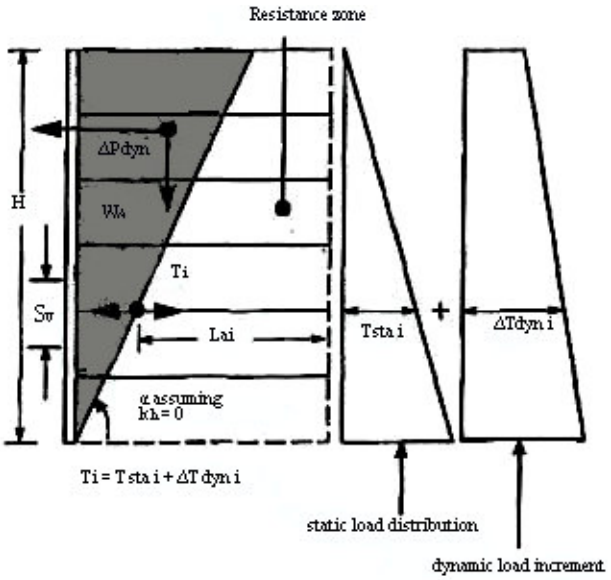

Figure 2.5. Calculations of tensile load, T_i, in a reinforcement layer for reinforced soil walls with extensible reinforcement using the FHWA (1996) method

$$\Delta T_{dyn\,i} = \frac{\Delta P_{dyn} L_{ai}}{\sum_{j=1}^{N} L_{aj}} \tag{2.9}$$

where N is the number of reinforcement layers, and L_a is tie anchorage length. This approach leads to redistribution of dynamic force to the lower reinforcement layers for internal stability calculations in structures with uniform reinforcement length. This strategy

is based on the results of finite element modeling of reinforced walls that used (inextensible) steel strips (Segrestin and Bastick, 1988). However, the dynamic increment force distribution shows the opposite trend to that used for external stability calculations in the same FHWA (1996) guidelines (see Figure 2.2). Although not demonstrated, it is clear that the FHWA method is the least conservative for the design of reinforcement forces, T_i, of all the methods reviewed. Furthermore, the FHWA approach is less likely to result in an increased number of reinforcement layers at the top of reinforced wall structures and increased reinforcement lengths to accommodate shallower internal failure surfaces with increasing horizontal acceleration, which is often the case using a rigorous interpretation retail on of M-O theory.

2.1.4. Two-part Wedge Failure Mechanism

The general solution for a trial two-part wedge failure mechanism with the slope subject to horizontal and vertical acceleration components is illustrated in Figure 2.6. The horizontal and vertical forces P_1 and V_1 acting on wedge 2 from wedge 1 are respectively:

$$P_1 = \frac{(1 \pm k_v)W_1 + B_1 A_1 k_h W_1}{\lambda \tan\phi_f + B_1 A_1} \tag{2.10}$$

$$V_1 = \lambda P_1 \tan\phi_f \tag{2.11}$$

where:

$$A_1 = \frac{1}{\sin\theta_1 - \tan\phi_f \cos\theta_1} \tag{2.12}$$

$$B_1 = \tan\phi_f \sin\theta_1 + \cos\theta_1 \tag{2.13}$$

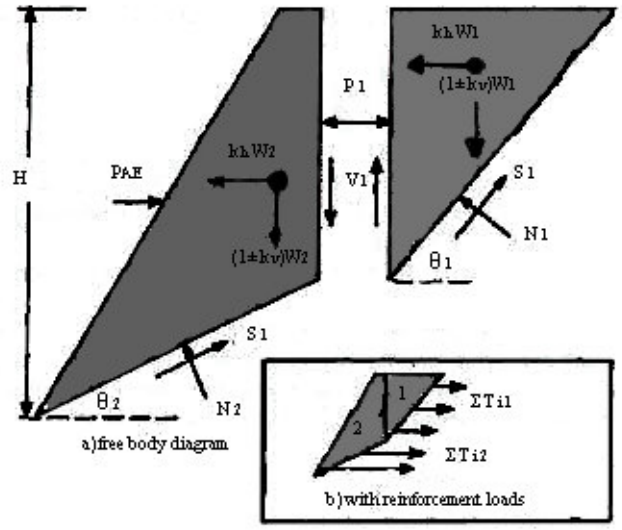

Figure 2.6. Two-part wedge analysis: (a) free-body diagram; and (b) with reinforcement forces

The quantity λ is the inter-wedge shear mobilization ratio and varies over the range $0 \leq \lambda \leq 1$. Parameter ϕ_f is the factored soil friction angle expressed as:

$$\phi_f = \tan^{-1}(\tan \phi / FS) \tag{2.14}$$

The horizontal out-of-balance force, P_{AE}, is calculated as:

$$P_{AE} = P_1 + k_h W_2 - B_2 A_2[(1 \pm k_v) W_2 + V_1] \tag{2.15}$$

where:

$$A_2 = \frac{1}{\tan \phi_f \sin \theta_2 - \cos \theta_2} \tag{2.16}$$

$$B_2 = \tan \phi_f \cos \theta_2 + \sin \theta_2 \tag{2.17}$$

By setting FS = 1 (i.e. $\phi = \phi_f$) an equivalent total active earth pressure coefficient for the most critical trial geometry (i.e. trial search that yields a maximum value for P_{AE} in the slope) can be calculated as:

$$K_{AE} = 2P_{AE}/\gamma H^2 \qquad (2.18)$$

This approach has been used by Bonaparte *et al.* (1986) to produce seismic design charts for geosynthetic reinforced soil slopes. The total requires design strength of the horizontal layers of reinforcement is taken as $\sum T_i = P_{AE}$. The two-part wedge approach with $\lambda = 0$ is used by the Geogrid Research Board (GRB 1990) to calculate K_{AE} according to Equations 2.15 and 2.18 for internal stability calculations.

The two-part wedge analysis degenerates to a single wedge analysis by restricting trial searches to $\theta_1 = \theta_2$ and setting $\lambda = 0$. All three solutions (M-O, single and two-part wedge) give the same solution for the horizontal component of total earth force when $\lambda = \omega = 0$.

An alternative strategy that extends the general approach used by Woods and Jewell (1990) for static loaded slopes to the seismic case (Bathurst 1994) is to rewrite Equation 2.15 as:

$$P_{AE} = P_1 - \frac{B_1 A_1 \sum T_{i1}}{\lambda \tan\phi_f + B_1 A_1} + k_h W_2 - \sum T_{i2} - B_2 A_2 \left[(1 \pm k_v) W_2 + V_1 \right] \qquad (2.19)$$

The factor of safety for a given two-part wedge geometry corresponds to the value of FS that yields $P_{AE} = 0$. The factor of safety for a slope corresponds to the minimum value of FS from a search of all potential failure geometries. It should also be noted that in this approach same global FS is applied to the reference design tensile strength of the reinforcement and pullout capacity defined by $T_{pull} = L_a C_i \sigma_v \tan\phi$. Equation 2.19 illustrates that the value of FS against collapse is independent of the location of the reinforcement layers for $\lambda = 0$.

2.1.5. Log Spiral Failure Mechanism

Log spiral failure mechanism Figure 2.7 have been used to calculate the out-of-balance force to be carried by horizontal reinforcement layers in slopes and walls under seismic loading (Leshchinky *et al.* 1995). An advantage of this method is that moment equilibrium is also satisfied (i.e. the problem is statically determinate). The trace of a log spiral surface is given by:

$$R = A\exp\left(-\tan\phi_f \times \xi\right) \tag{2.20}$$

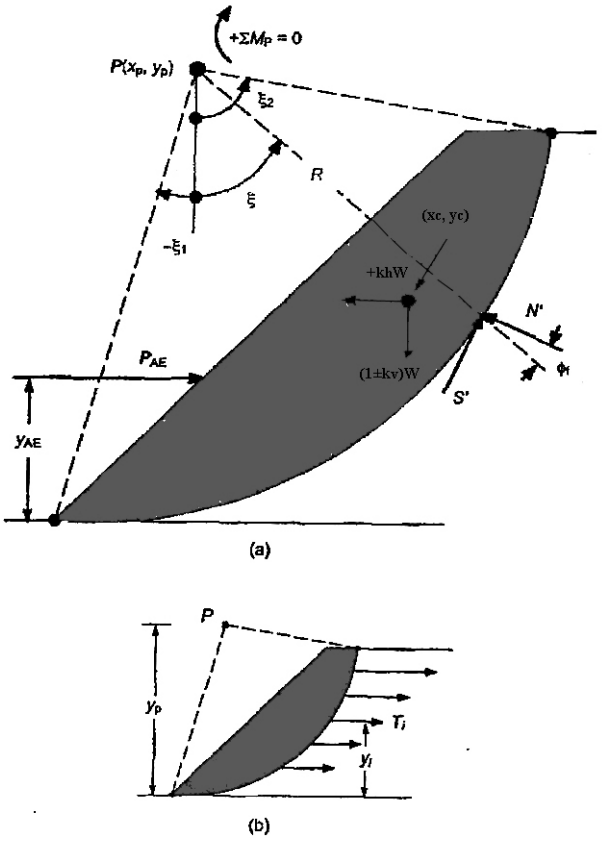

Figure 2.7. Log spiral analysis: (a) free-body diagram; and (b) with reinforcement forces

For an assumed surface (i.e. for any three independent parameters defining a log spiral, x_p, y_p and A), the moment equilibrium about the pole, P, can be explicitly written as:

$$M_p = (1 \pm k_v)W(x_c - x_p) + k_h W(y_p - y_c) - P_{AE}(y_p - y_{AE}) = 0 \qquad (2.21)$$

Note that the moment about the log spiral pole is independent of the distribution of normal and shear stresses over the log spiral because its resultant must pass through pole. The point (7) of application of the components of seismic inertial forces is taken at the centre of the failure mass. The critical mechanism corresponds to the trace that yields the maximum value of P_{AE} required to satisfy Equation 2.21. Clearly the balance horizontal force P_{AE} will influence the magnitude of P_{AE}. Here it is assumed a *priori* that y_{AE} = H/3. the calculation of an equivalent dynamic active earth pressure, K_{AE}, now follows Equation 2.18 with FS = 1 (i.e. $\phi = \phi_f$).

In practice, the factor of safety against collapse of a reinforced slope can be determined by replacing $P_{AE}(y_p - y_{AE})$ with $\sum T_i(y_p - y_i)$ in Equation 2.21 and finding the minimum value for FS from a search of all potential failure geometries that yields $\sum Mp = 0$. This value corresponds to the minimum factor of safety for the reinforced soil slope (Leshchinsky 1995). The formulation of Equation 2.21 illustrates that the FS against collapse is a function of the location of the reinforcement layers.

2.1.6. Circular Slip Failure Mechanism

Conventional methods of slices can be modified to account for the additional restoring moment due lo reinforcement layers. The general case can be referred to in Figure 2.8. Moment equilibrium leads to the following equation to calculate the factor of safety FS against collapse:

$$FS = \frac{M_R + \Delta M_R}{M_D} \qquad (2.22)$$

where M_R is the moment resistance due to soil shear strength, ΔM_R is the increase in moment resistance due to the reinforcement, and M_D is the driving moment. Introducing

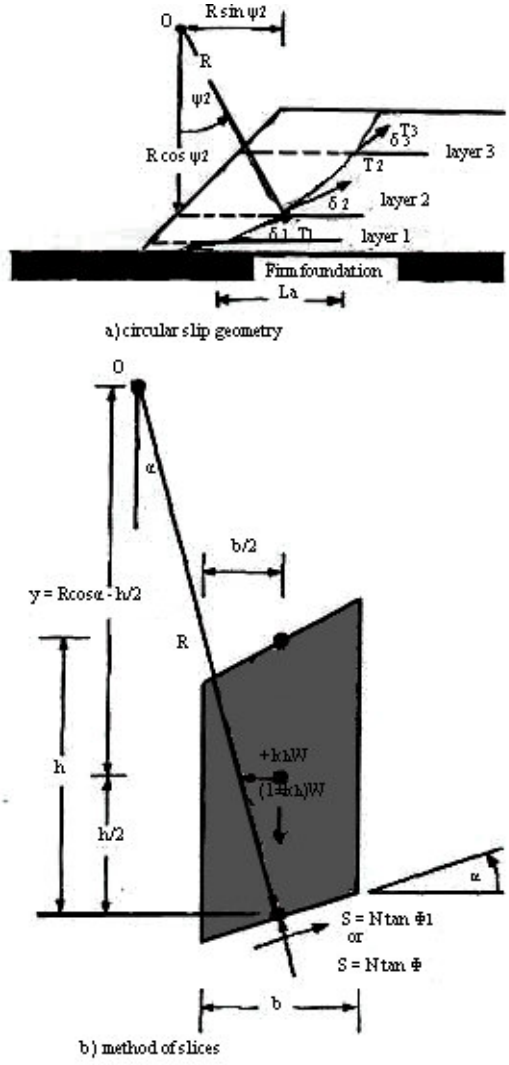

Figure 2.8. Circular slip analysis: (a) circular slip geometry; and (b) method of slices

k_v, into the derivations for Bishop's Simplified Method (e.g. Fredlund and Krahn 1976) results in the driving moment calculated as:

$$M_D = \sum W\left[(1 \pm k_v)R\sin\alpha + k_h y\right] \tag{2.23}$$

The moment resistance due To cohesionless soil shear strength is:

$$M_R = (1 \pm k_v)R\sum\left(\frac{W\tan\phi\sec\alpha}{1+\tan\alpha\tan\phi_f}\right) \tag{2.24}$$

The additional resisting moment due to the tensile capacity of the reinforcement is calculated as:

$$\Delta M_R = R\sum T_i \cos(\omega_i - \delta_i) \tag{2.25}$$

The summation term in equation (2.25) considers the available reinforcement tensile force in each layer (lesser of tensile reinforcement strength based on over-stressing or pullout) and the orientation, δ_i, of the force with respect to the horizontal. For flexible geosynthetic reinforcement products, the restoring force, T_i, can be argued to act tangent to the slip surface at the incipient collapse or the slope. This assumption leads to the summation term in equation 2.25 becoming $\sum T_i R$. This approach is used in FHWA. (1996) guidelines together with $k_v = 0$. It is important to note that in the above formulation, the influence of reinforcement capacity, T_i, and horizontal acceleration term, k_h, on base sliding resistance is not considered.

An alternative strategy is to modify the 'Ordinary Method' (e.g. Fredlund and Krahn, 1976) In this approach, equations for vertical and horizontal equilibrium of slices include forces due to acceleration components and reinforcement forces. Hence, these parameters directly affect base sliding resistance. This resisting moment term in equation 2.22 becomes:

$$M_R = R\sum\left[(1 \pm k_v)W\cos\alpha - k_h W\sin\alpha\right]\tan\phi \tag{2.26}$$

and the incremental resisting moment due to reinforcement layers is:

$$\Delta M_R = R\sum T_i\left[\cos(\omega_i - \delta_i) + \sin(\omega_i - \delta_i)\tan\phi\right] \tag{2.27}$$

where the summation term in equation 2.27 is with respect to reinforcement layers. An advantage of the modified 'Ordinary Method' is that the right-hand side of equation 2.22 is a linear function of FS. This approach is used by PWRI (1992) in Japan with $\delta_i = 0$ for retaining walls, and $\delta_i = \omega_i$ for slopes. In the Japanese approach, the distribution of total reinforcement load is assumed to be uniform with depth for slopes less than 45°

from horizontal. For steeper slopes, including walls, the static portion of required reinforcement load is assumed to increase linearly with depth below the crest, while the additional seismic portion is assumed to be distributed uniformly. FHWA (1996) guidelines allow the global factor of safety, FS, to be as low as 1.1 for the seismic design of slopes using pseudo-static methods.

2.1.7. Selection of Seismic Coefficients

In conventional pseudo-static methods of analysis, the choice of horizontal seismic coefficient, k_h, for design is related to specified horizontal peak ground acceleration for the site, a_h. The relationship between a_h and a representative value of k_h is nevertheless complex and there does not appear to be a general consensus in the literature on how to relate these parameters. For example, Whitman (1990) reports that values of k_h from 0.05 to 0.15 are typical values for the design of conventional gravity wall structures and these values correspond to 1/3 to 1/2 of the peak acceleration of the design earthquake. Bonaparte et al (1986) used $k_h = 0.85a_h/g$ to generate design charts for geosynthetic-reinforced slopes under seismic loading using the two-part wedge method of analysis.

However, the results of finite element modeling of reinforced soil walls (Segrestin and Bastick, 1988; Cai and Bathurst, 1995) limited half-scale experimental work (Chida et al., 1982) and FLAC modeling (Bathurst and Hatami l998a) have shown that the average acceleration of the composite soil mass may be equal to or greater than a_h depending on a number of factors including, wall height, wall toe boundary (i.e. degree of toe restraint), base acceleration intensity, ratio of ground motion predominant frequency to wall fundamental frequency, f_g/f_l, soil properties and, to a lesser extent, the reinforcement stiffness.

Current FHWA guidelines use an equation proposed by Segrestin and Bastick (1988) that relates k_h to a_h according to:

$$k_h = \frac{a_h}{g}\left(1{,}45 - \frac{a_h}{g}\right) \tag{2.28}$$

This formula results in $k_h > a_h/g$ for $a_h < 0{,}45g$. However, as clearly stated by Segrestin and Bastick, equation 2.28 should be used with caution because it is based on the results of finite element modeling of steel-reinforced soil walls up to 10.5 m high that were subjected to ground motions with a very high predominant frequency of 8 Hz. The results of finite element modeling reported by Cai and Bathurst (1995) for a 3.2 m high geosynthetic-reinforced segmental retaining wall with $a_h = 0.25$ and a predominant frequency range of 0.5 – 2 Hz; gave a distribution of peak horizontal acceleration through the height of the composite mass and retained soil that was. For practical purposes, uniform and equal to the base peak, input acceleration These observations are consistent with the results of Chida *et al.* (1982) who constructed 4.4 m high steel-rein forced soil wall models and showed that the average peak horizontal acceleration in the soil behind the walls was equal to the peak ground acceleration for ground motion frequencies less than 3 Hz.

The general solutions to pseudo-static methods of analysis admit both vertical and horizontal components of seismic-induced internal forces. The choice of positive or negative k_v, values influences the magnitude of dynamic earth forces calculated using equations 2.1 and 2.2. In addition, the resistance terms in factor of safely expressions for internal and external stability of walls and slopes that include the vertical component of seismic force are influenced by the choice of sign for k_v. An implicit assumption in many of the papers on pseudo-static design of conventional gravity wall structures cited in the literature is that the vertical component of seismic body forces acts upward. However, the designer must evaluate both positive and negative values of k_v to ensure that the most critical condition is considered in dynamic stability analyses if non-zero values of k_v are assumed to apply. For example, Fang and Chen (1995) have demonstrated in a series of example calculations that the magnitude of P_{AE} may be 12% higher for the case when the vertical seismic force acts downward ($+k_v$) compared to the case when it acts upward ($-k_v$). Nevertheless, selection of a non-zero value of k_v implies that peak horizontal and vertical accelerations are time coincident, which is an unlikely occurrence in practice. For example, Madabhushi (1996) investigated the arrival time of horizontal and vertical stress waves to selected recording sites. He concluded that since the horizontal and vertical waves arrive at different times, the design ground acceleration coefficients for retaining walls do not need to be combined at their

maximum values. The assumption that peak vertical accelerations do not occur simultaneously with peak horizontal accelerations is made in the current FHWA and AASHTO guidelines for the seismic design of mechanically stabilized soil retaining walls and in Japan (PWRI, 1992).

Seed and Whitman (1970) have suggested that $k_v = 0$ is a reasonable assumption for the practical design of conventional gravity structures using pseudo-static methods. Wolfe *et al.* (I978) studied the effect of combined horizontal and vertical ground acceleration on the seismic stability of reduced-scale model reinforced earth walls using shaking table tests. They concluded that the vertical component of seismic motion may be disregarded in terms of practical seismic stability design. Their conclusion can also be argued lo apply to geosynthetic-reinforced walls. Nevertheless, significant vertical accelerations may occur at sites located at short epicentral distances and engineering judgement must be exercised in the selection of vertical and horizontal seismic coefficient to be used in pseudo-static seismic analyses.

In order to address specific concerns raised by Allen (1993) related to facing stability of geosynthetic-reinforced segmental retaining walls during a seismic event that includes vertical ground accelerations, parametric analyses were carried out by Bathurst and Cai (1995) to investigate the combined effect of horizontal and vertical acceleration using the range $k_v = - 2k_h/3$ to $+ 2k_h/3$. The upper limit on the ratio k_v, to k_h is equal to the calculated ratio of peak vertical ground acceleration to peak horizontal ground acceleration from seismic data recorded in the Los Angeles area (Stewart *et al.* 1994). The results are shown in Figure 2.9 and illustrate that for $k_h < 0$ 35 the effect on total dynamic earth pressure is not significant.

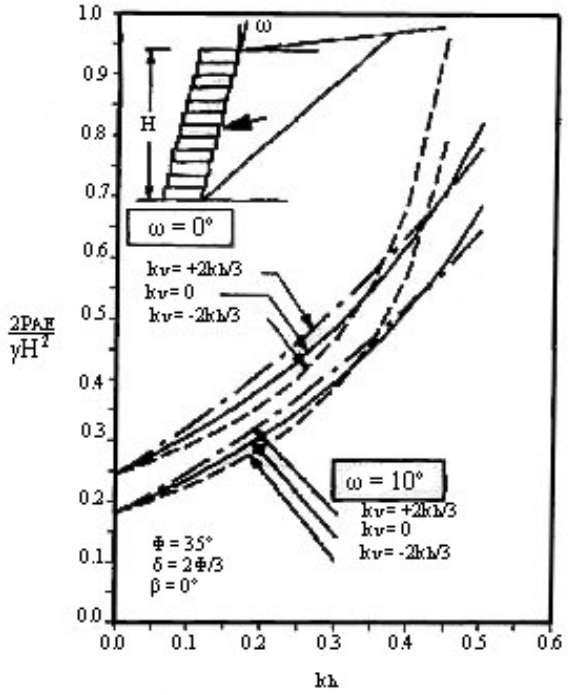

Figure 2.9. Influence of seismic coefficients, k_h and k_v and wall inclination angle, ω, on dynamic earth force, P_{AE}

Based on experience with the performance of conventional and reinforced soil retaining walls during the Kobe earthquake, Tatsuoka el al. (1998) reviewed the choice of horizontal seismic coefficient value used in pseudo-static design methods in Japan. They suggested that the design k_h value for geosynthetic-reinforced soil walls with full-height rigid facings should be taken as 0.3. This value is less than their recommended value of 0.35 for unreinforced cantilever walls and considerably less than their recommended value of 0.4 for conventional gravity type retaining walls. They attributed the selection of the design value of k_h = 0.3 for reinforced soil wall structures to:

- typically conservative assumptions for soil strength.
- positive structural dynamic effects (e.g. wall ductility and flexibility}
- a global factor of safety value that is normally taken to be larger than unity.

In practice, the final choice of k_h may be based on local experience, or prescribed by local building codes or other regulations. The magnitude of a_h for a particular location in the United States, can be found in USGS (2000), and in AASHTO (1998) and NEHRP (1994) guidelines. Similar data can be found in the CFEM (1993) for Canada. Readers may refer to the book by Paz (1994) for information on seismic codes for most other countries. The textbooks by Kramer (1996a) and Okamoto (1984) and agency documents by AASHTO and NEHRP provide valuable in formation on the effect of foundation conditions on attenuation or amplification of bedrock source ground motion.

Finally, FHWA (1996) guidelines for reinforced soil wall structures caution that pseudo-static design methods should be restricted to sites where peak horizontal ground acceleration is not expected to exceed 0,29g. For more intense earthquakes, large structure displacements may occur and the services of a specialist are recommended. As a minimum requirement, retaining wall structures should be analyzed using a Newmark-type sliding block approach (Section 2.2.1), For reinforced soil slopes as flexible structures, FHWA (1996) guidelines allow peak horizontal ground acceleration values published by AASHTO (1998) to be reduced by 50%.

2.1.8. Comparisons Between Selected Pseudo-Static Methods

A comparison of total active earth forces calculated using wedge and log spiral pseudo-static methods is illustrated in Figure 2.10 (a) for frictionless soil/facing interfaces ($\delta = 0$). In these calculations, fully mobilized inter-wedge friction was assumed ($\lambda = 1$) and the point of equivalent total earth force application was taken as H/3. Figure 2.10 (a) shows that for vertical faced slopes and walls ($\omega = 0$) the magnitude of P_{AE} from different pseudo-static methods is the same. However, for shallow slopes, there can be a significant difference between the methods. In particular, the M-O method may be non-conservative at high horizontal ground accelerations. For walls, the choice of earth pressure theory is not a concern, but for slopes the choice of theory must be considered carefully. In conventional tie-back methods of design, it is necessary that reinforcement lengths extend beyond the assumed active failure volume in order that pullout resistance is available for each layer. This is of particular concern towards the top of reinforced wall and slope structures. All rigorous pseudo-static methods consistently predict that

the minimum required reinforcement length will increase with increasing horizontal ground acceleration (Figure 2.10 (b) and Figure 2.10 (c)) and, hence, reinforcement lengths may have to be increased for reinforced soil structures, particularly towards the crest.

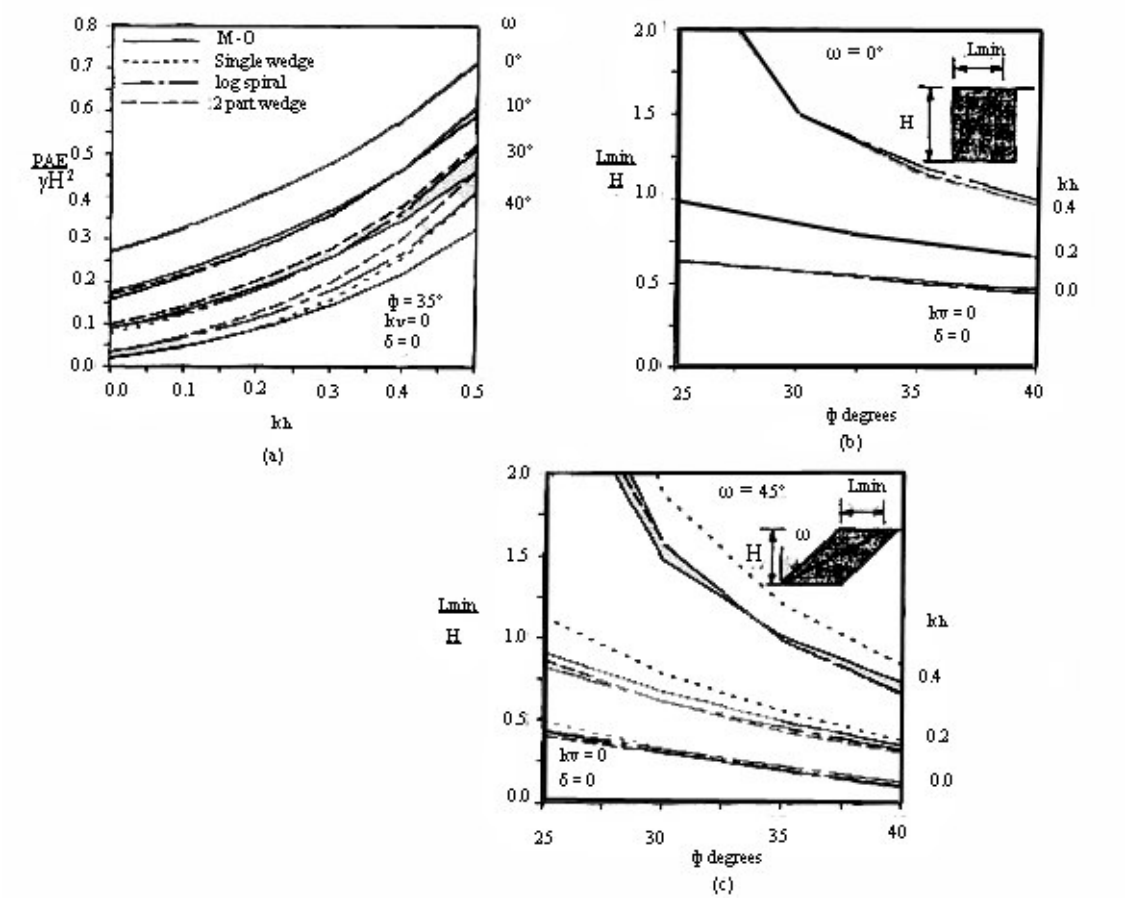

Figure 2.10. Comparison of wedge and log spiral pseudo-static methods (L_{min} = minimum length of reinforcement to contain failure volume; note: L_{min} may not be at the top of the reinforced mass): (a) normalized active earth force; (b) maximum width of failure volume (vertical face); and (c) maximum width of failure volume (sloped face)

2.1.9. Pseudo-dynamic Methods

A pseudo-dynamic earth pressure theory has been proposed by Steedman and Zeng (1990) to account for the influence of phase difference over the height of a vertical retaining wall. The approach recognizes that a base acceleration input will propagate up

through the retained soils at a speed that corresponds to the shear velocity of the soil. The general approach has been extended to the case of cohesionless slopes by Sabhahit *et al.* (1996). Introducing an interface friction angle, δ, and setting $k_v = 0$, leads to a further refinement (Figure 2.11), The horizontal acceleration is assumed to vary as:

$$a(z, t) = a_0 \sin\left[\omega\left(t - \frac{H - z}{V_s}\right)\right] \tag{2.29}$$

where ω is the angular frequency, V_s is the shear wave velocity of the cohesionless soil, a_0 is the peak base acceleration, and t is time. Horizontal slices of the assumed failure wedge with linear failure surface, α have incremental mass calculated as:

$$m(z) = \frac{\gamma}{g}(H - z)(\cot\alpha - \tan\omega)dz \tag{2.30}$$

The total active earth force is computed as:

$$P_{AE}(t) = \frac{Q_h(t)\cos(\alpha - \phi)}{\cos(\delta - \alpha + \phi)} + \frac{W\sin(\alpha - \phi)}{\cos(\delta - \alpha + \phi)} \tag{2.31}$$

where:

$$Q_h(t) = \int_0^H m(z)a(z,t)dz \tag{2.32}$$

The calculation of an equivalent dynamic coefficient of earth pressure, K_{AE}, follows from equation 2.18. The pseudo-dynamic approach leads to values of P_{AE} (t) that in the limit $V_s \rightarrow \infty$ give the pseudo-static value according to M-O theory. The pseudo-dynamic approach allows tile location, H_d, of the dynamic force increment ΔP_{dyn} (the first term in equation 2.31) to be determined numerically for a range of base motion frequencies. The solution is independent of soil friction angle, ϕ, and slope angle, ω, but is dependent

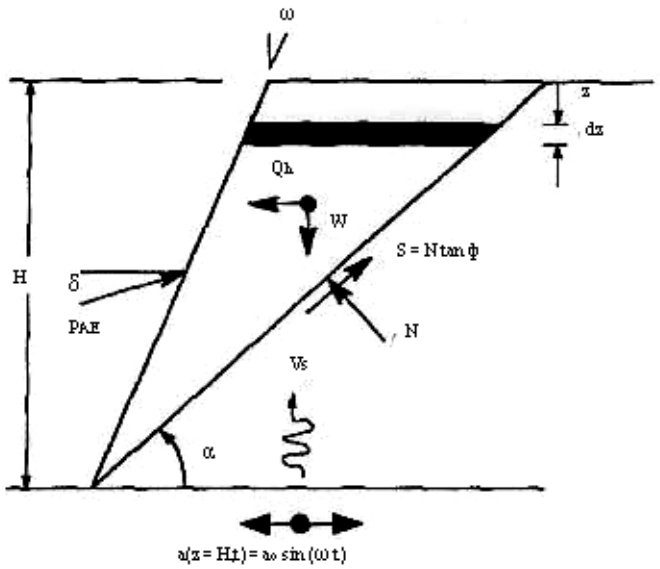

Figure 2.11. Pseudo-dynamic method

on shear velocity (soil density and shear modulus) and period., T_p, of the assumed sinusoidal horizontal acceleration function. The results of the calculations are illustrated in Figure 2.12 and show that for low frequency excitation, the point of application is at H_d = H/3 above the toe of the total mass but will increase at higher frequencies. It appears that the pseudo-static M-O method is reasonable for overturning/base eccentricity design calculations for a wide range of base motion frequencies.

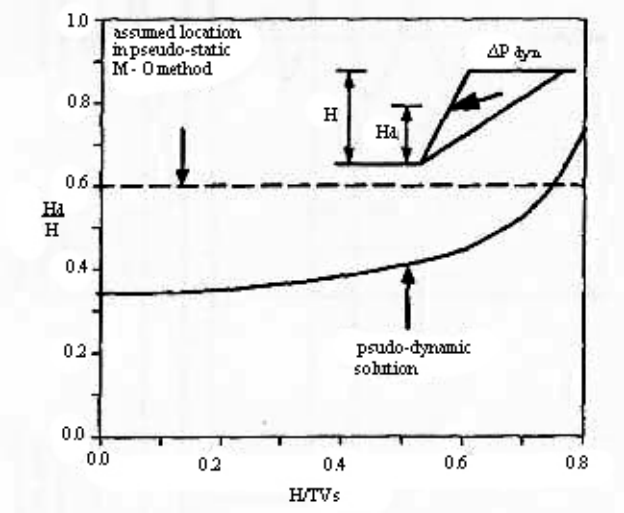

Figure 2.12. Point of application of dynamic force increment

2.2. Displacement Calculations

As with all limit-equilibrium methods of analysis, pseudo-static approaches cannot explicitly include wall or slope deformations. This is an important shortcoming since failure of geosynthetic-reinforced soil walls, in particular, may be manifested as unacceptable movement without structural collapse. The permanent displacement of a geosynthetic-reinforced soil structure due to horizontal sliding/shear mechanisms can be estimated using one of the two general approaches, as described below.

2.2.1. Newmark's Method and Variations

For a given input acceleration time history, Newmark's double integration method for a sliding mass can be used to calculate permanent displacement (Newmark, 1965). According to Newmark's theory, a potential sliding body is treated as a rigid-plastic monolithic mass under the action of seismic forces. Permanent displacement of the mass takes place whenever the seismic force induced on the body (plus the existing static force) overcomes the available resistance along, a potential sliding/shear surface. Newmark's method requires that the critical acceleration, k_c, to initiate sliding or shear failure be determined for each translation failure mechanism. The value of k_c can be determined by searching for values of k_h that give a factor of safety of unity in pseudo-static factor of safety expressions. The critical acceleration is then applied to the horizontal ground acceleration record at the site and double integration is performed to calculate cumulative displacements, as illustrated in Figure 2.13 where g is the gravitational constant, a(t) is the horizontal ground acceleration function with time t, $a_m = k_m g$ is the peak value of a(t), and $a_c = k_c g$ is the critical horizontal acceleration of the sliding block. For a given ground acceleration time history and a known critical acceleration of the sliding mass, the earthquake-induced displacement is calculated by integrating those portion of the acceleration history that are above the critical acceleration and those portions that are below until the relative velocity between the sliding mass and the sliding base reduces to zero.

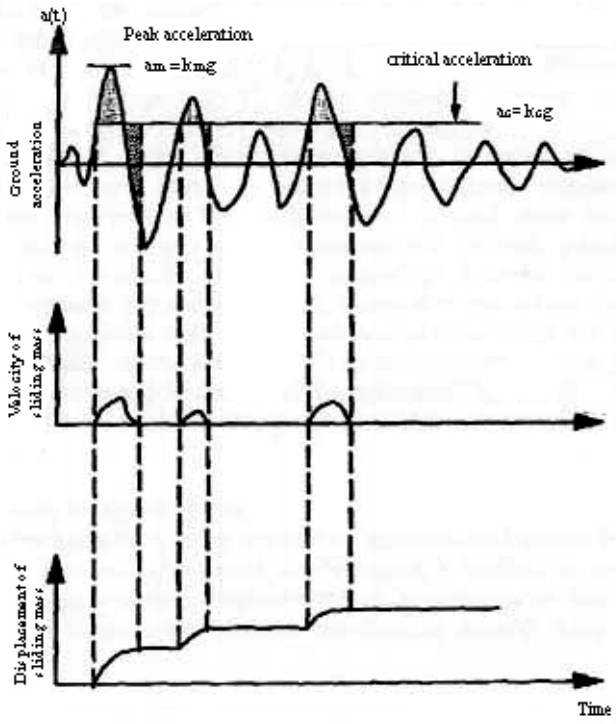

Figure 2.13.Calculation of permanent displacements (unidirectional displacement) using Newmark's method

A number of researchers have postulated that the critical acceleration value to initiate slip should be based on the peak shearing resistance of the soil (e.g. ϕ_{peak}) but thereafter residual strength values should be used (e.g. Elms and Richards, 1990; Chugh, 1995). Alternatively, conservativeh estimates of seismic-induced displacements should be based on residual strength values if a single value of ϕ is adopted to simplify analyses.

2.2.2. Empirical Approaches

If the input acceleration data at a site are specified by characteristic parameters such as the peak ground acceleration and the peak ground velocity, then empirical methods that correlate the expected permanent displacement to the characteristic parameters of the earthquake, and a critical acceleration ratio for the structure, are required. Alternatively, if the tolerable permanent displacement of the structure is specified, based on serviceability criteria, the wall can then be designed using an empirical method

so that, expected permanent displacements do not exceed specified values. Newmark's sliding block theory has been widely used to establish empirical relationships between the expected permanent displacement and characteristic seismic parameters of the input earthquake by integrating existing acceleration records. The critical acceleration ratio, which is the ratio of the critical acceleration, $k_c g$, of the sliding block to the peak horizontal acceleration, $k_m g$, of the earthquake, has been shown to be an important parameter that affects the magnitude of the permanent displacement. Thus, the seismic displacement of a potential sliding soil mass computed using Newmark's theory has been traditionally correlated with the critical acceleration ratio k_c/k_m, and other representative characteristic seismic parameters, such as the peak ground acceleration, $k_m g$, the peak ground velocity, V_m, and the predominant period, T, of the acceleration spectrum (e.g. Newmark, 1965; Sarma, 1975; Franklin and Chang. 1977).

Cai and Bathurst (1996b) have reformulated a number of existing displacement methods based on non-dimensionalized displacement terms that are common to the methods, and divided them into two separate categories based on the characteristic seismic parameters referenced in each method. Example relationships between the dimensionless displacement term, $d/\upsilon^2_m/k_m g)$, where d is the actual expected permanent displacement, and the critical acceleration ratio are shown in Figure 2.14. Other curves are available in the literature but it should be noted that any empirical curve will be influenced by the earthquake data that is used to establish the curve and the interpretation of the original data.

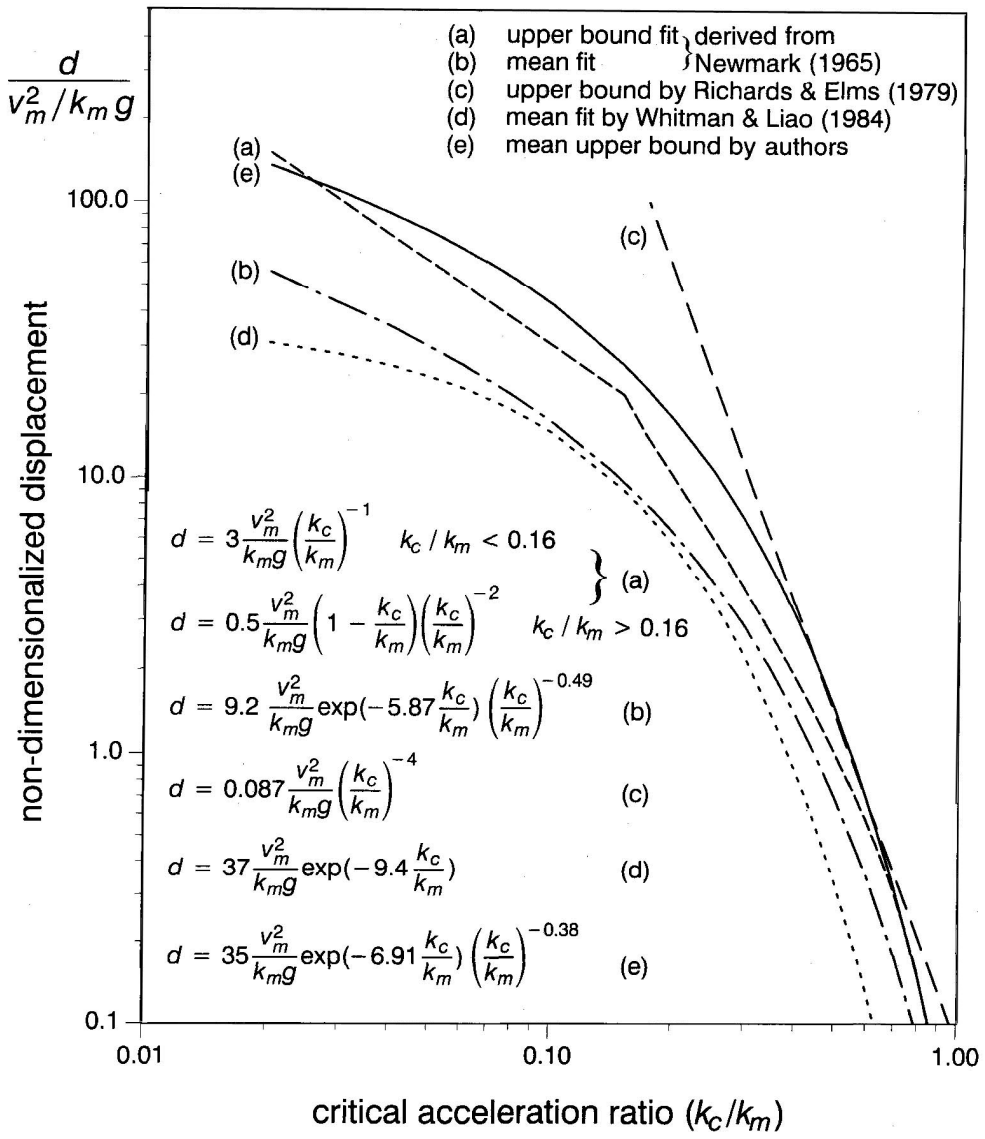

Figure 2.14.Nondimensionalized displacement in terms of $d/(v_m^2/k_m g)$ versus critical acceleration ratio k_c/k_m (after Cai and Bathurst 1996)

3. DESIGN OF GEOSYNTHTIC REINFORCED SEGMENTAL RETAINING WALLS

3.1. Modes of Failure

Stability analyses for geosynthetic reinforced segmental retaining wall systems under static and seismic loading conditions involve separate calculations to establish factors of safety against external, internal and facing modes of failure (Figure 1.2).

External stability calculations consider the reinforced soil zone and the facing column as a monolithic gravity structure. The evaluation of factors of safety against base sliding, overturning about the toe, and foundation bearing capacity is similar to that used for conventional reinforced concrete gravity structures.

Internal stability analyses for geosynthetic reinforced soil walls are carried out to ensure that the structural integrity of the reinforced zone is preserved with respect to reinforcement over-stressing within the reinforced zone, pullout of geosynthetic reinforcement layers from the anchorage zone and internal sliding along a reinforcement layer.

Facing stability analyses are carried out to ensure that the facing column is stable at all elevations above the toe of the wall and connections between the facing units and reinforcement layers are not over-stressed.

Minimum recommended factors of safety for static and seismic design of geosynthetic reinforced SRW structures are given in Table 3.1.

In general, minimum recommended factors of safety for seismic design are taken as 75% of the values recommended for statically loaded structures following AASHTO/ FHWA practice.

Table 3.1. Recommended Minimum Factors of Safety for Design of Geosynthtic Reinforced SRW Structures

Failure Mode		Static	Seismic
a) Base Sliding	FS_{sl}	1.5	1.1
b) Overturning	FS_{ot}	1.5*	1.1
c) Bearing Capacity	FS_{bc}	2.0	1.5
Global Stability	FS_{gl}	1.3 – 1.5	1.1
d) Tensile over-stress	FS_{os}	1.0	1.0
e) Pullout	FS_{po}	1.5	1.1
f) Internal sliding	FS_{sli}	1.5	1.1
g) Shear (bulging)	FS_{sc}	1.5	1.1
h) Connection	FS_{cs}	1.5	1.1
i) Local Overturning**	FS_{otl}	1.5	1.1
j) Crest Toppling	FS_{otc}	1.5	1.1

3.2. External Stability

External stability calculations are similar to those carried out for conventional (gravity) SRW structures with the gravity mass now taken as the composite mass formed by the reinforced soil zone and the facing column. The facing column may comprise a significant part of the gravity mass, particularly for low height structures (and hence generate additional inertial forces during a seismic event). For brevity, this gravity mass is called the reinforced mass or reinforced zone in this document

The dynamic earth pressure distribution shown in Figure 2.2 f is used to calculate the destabilizing forces in otherwise conventional expressions for the factor of safety against sliding along the foundation surface, overturning about the toe of the structure and bearing capacity failure of the foundation soils. $k_h = a_c/2g$ is used to calculate the magnitude of the uniformly applied horizontal seismic coefficient value k_h, in all external stability calculations (i.e. $k_h = k_h(ext)$).

The peak friction angle is taken as $\phi = \phi_b$ in earth pressure and force calculations. The calculation of force components P_{AH} and ΔP_{dynH} assumes full mobilization of inter face friction between the reinforced soil zone and the retained soil (i.e. $\delta = \phi$ with ϕ equal to lesser of ϕ_r and ϕ_b values).

The simplified geometry and body forces illustrated in Figure 3.2 are used in the external stability calculations to follow. Here;

W_i = total weight of the reinforced zone extending from the back of the facing column to length L_{min} beyond the face of the wall and having constant height H;

W_β = contribution of the wedge of soil in the slope above the crest of the wall at height H; and

W_w = total weight of the facing column.

$$W_w = N_w L_w H_w \gamma_w = L_w H \gamma_w \tag{3.1}$$

The results of parametric analyses reported by Bathurst and Cai (1995) have illustrated that as the backslope angle β for the infinite slope case increases, the factors of safety against external stability modes of failure diminish rapidly and reasonable solutions even for modest values of ground acceleration are not possible. This result is due in part to the formulation of earth forces calculated using the M-O method and the conservative estimates of soil strength parameters that are routinely used for the design and analysis of geosynthetic reinforced wall systems. In order to prevent this problem from developing the following empirical rule is proposed in this design guideline: Regardless of the wall geometry and reinforcement lengths the maximum value of the reinforced zone width L_{min} (Figure 3.2) is restricted to the height of the wall H. Hence $L_{min} \leq H$. This approach has been adopted by the Reinforced Earth Company (RECO 1990) for the design of steel strip reinforced soil wails for the same reasons given above.

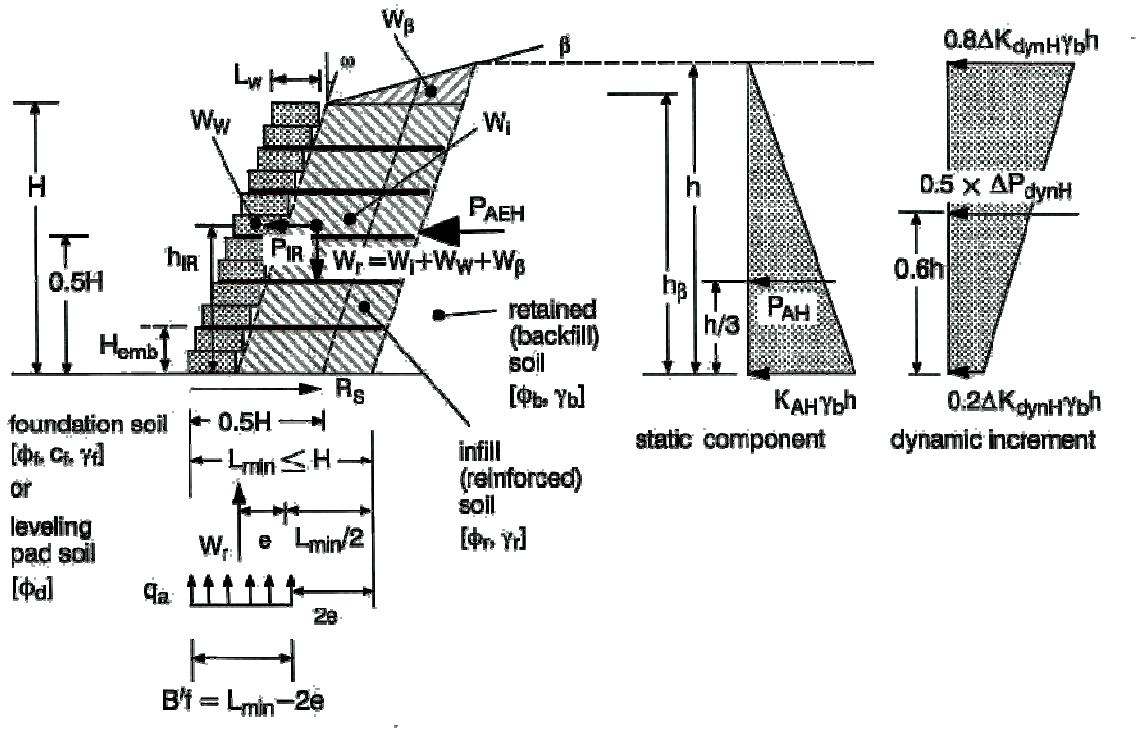

Figure 3.1. Geometry and forces in external stability calculations for reinforced SRW structures

The total weight of the reinforced soil zone is:

$$W_r = W_w + W_i + W_\beta \tag{3.2}$$

The total weight W_r is used to calculate resisting terms in factor of safety expressions for base sliding and overturning and the applied load in bearing capacity calculations. Quantities W_i and W_β can be calculated using the following expressions:

$$W_i = (L_{min} - L_w)H\gamma_r \tag{3.3}$$

$$W_\beta = \frac{1}{2}\gamma_r (L_{min} - L_w)^2 \left(\frac{\tan\beta}{1 - \tan\beta\tan\omega}\right) \tag{3.4}$$

The quantity P_{IR} in Figure 3.2 denotes the horizontal inertial force due to the reinforced mass used in external stability factor of safety calculations. Different strategies have been proposed in North America to compute $P_{IR} < k_h W_r$ to ensure reasonable designs

(Bathurst and Alfaro 1996). The justification is based on the expectation that horizontal inertial forces induced in the reinforced mass and the retained (backfill) soil zone will not reach peak values at the same time during a seismic event.

The method adopted here uses the AASHTO/FHWA approach and assumes that the horizontal inertial force P_{IR} is due to an equivalent mass comprising the facing column and a portion of the reinforced soil zone extending to a distance 0.5 H beyond the face of the wall. The general approach is illustrated in Figure 3.2 and applies to any infinite backfill slope condition (i.e. $\beta > 0$). The inertial force P_{IR} is calculated using:

$$P_{IR} = k_h \, (ext) \, (W_w + W'_i + W'_\beta) \tag{3.5}$$

Where the reduced inertial zone weights W'_i and W'_β are calculated by substituting L_{min} = 0,5 H in equation 3.3 and 3.4. Hence:

$$W'_i = (0{,}5H - L_w)H\gamma_r \tag{3.6}$$

$$W'_\beta = \frac{1}{2}\gamma_r (0{,}5H - L_w)^2 \left(\frac{\tan\beta}{1 - \tan\beta \tan\omega} \right) \tag{3.7}$$

The dynamic earth force P_{AE} is applied at the back of the reinforced mass described by the minimum reinforcement length L_{min} and height h. The quantity h can be calculated as:

$$h = H + (L_{min} - L_w)\left(\frac{\tan\beta}{1 - \tan\beta \tan\omega} \right) \tag{3.8}$$

For structures with a horizontal backslope ($\beta = 0$) the problem geometry is simplified since h = H.

The horizontal component of dynamic earth force P_{AEH} acting over depth at the back of the reinforced zone is calculated using the following expression:

$$P_{AEH} = P_{AH} + 0{,}5 \times \Delta P_{dynH} = \frac{K_{AH}\gamma_b h^2}{2} + 0{,}5 \times \frac{\Delta K_{dynH}\gamma_b h^2}{2} \quad (3.9)$$

Note that only 50% of the dynamic earth force increment, ΔP_{dynH}, acting over height h is considered in external stability calculations.

The application of the dynamic increment of backfill soil force ΔP_{dynH} differs from the method used by AASHTO/FHWA. AASHTO/FHWA apply ΔP_{dynH} to the back of the inertial zone identified by the dashed line at distance 0.5H behind the wall face in Figure 3.2. For sloped backfills the method used in this document is slightly more conservative but greatly simplifies calculations. For horizontal backfills there is no difference between methods with respect to location of the dynamic force increment. However, AASHTO/FHWA guidelines assume that the interface friction angle at the boundary between the reinforced zone and backfill soil is equal in magnitude to the angle of the constant slope behind the wall crest (i.e. $\delta = \phi$). However, there is no justification for linking interface friction angle to slope angle. The magnitude of earth pressures for external stability calculations in this document will almost always be less than AASHTO/FHWA values since $\delta = \phi \geq \beta$. In addition, AASHTO/FHWA assumes that $\omega = 0$ for walls with $\omega < 10°$ and this leads to higher earth pressures and hence more conservative static and seismic designs for reinforced SRW structures using their method. The interpretation of Coulomb and M-O earth pressure theory used in NCMA document provides a seamless transition between the analysis and design of statically loaded structures described in the DMSRW and the methodology for seismic loaded SRW structures.

3.2.1. Base Sliding (Figure 3.1 (a))

The factor of safety against base sliding FS_{sl} at the bottom of the reinforced mass (i.e. bottom of the lowermost facing unit and reinforced soil zone) can be expressed as:

$$FS_{sl} = \frac{R_S}{P_{IR} + P_{AH} + 0{,}5 \times \Delta P_{dynH}} \quad (3.10)$$

The base sliding resistance force, R_S, (Figure 3.2) is calculated as follows:

a) If the reinforced soil (infill) or drainage fill controls:

$$R_S = C_{ds}\, W_r \tan\phi \tag{3.11}$$

with $\phi = \phi_d$ or ϕ_r whichever value has the least magnitude.

b) If the foundation soil controls:

$$R_S = C_{ds}\, [c_f\, L_{min} + Wr \tan\phi_f] \tag{3.12}$$

Here the quantity C_{ds} is the coefficient of direct sliding and cannot exceed unity. For soil to soil interfaces the value for this parameter can be assumed to be equal to one. For the case of a geosynthetic layer placed at the base of the reinforced soil zone, $C_{ds} < 1$ maybe appropriate.

The calculated value of FS_{sl} should not be less than 1.1 (Table 3.1)

3.2.2. Base Overturning (Figure 3.2 (b))

The factor of safety FS_{ot} against overturning about the toe of the facing column can be expressed as the ratio of the resisting moment M_r and driving moment M_o:

$$FS_{ot} = \frac{M_r}{M_o} \tag{3.13}$$

The resisting moment is calculated as:

$$M_r = W_w X_w + W_i X_i + W_\beta X_\beta \tag{3.14}$$

where X_w is the horizontal distance from the toe of the wall to the center of gravity of the entire facing column and can be calculated using:

$$X_w = \frac{1}{2}\left[(N_w - 1)H_w \tan\omega\right] + L_g \tag{3.15}$$

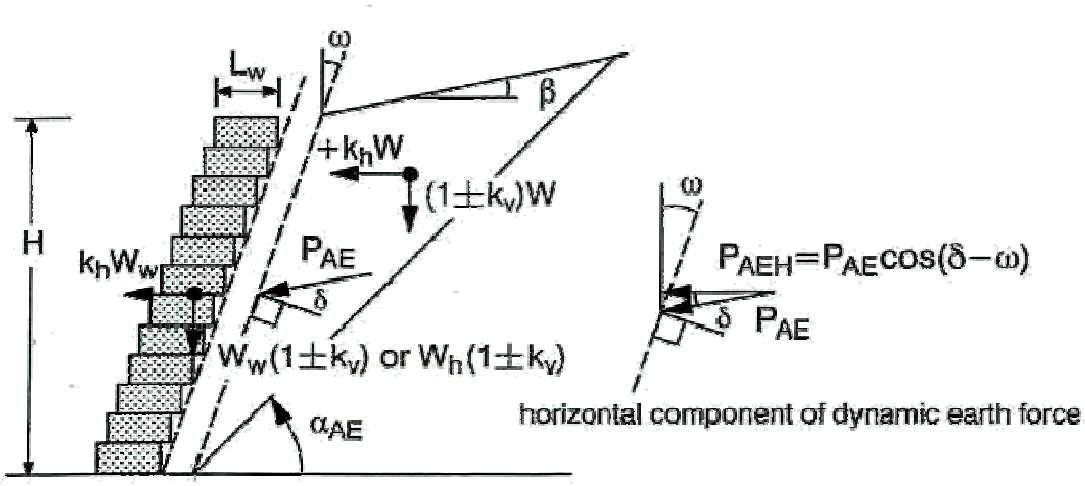

Figure 3.2. Resisting moments for base overturning in external stability calculations for reinforced SRW structures

Moment arm quantities X_i and X_β illustrated in Figure 3.3 are calculated as follows:

$$X_i = \frac{L_{min} + L_w + H\tan\omega}{2} \tag{3.16}$$

$$X_\beta = H\tan\omega + \frac{1}{3}\left(L_w + 2L_{min}\right) \tag{3.17}$$

The driving moment is calculated as:

$$M_o = P_{IR}\,h_{IR} + P_{AH}\,\frac{h}{3} + 0{,}5 \times \Delta P_{dynH}\,0{,}6h \tag{3.18}$$

Here:

$$h_{IR} = \frac{k_h(ext)W_w \frac{H}{2} + k_h(ext)W_i' \frac{H}{2} + k_h(ext)W_\beta' h_\beta}{P_{IR}} \quad (3.19)$$

$$h_\beta = H + \frac{1}{3}(L_{min} - L_w)\tan\beta \quad (3.20)$$

The calculated value of FS_{ot} should not be less than 1.1 Table 3.1

3.2.3. Bearing Capacity (Figure 3.2 (c))

Conventional bearing capacity analyses are carried out with respect to the base width L of the reinforced (infill) soil mass is assumed to act as a continuous strip footing and must have sufficient width L to prevent overstressing of the foundation soils that may lead to shear failure of the foundation soils or excessive settlement.

Meyerhof stress distribution approach is utilized to ensure a conservative estimate of applied bearing stress. The effect of eccentricity of the resultant bearing force (net foundation load) (Figure 3.2) is to restrict compressive bearing pressures to an equivalent bearing area B'_f calculated as:

$$B'_f = L_{min} - 2e \quad (3.21)$$

The Meyerhof bearing capacity approach for statically loaded geosynthetic reinforced SRW structures is modified here to include the additional base loading eccentricity developed by the external dynamic force increment ΔP_{dynH} and the inertial force P_{IR}. The factor of safety against bearing capacity failure is expressed as:

$$FS_{bc} = \frac{q_{ult}}{q_a} \quad (3.22)$$

where q_{ult} is the ultimate bearing capacity of the foundation soil and q_a the applied bearing stress at the base of the reinforced soil mass and facing column (composite mass). The magnitude of q_{ult} is calculated as follows:

$$q_{ult} = c_f N_c + \frac{1}{2}\gamma_f B_f' N_\gamma + \gamma_f H_{emb} N_q \tag{3.23}$$

values of bearing capacity coefficients N_c, N_γ and N_q are shown in Table 3.2.

Consistent with the method used in the DMSRW the eccentricity term e can be calculated with respect to the center of the base of the reinforced zone (i.e. at distance $L_{min}/2$ from the toe of the wall) as follows:

$$e = \frac{P_{IR} h_{IR} + P_{AH} \frac{h}{3} + 0.5 \times \Delta P_{dynH} 0.6h}{W_r} - \frac{W_w\left(X_w - \frac{L_{min}}{2}\right) - W_i\left(X_i - \frac{L_{min}}{2}\right) - W_\chi\left(X_\beta - \frac{L_{min}}{2}\right)}{W_r} \tag{3.24}$$

The applied bearing capacity stress at the base of the reinforced zone is calculated as:

$$q_a = \frac{W_r}{B_f'} \tag{3.25}$$

The calculated value of FS_{bc} should not be less than 1.5. (Table 3.1)

Table 3.2. Bearing capacity factors

ϕ^+ (deg)	N_c	N_q	N_γ	N_q/N_c	$\tan\phi$
0	5.14	1.00	0.00	0.20	0.00
1	5.38	1.09	0.07	0.20	0.02
2	5.63	1.20	0.15	0.21	0.03
3	5.90	1.31	0.24	0.22	0.05
4	6.19	1.43	0.34	0.23	0.07
5	6.49	1.57	0.45	0.24	0.09
6	6.81	1.72	0.57	0.25	0.11
7	7.16	1.88	0.71	0.26	0.12
8	7.53	2.06	0.86	0.27	0.14
9	7.92	2.25	1.03	0.28	0.16
10	8.35	2.47	1.22	0.30	0.18
11	8.80	2.71	1.44	0.31	0.19
12	9.28	2.97	1.69	0.32	0.21
13	9.81	3.26	1.97	0.33	0.23
14	10.37	3.59	2.29	0.35	0.25
15	10.98	3.94	2.65	0.36	0.27
16	11.63	4.34	3.06	0.37	0.29
17	12.34	4.77	3.53	0.39	0.31
18	13.10	5.26	4.07	0.40	0.32
19	13.93	5.80	4.68	0.42	0.34
20	14.83	6.40	5.39	0.43	0.36
21	15.82	7.07	6.20	0.45	0.38
22	16.88	7.82	7.13	0.46	0.40
23	18.05	8.66	8.20	0.48	0.42
24	19.32	9.60	9.44	0.50	0.45
25	20.72	10.66	10.88	0.51	0.47
26	22.25	11.85	12.54	0.53	0.49
27	23.94	13.20	14.47	0.55	0.51
28	25.80	14.72	16.72	0.57	0.53
29	27.86	16.44	19.34	0.59	0.55
30	30.14	18.40	22.40	0.61	0.58
31	32.67	20.63	25.99	0.63	0.60
32	35.49	23.18	30.22	0.65	0.62
33	38.64	26.09	35.19	0.68	0.65
34	42.16	29.44	41.06	0.70	0.67
35	46.12	33.30	48.03	0.72	0.70
36	50.59	37.75	56.31	0.75	0.73
37	55.63	42.92	66.19	0.77	0.75
38	61.35	48.93	78.03	0.80	0.78
39	67.87	55.96	92.25	0.82	0.81
40	75.31	64.20	109.41	0.85	0.84
41	83.86	73.90	130.22	0.88	0.87
42	93.71	85.38	155.55	0.91	0.90
43	105.11	99.02	186.54	0.94	0.93
44	118.37	115.31	224.64	0.97	0.97
45	133.88	134.88	271.76	1.01	1.00
46	152.10	158.51	330.35	1.04	1.04
47	173.64	187.21	403.67	1.08	1.07
48	199.26	222.31	496.01	1.12	1.11
49	229.93	265.51	613.16	1.15	1.15
50	266.89	319.07	762.89	1.20	1.19

+ USE ϕ_f, THE PHI ANGLE FOR FOUNDATION SOILS

3.3. Internal Stability

3.3.1. Reinforcement Loads

The contributory area approach used for the static stability analysis of segmental retaining walls is extended to the dynamic loading case **(Fig)**. In this method the reinforcement layers are modeled as tie-backs with the tensile force, Fi, in layer i equal to the earth pressure integrated over the contributory area, S_{vi}, at the back of the facing column plus the corresponding wall inertial force increment. Hence:

$$F_i = k_h(\text{int})\Delta W_{wi} + F_{stai} + F_{dyni} \tag{3.26}$$

where: $k_h(\text{int})\Delta W_{wi}$ = wall inertial force increment; F_{stai} = static component of reinforcement load; and F_{dyni} = dynamic component of reinforcement load. The quantity ΔW_{wi} is the weight of the facing falling with the contributory area S_{vi} of the corresponding reinforcement layer and hence can be calculated as follows:

$$\Delta W_{wi} = S_{vi} L_w \gamma_w \tag{3.27}$$

referring to Figure 3.4:

$$F_{stai} = K_{AH} \gamma_r z_{vi} S_{vi} \tag{3.28}$$

$$F_{dyni} = \left[0.8 - 0.6 \frac{z_{vi}}{H} \right] \Delta K_{dynH} \gamma_r H S_{vi} \tag{3.29}$$

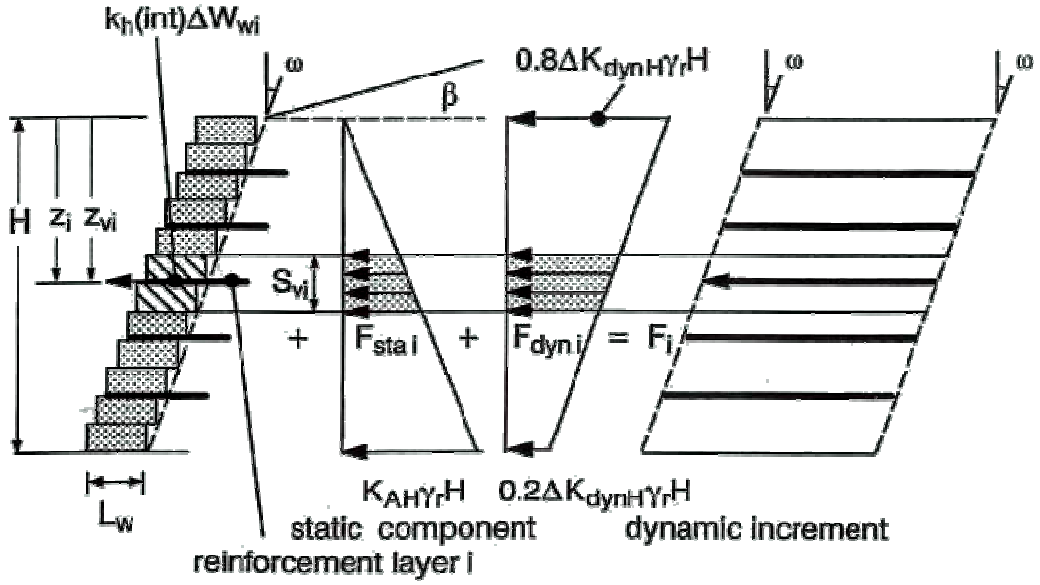

Figure 3.3. Geometry and forces used to calculate reinforcement loads for reinforced SRW structures

The quantity z_{vi} is the distance from the crest of the wall to the mid-elevation of the contributory area S_{vi}. For constant reinforcement spacings $z_{vi} = z_i$. For non-uniform spacings $z_{vi} \neq z_i$. The contributory area for the topmost reinforcement layer is taken from the wall crest to mid-elevation between the first and second reinforcement layers from the crest. The contributory area for the bottommost layer is taken from the mid-elevation between the bottom layer and the layer immediately above, and the base elevation of the reinforced soil mass. The value of horizontal seismic coefficient ($k_h = k_h(int)$) used to calculate the wall inertial force increment ($k_h(int)\ \Delta W_{wi}$ in Equation 3.26) and dynamic component of reinforcement load (i.e. ΔK_{dynH} term in Equation 3.29) is determined from Equation 2.28**.**

3.3.2. Over-stressing of Reinforcement (Figure 3.2 (d))

The dynamic factor of safety, FS_{os}, against over-stressing of reinforcement layer I is given by:

$$FS_{os} = \frac{T_{a(dyn)}}{F_i} \tag{3.30}$$

Here, $T_{a(dyn)}$ is the allowable tensile load for the reinforcement under seismic loading. AASHTO/FHWA guidelines recommend that the allowable strength for seismic loaded structures can be calculated using the same reduction factor approach used for statically loaded structures but with the creep reduction factor $RF_{CR} = 1$. Equivalently, the allowable strength calculated according to the DMSRW for statically loaded structures can be modified according to:

$$T_{a\,(dyn)} = T_a \times RF_{CR} \tag{3.31}$$

The calculated value of FS_{os} should not be less that 1.0 (Table 3.1). In other words, $T_{a\,(dyn)} > F_i$.

3.3.3. Reinforcement Anchorage (Figure 3.2 (e))

The reinforcement tensile load F_i must be carried by the reinforcement anchorage length which is located between the internal active failure plane (oriented at α_{ae} from horizontal) and the reinforcement free end (Figure 3.5). A common approach for anchorage capacity design is to use a simple Coulomb-type interface model in which anchorage capacity is taken to be linearly proportional to anchorage length, overburden pressure and soil shear strength.

The anchorage capacity $T_{pull\,i}$, corresponding to reinforcement layer i is calculated as follows:

$$T_{pull\,i} = 2L_{Ai}C_i\sigma_{vi}\tan\phi_r \tag{3.32}$$

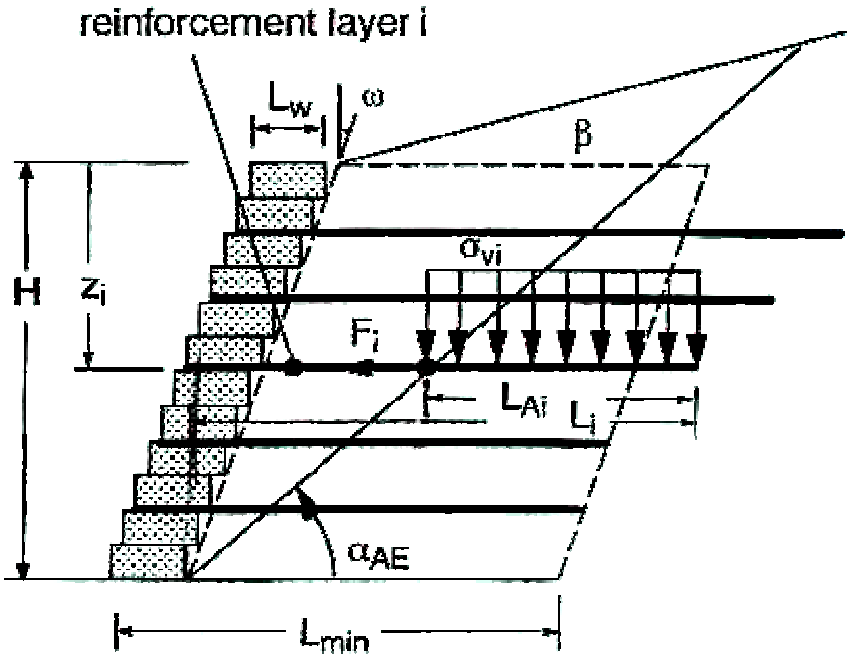

Figure 3.4. Geometry and forces used to calculate anchorage capacity of reinforcement layers in SRW structures

where:

L_{Ai} = anchorage length for reinforcement layer i;

C_i = the coefficient of interaction for pullout;

σ_{vi} = average overburden pressure acting over anchorage length L_{Ai}; and

ϕ_r = peak friction angle of reinforced (infill) soil.

The anchorage length L_{Ai} can be calculated as follows:

$$L_{Ai} = L_i - L_w + (H - z_i)\left[\tan\omega - \tan\left(\frac{\pi}{2} - \alpha_{AE}\right)\right] \tag{3.33}$$

Here L_i is the total length of reinforcement layer i taken from the front face of the wall to the soil embedded end of the layer, and α_{AE} is calculated in accordance with Equation 2.6

using θ = 0. The average normal stress acting over the anchorage length can be calculated using the following expression:

$$\sigma_{vi} = \gamma_r \left[z_i + \left(\frac{H - z_i}{\tan \alpha_{AE}} - H \tan \omega + \frac{L_{Ai}}{2} \right) \tan \beta \right] \tag{3.34}$$

The factor of safety against pullout failure is expressed as:

$$FS_{po} = \frac{T_{pulli}}{F_i} \tag{3.35}$$

The calculated value of FS_{po} should not be less than 1.1 (Table 3.1)

3.3.4. Internal Sliding (Figure 3.2 (f))

The factor of safety against internal sliding FS_{sli} = along a reinforcement layer located at depth z below the crest of the wall can be expressed as:

$$FS_{sli} = \frac{R_S(z_i)}{\Delta P_{IR}(z_i) + P_{AEH}(z_i)} \tag{3.36}$$

The internal force contribution $\Delta P_{IR}(z_i)$ is calculated as:

$$\Delta P_{IR}(z_i) = k_h(\text{ext})\left(\Delta W_w(z_i) + \Delta W_i'(z_i) + \Delta W_\beta'\right) \tag{3.37}$$

The value of k_h (ext) used to calculate the inertial force contribution is determine from $k_h = a_c/2g$. Quantity $\Delta W_w(z_i)$ is the total weight of the facing column above the sliding surface located at depth z_i. Similar to the approach adopted for base sliding, the reduced reinforced zone weight $\Delta W_i'(z_i)$ is calculated using:

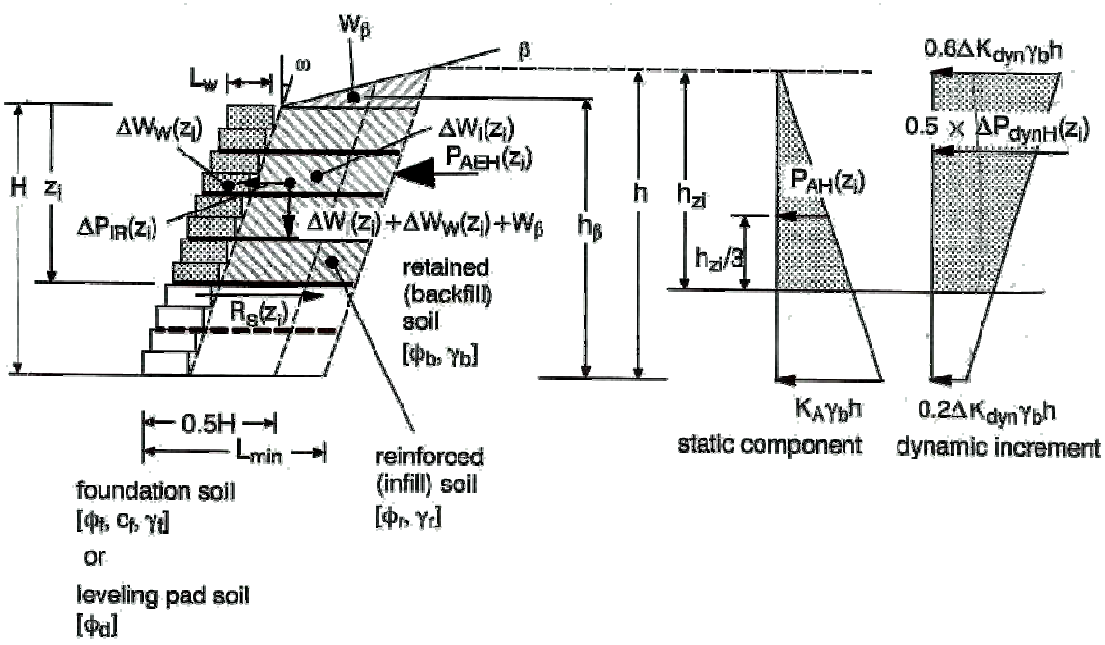

Figure 3.5. Geometry and forces used to calculate internal sliding of reinforcement layers in reinforced SRW structures

$$\Delta W_i'(z_i) = (0.5H - L_w)z_i\gamma_r \tag{3.38}$$

Finally, the reduced reinforced zone weight in the slope above the reinforced mass, W'_β, is calculated using Equation 3.7.

The horizontal component of dynamic earth force $P_{AEH}(z_i)$ acting over the depth h_{zi} at the back of the reinforced zone is calculated using the following expression;

$$P_{AEH}(z_i) = P_{AH}(z_i) + 0.5 \times \Delta P_{dynH}(z_i) = \frac{K_{AH}\gamma_b h_{zi}^2}{2} + \left[0.8h_{zi} - 0.3\frac{h_{zi}^2}{h}\right]\Delta K_{dynH}\gamma_b h \tag{3.39}$$

The value of k_h, used to calculate the horizontal component of the dynamic force increment ($\Delta P_{dynH}(z_i)$) is determined from $k_h = a_c/2g$ (i.e. $k_h = k_h(ext)$. The quantity h_{zi} can be calculated as:

$$h_{zi} = z_i + (L_{min} - L_w)\left(\frac{\tan\beta}{1 - \tan\beta\tan\omega}\right) \quad (3.40)$$

For structures with a horizontal backslope ($\beta = 0$) the problem geometry is simplified since $h_{zi} = z_i$. The sliding resistance $R_S(z_i)$ corresponding to interface i is calculated using:

$$R_S(z_i) = V_u(z_i) + C_{ds}\left(\Delta W_i(z_i) + W_\beta\right)\tan\phi_r \quad (3.41)$$

The quantity $V_u(z_i)$ is the peak interface shear capacity between facing column units calculated using:

$$V_u(z_i) = a_u + \Delta W_h(z_i)\tan\lambda_u \quad (3.42)$$

The quantity C_{ds} in Equation 3.41 is the coefficient of direct sliding for the soil-geosynthetic interface and cannot exceed unity. Quantity $\Delta W_i(z_i)$ is calculated as:

$$\Delta W_i(z_i) = (L_{min} - L_w)z_i\gamma_r \quad (3.43)$$

and W_β is calculated using equation 3.4

Only 50% of the external dynamic earth force increment, $\Delta Pd_{ynH}(zi)$, acting over the height h_{zi} is considered for internal sliding stability calculations. The calculation of force components $P_{AH}(z_i)$and $\Delta P_{dynH}(z_i)$ assumes full mobilization of interface friction between the reinforced soil zone and the retained soil (i.e.$\delta = \phi$ with ϕ equal to the lesser of ϕ_r and ϕ_b).

The calculated value of FS_{sli} should not be less than 1.1 (Table 1.1).

3.4. Facing Stability

In pseudo-static seismic analysis of the facing stability of reinforced SRW structures, the following potential failure mechanisms must be examined: interface shear failure; overturning; crest toppling; and connection failure (Figure 2.2).

3.4.1. Interface Shear (Figure 3.2 (g))

The influence of interface shear transmission on facing column stability can be analyzed by treating the facing column as a beam in which the integrated lateral pressure (i.e. distributed load) must equal the sum of the reactions (forces in reinforcement layers). The calculation of interface shear force under dynamic loading must include the effect of wall facing inertia. The general approach is illustrated in Figure 3.7. The locally maximum interface shear forces will occur at reinforcement elevations.

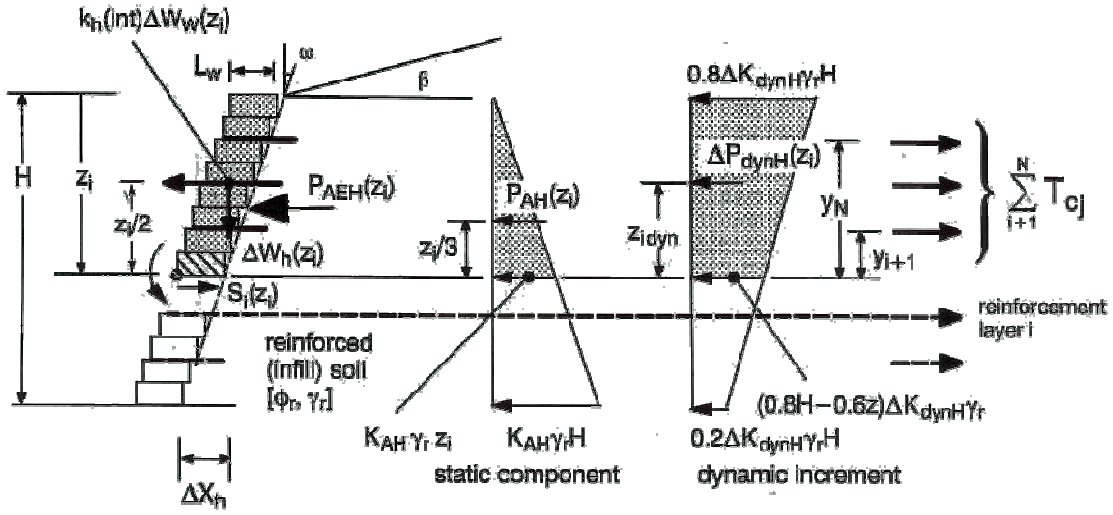

Figure 3.6. Geometry and forces used to calculate interface shear (bulging) and overturning of the facing column for reinforced SRW structures

The out-of-balance horizontal force S_i transmitted to an interface at depth z_i (corresponding to reinforcement layer i) is the difference in magnitude between the horizontal

component of dynamic earth force plus facing column inertia) force and the sum of the horizontal loads carried by the reinforcement layers above the target interface. Hence:

$$S_i(z_i) = k_h(\text{int})\Delta W_w(z_i) + P_{AEH}(z_i) - \sum_{i+1}^{N} F_j \tag{3.44}$$

Here N is the number of reinforcement layers. The horizontal component of dynamic earth force $P_{AEH}(z_i)$ acting over the depth z_i at the back of the facing column is calculated using the following expression;

$$P_{AEH}(z_i) = P_{AH}(z_i) + \Delta P_{dynH}(z_i) = \frac{K_{AH}\gamma_r z_i^2}{2} + \left[0.8z_i - 0.3\frac{z_i^2}{H}\right]\Delta K_{dynH}\gamma_r H \tag{3.45}$$

Coefficients of earth pressure (K_{AH} and ΔK_{dynH}) are calculated using $\phi = \phi_r$ and $0 \le \delta \le \phi_r$. Typically δ is taken as $2\phi_r/3$ for facing stability calculations. Quantity ΔK_{dynH} in Equation 3.45 is calculated using $k_h=k_h(\text{int})$ (Equation 2.28)**.** The summation of reinforcement reactions can be calculated using Equation 3.26. The factor of safety against interface shear failure (FS_{sc}) at a reinforcement layer is:

$$FS_{sc} = \frac{V_u(z_i)}{S_i(z_i)} \tag{3.46}$$

where $V_u(z_i)$ is the peak shear capacity of the interface calculated using Equation 3.42, The selection of interface shear strength parameters should be based on the results of laboratory interface shear data simulating the geosynthetic-modular block interface.

The calculated value of FS_{sc} should not be less than 1.1 (Table 3.1).

3.4.2. Connection Failure (Figure 3.2 (h))

The dynamic factor of safety, FS_{cs}, against connection failure of the reinforcement layer with the facing column can be expressed as:

$$FS_{cs} = \frac{T_{ci}}{F_i} \tag{3.47}$$

Here, F_i is the tensile load in the reinforcement layer i calculated using Equation 3.26 and T_{ci} is the peak connection capacity for that layer calculated as:

$$T_{ci} = a_{cs} + \Delta W_h(z_i)\tan\lambda_{cs} \tag{3.48}$$

The quantity a_{cs} is the minimum available peak connection strength in kN/m and λcs is the apparent peak interface friction angle describing the connection failure envelope (degrees) corresponding to the range of normal weight over which $\Delta W_h(zi)$ applies.

The calculated value of FS_{cs} should not be less than 1.1 (Table 3.1).

3.4.3. Local Overturning (Figure 3.2 (i))

The distribution of internal moments at interface elevations can also be calculated using the beam analog described in Section 3.4.1 for interface shear stability calculations. Internal moments that cause net outward moment at the toe of a facing unit, provide a possible failure mechanism for which an adequate factor of safety should be checked. Local peak destabilizing moments will occur at reinforcement elevations.

The factor of safety FS_{otl} against local overturning about the toe of the facing column at depth z_i below the crest of the wall can be expressed as the ratio of the resisting moments to driving moments:

$$FS_{otl} = \frac{M_r(z_i) + \sum_{i+1}^{N} T_{cj} \times y_j}{M_o(z_i)} \tag{3.49}$$

The resisting moment $M_r(z_i)$ due to the facing column is calculated using:

$$M_r(z_i) = \Delta W_h(z)\Delta X_h(z) \tag{3.50}$$

where:

$$\Delta X_h = \frac{1}{2}\left[(N_z - 1)H_w \tan\omega\right] + L_g \tag{3.51}$$

and the driving moment due to earth forces, $M_o(z_i)$, is calculated using:

$$M_o(z_i) = k_h \Delta W(z_i)\frac{z_i}{2} + \frac{P_{AH}(z_i)z_i}{3} + \Delta P_{dynH}(z_i)y_{dyn}(z_i) \tag{3.52}$$

$$= k_h \Delta W(z_i) + \frac{K_{AH}\gamma_b z^3}{6} + \left[\left(0.8z_i - 0.3\frac{z_i^2}{H}\right)\Delta K_{dynH}\gamma_b H\right] y_{dyn}(z)$$

where:

$$y_{dyn}(z_i) = \frac{0.4Hz_i - 0.1z_i^2}{0.8H - 0.3z_i} \tag{3.53}$$

The value of k_h used in this moment calculation is based on the value from Equation 2.28 (i.e. $k_h = k_h(int)$). The summation with T_{cj} X y_j terms in Equation 3.49 de notes the resisting moment due to the peak connection capacities of reinforcement layers and their corresponding moment arms from the target point of rotation.

The calculated value of FS_{otl} should not be less than 1.1 (Table 3.1).

3.4.4. Crest Toppling (Figure 3.2 (j))

Local (crest) toppling refers to the overturning of the top unreinforced portion of the facing column (Figure 3.2 j)**.** This analysis is identical to that described in Section 3,4.3 for conventional gravity structures but using $k_h = k_h(int)$ (i.e. Equation 3.49 neglecting summation term). The critical portion of the facing column is taken as the height of wall starting at the elevation of the topmost layer of reinforcement.

The calculated value of FS_{otc} should not be less than 1.1 (Table 3.1).

4. METHODOLOGY

To determine the influence of several parameters on the earthquake induced deformation of geosynthetic reinforced segmental retaining walls, NCMA's Segmental Retaining Walls - Seismic Design Manual and Newmark's displacement method is used. Instead of calculation all the values by hand, MS Excel program is used.

4.1. Assumptions Made in the Analysis

1. SRW structures are free-standing and able to displace horizontally at the base and yield laterally through the height of the wall and at the wall crest.
2. Reinforced and retained soils are cohesionless (i.e. purely frictional soils), un-saturated and homogeneous. Soil strength is described by the Mohr-Coulomb failure criterion. In many cases the apparent cohesive strength component of the free-draining soils is ignored, which is a conservative (i.e. safe) assumption for design.
3. Vertical ground acceleration is zero.
4. Constant (infinite) backslope angle and constant horizontal foreslope angle.
5. Reinforced soils are placed to a depth corresponding to the full height of the stacked standard facing units.
6. Capping units are assumed to have a negligible effect on stability analyses and if present are attached to the facing column in such a manner that they cannot be dislodged during ground shaking.
7. No permanent surcharge or footing loads exist at the top or behind the facing column.
8. The base of the facing column is horizontal.
9. Global instability involving failure of soil volumes beyond the base of the geosynthetic reinforced soil zone is not considered.
10. SRW structures are built on competent foundations for which excessive settle ment, squeezing or liquefaction are not potential sources of instability.

4.2. Material Properties

Table 4.1. Material Properties for Calculated Wall

Input Data	Properties	Values
Backfill Soil	Friction angle (Φ_b)	32°
	Unit Weight(γ_b	20 kN/m
	Mobilized interface friction angle (δb)	32°
Reinforced Soil	Friction angle (Φ_r)	32°
	Unit Weight(γ_r	20 kN/m
	Mobilized interface friction angle (δ_r)	21.3°
Geosynthetic	Ultimate Strength (T_{ult})	40 kN/m
	Allowable Strength (T_a)	10 kN/m
	Creep Reduction Factor RF_{CR}	1,66
Soil-Geosynthetic	Coefficient of Direct Sliding	1,00
Segmental Block	Height (H_w)	0,2 m
	Length (L_w)	0,2 m, 0,4 m
	Unit Weight(γ_w	23 kN/m^3
	Block-Block interface shear (Formula 3.42)	a_u = 6 kN/m λ_u = 30°
	Block-Geosynthetic interface shear (Formula 3.48)	a_{cs} = 6 kN/m λ_{cs} = 30°
Wall	Height (H)	2 m, 4 m, 6 m, 8 m, 10 m
	Setback (ω)	0°, 3°
	Backslope Angle (β)	0°
	Reinforcement Spacing	0,2 m, 0,4 m
	Reinforcement Length/Height of Wall	0,70, 1,00
Seismic Data (Sakarya Earthquake)	Peak Ground Acceleration a_m	0,628 g
	Peak Ground Velocity v_m	0,277 m/sn

4.3. Determination of Critical Accelerations

Permanent displacements are assumed to calculate each time the critical acceleration a_c ($a_c = k_c g$, where k_c is the critical horizontal seismic coefficient), associated with each three displacement mechanisms; (1) external sliding along the base of total structure; (2) internal sliding along a reinforcement layer and through the facing column; and (3) block interface shear between facing column units; is exceeded by the horizontal input (ground) acceleration $a(_t)$.

The critical horizontal acceleration coefficient (k_c) for any given set of input parameters corresponds to the value of k_h that gives $FS_{dyn} = 1.0$.

4.4. Calculation of Permanent Displacements

The permanent displacement of a geosynthetic-reinforced segmental soil retaining wall due to the sliding or shear mechanisms introduced earlier can be estimated using one of two general approaches. For a given input acceleration time history Newmark's double-integration method (Newmark 1965) for a sliding block can be used to calculate the permanent displacement. However, if the input acceleration data are specified only by characteristic parameters such as the peak ground acceleration and the peak ground velocity, then empirical methods that correlate the expected permanent displacement and the characteristic parameters of the earthquake are required. Alternatively, if the tolerable permanent displacement of the structure is specified, based on serviceability criteria, the wall can then be designed using the empirical-method approach so that expected permanent displacements do not exceed specified values.

4.4.1. Newmark’s Double Integration Method

Most displacement-based methods have been formulated based on the sliding-block theory proposed by Newmark (1965). According to this theory, the potential sliding soil body is treated as a rigid-plastic monolithic mass under the action of seismic forces. Permanent displacement of the mass takes place whenever the seismic force acting on the soil mass (plus the existing static force) overcomes the available resistance along the

potential sliding surface. The corresponding acceleration that causes this seismic force is the critical acceleration of the sliding soil mass. Given an earthquake record, the accumulated permanent displacement of the sliding soil body is computed by numerically integrating twice the acceleration time history, with the critical acceleration used as the reference datum. This procedure is illustrated in Figure 4.1, where g is the gravitational constant, a(t) is the horizontal ground acceleration function with time t, $a_m = k_m g$ (where k_m is the peak horizontal acceleration coefficient) is the peak value of a(t), and $a, = kcg$ is the critical horizontal acceleration of the sliding block. For a given ground acceleration time history and a known critical acceleration of the sliding mass, the earthquake-induced displacement is calculated by integrating those portions of the acceleration history that are above the critical acceleration and those portions that are below until the relative velocity between the sliding mass and the sliding base reduces to zero.

Newmark's sliding-block theory has been widely used to establish empirical relationships between the expected permanent displacement and characteristic seismic parameters of the input earthquake by integrating existing acceleration records. The critical acceleration ratio, which is the ratio of the critical acceleration ($k_c g$) of the sliding block to the peak horizontal acceleration ($k_m g$) of the earthquake, has been shown to be an important parameter that affects the magnitude of the permanent displacement. Thus, the seismic displacement of a potential sliding soil mass computed using Newmark's theory has been traditionally correlated with the critical acceleration ratio (k_c/k_m) and other representative characteristic seismic parameters such as the peak ground acceleration ($k_m g$), the peak ground velocity v_m, and the predominant period (T) of the acceleration spectrum (e.g., Newmark 1965; Sarma 1975; Franklin and Chang 1977). The writers have reformulated a number of existing displacement methods based on nondimensionalized displacement terms that are common to the methods and divided them into two separate categories based on the characteristic seismic parameters referenced in each method (Cai and Bathurst 1996). The first category of methods uses the peak ground acceleration ($k_m g$) and peak ground velocity (v_m) as characteristic parameters, and the second category of methods uses the peak ground acceleration ($k_m g$) and the predominant period (T) of the ground acceleration spectrum.

For brevity, only the first category of methods is presented in Figure 2.13. These methods give correlations between the dimensionless displacement term $d/(v_m^2/k_m g)$, where d is the actual expected permanent displacement, and the critical acceleration ratio (k_c/k_m). In Figure 2.13, there are three upper bound displacement curves (a, c, e) and two mean displacement curves (b, d) that are derived based on different sources of earthquake data.

It should be pointed out, however, that since these methods have been formulated based on different earthquake data, the selection of which method to use should be based on careful evaluation of the characteristics of the earthquake record and the site conditions under consideration. It should also be noted that the values of permanent displacement given by each method are only order-of-magnitude estimates rather than accurate predictions. Engineering judgement plays an important role in the interpretation of results using the methods given in Figure 2.13.

In this study Newmark's double integration and Bathurst and Cai's mean upper bound methods are used for calculation of permanent displacement.

Some examples of the calculation of the critical acceleration coefficient (k_c) and permanent displacements according to reinforcement length, wall height, facing column, reinforcement spacing and wall inclination angle are shown in the following tables and figures.

4.5. Seismic Data

As seismic data, Sakaria Earthquake, which maximum acceleration and velocity are 0.628g and 0.277 m/sn respectively, is taken, and it's diagram is shown in Figure 4.1.

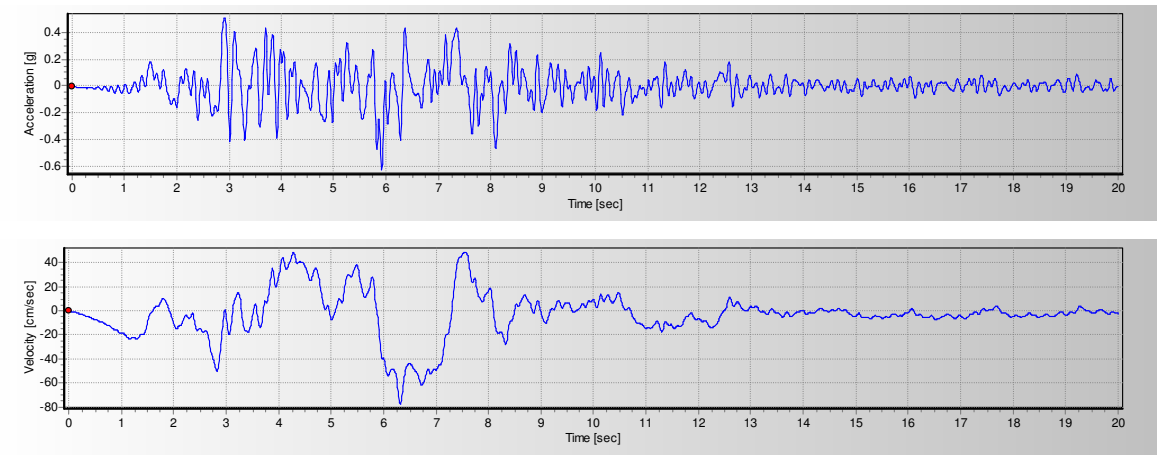

Figure 4.1. Seismic data of Sakarya Earthquake.

Table 4.2. Calculation of kc for H = 6 m, L = 4,2 m, Spacing = 0,2 m, Lw = 0,2 m, β = 3°

External Base Sliding

k_c	0,426		H	6,00
θ	23,07		L	4,20
K_A	0,255		K_{AH}	0,22
K_{AE}	0,779		K_{AEH}	0,68
ΔK_{dyn}	0,524		ΔK_{dynH}	0,46
W_w	27,60		H_h	3,80
W_i	480,00		W_i'	336,00
W_r	507,60		N_h	19
R_S	317,250		W_h	17,50
P_{IR}	154,89			
P_{AEH}	162,79			
FS_{sl}	1,00			

Internal Sliding

Layer Number	Elevation	Depth	S_{vi}	Z_{vi}	L_i	H
1	0,20	5,80	0,30	5,85	4,20	6,00
2	0,40	5,60	0,20	5,60	4,20	6,00
3	0,60	5,40	0,20	5,40	4,20	6,00
4	0,80	5,20	0,20	5,20	4,20	6,00
5	1,00	5,00	0,20	5,00	4,20	6,00
6	1,20	4,80	0,20	4,80	4,20	6,00
7	1,40	4,60	0,20	4,60	4,20	6,00
8	1,60	4,40	0,20	4,40	4,20	6,00
9	1,80	4,20	0,20	4,20	4,20	6,00
10	2,00	4,00	0,20	4,00	4,20	6,00
11	2,20	3,80	0,20	3,80	4,20	6,00
12	2,40	3,60	0,20	3,60	4,20	6,00
13	2,60	3,40	0,20	3,40	4,20	6,00
14	2,80	3,20	0,20	3,20	4,20	6,00
15	3,00	3,00	0,20	3,00	4,20	6,00
16	3,20	2,80	0,20	2,80	4,20	6,00
17	3,40	2,60	0,20	2,60	4,20	6,00
18	3,60	2,40	0,20	2,40	4,20	6,00
19	3,80	2,20	0,20	2,20	4,20	6,00
20	4,00	2,00	0,20	2,00	4,20	6,00
21	4,20	1,80	0,20	1,80	4,20	6,00
22	4,40	1,60	0,20	1,60	4,20	6,00
23	4,60	1,40	0,20	1,40	4,20	6,00
24	4,80	1,20	0,20	1,20	4,20	6,00
25	5,00	1,00	0,20	1,00	4,20	6,00
26	5,20	0,80	0,20	0,80	4,20	6,00
27	5,40	0,60	0,20	0,60	4,20	6,00
28	5,60	0,40	0,20	0,40	4,20	6,00
29	5,80	0,20	0,30	0,15	4,20	6,00

Layer Number	Elevation	Depth	ΔW_w	$\Delta W_i'$	$\Delta P_{IR}(z)$	h_{zi}	$P_{AEH}(z)$	$V_u(z)$	ΔWi	$R_S(z)$	FS_{sli}
1	0,20	5,80	26,68	324,80	156,06	5,80	151,15	16,94	464,00	306,94	1,00
2	0,40	5,60	25,76	313,60	150,68	5,60	144,88	16,94	448,00	296,94	1,00
3	0,60	5,40	24,84	302,40	146,60	5,40	140,00	16,94	432,00	286,94	1,00
4	0,80	5,20	23,92	291,20	142,43	5,20	135,18	16,94	416,00	276,94	1,00
5	1,00	5,00	23,00	280,00	137,56	5,00	129,74	16,94	400,00	266,94	1,00

Table 4.2. Calculation of kc for H = 6 m, L = 4,2 m, Spacing = 0,2 m, Lw = 0,2 m, β = 3° (Continued)

6	1,20	4,80	22,08	268,80	132,64	4,80	124,35	16,94	384,00	256,94	1,00
7	1,40	4,60	21,16	257,60	127,67	4,60	119,00	16,94	368,00	246,94	1,00
8	1,60	4,40	20,24	246,40	122,65	4,40	113,70	16,94	352,00	236,94	1,00
9	1,80	4,20	19,32	235,20	117,59	4,20	108,43	16,94	336,00	226,94	1,00
10	2,00	4,00	18,40	224,00	112,96	4,00	103,81	16,94	320,00	216,94	1,00
11	2,20	3,80	17,48	212,80	107,77	3,80	98,60	16,93	304,00	206,93	1,00
12	2,40	3,60	16,56	201,60	102,54	3,60	93,41	16,35	288,00	196,35	1,00
13	2,60	3,40	15,64	190,40	97,25	3,40	88,25	15,78	272,00	185,78	1,00
14	2,80	3,20	14,72	179,20	91,92	3,20	83,11	15,20	256,00	175,20	1,00
15	3,00	3,00	13,80	168,00	86,54	3,00	77,98	14,63	240,00	164,63	1,00
16	3,20	2,80	12,88	156,80	81,11	2,80	72,86	14,05	224,00	154,05	1,00
17	3,40	2,60	11,96	145,60	75,63	2,60	67,75	13,48	208,00	143,48	1,00
18	3,60	2,40	11,04	134,40	70,10	2,40	62,65	12,90	192,00	132,90	1,00
19	3,80	2,20	10,12	123,20	64,53	2,20	57,54	12,33	176,00	122,33	1,00
20	4,00	2,00	9,20	112,00	58,90	2,00	52,43	11,75	160,00	111,75	1,00
21	4,20	1,80	8,28	100,80	53,45	1,80	47,68	11,18	144,00	101,18	1,00
22	4,40	1,60	7,36	89,60	47,90	1,60	42,86	10,60	128,00	90,60	1,00
23	4,60	1,40	6,44	78,40	42,25	1,40	37,95	10,03	112,00	80,02	1,00
24	4,80	1,20	5,52	67,20	36,51	1,20	32,94	9,45	96,00	69,45	1,00
25	5,00	1,00	4,60	56,00	30,78	1,00	28,06	8,87	80,00	58,87	1,00
26	5,20	0,80	3,68	44,80	25,02	0,80	23,18	8,30	64,00	48,30	1,00
27	5,40	0,60	2,76	33,60	19,27	0,60	18,51	7,72	48,00	37,72	1,00
28	5,60	0,40	1,84	22,40	13,38	0,40	13,76	7,15	32,00	27,15	1,00
29	5,80	0,20	0,92	11,20	7,27	0,20	9,32	6,57	16,00	16,57	1,00

Layer Number	k_c	θ	K_A	K_{AE}	ΔK_{dyn}	K_{AH}	K_{AEH}	ΔK_{dynH}
1	0,444	23,94	0,26	0,75	0,49	0,22	0,65	0,43
2	0,444	23,94	0,26	0,75	0,49	0,22	0,65	0,43
3	0,448	24,13	0,26	0,75	0,50	0,22	0,66	0,44
4	0,452	24,32	0,26	0,76	0,51	0,22	0,67	0,44
5	0,454	24,42	0,26	0,77	0,51	0,22	0,67	0,45
6	0,456	24,51	0,26	0,77	0,52	0,22	0,68	0,45
7	0,458	24,61	0,26	0,78	0,52	0,22	0,68	0,46
8	0,460	24,70	0,26	0,78	0,53	0,22	0,68	0,46
9	0,462	24,80	0,26	0,79	0,53	0,22	0,69	0,46
10	0,466	24,99	0,26	0,80	0,54	0,22	0,70	0,47
11	0,468	25,08	0,26	0,80	0,55	0,22	0,70	0,48
12	0,470	25,17	0,26	0,81	0,55	0,22	0,70	0,48
13	0,472	25,27	0,26	0,81	0,56	0,22	0,71	0,49
14	0,474	25,36	0,26	0,82	0,56	0,22	0,71	0,49
15	0,476	25,45	0,26	0,82	0,57	0,22	0,72	0,49
16	0,478	25,55	0,26	0,83	0,57	0,22	0,72	0,50
17	0,480	25,64	0,26	0,83	0,58	0,22	0,73	0,50
18	0,482	25,73	0,26	0,84	0,58	0,22	0,73	0,51
19	0,484	25,83	0,26	0,84	0,59	0,22	0,74	0,51
20	0,486	25,92	0,26	0,85	0,59	0,22	0,74	0,52
21	0,490	26,10	0,26	0,86	0,60	0,22	0,75	0,53
22	0,494	26,29	0,26	0,87	0,61	0,22	0,76	0,54
23	0,498	26,47	0,26	0,88	0,63	0,22	0,77	0,55
24	0,502	26,66	0,26	0,89	0,64	0,22	0,78	0,56
25	0,508	26,93	0,26	0,91	0,66	0,22	0,80	0,57
26	0,516	27,29	0,26	0,94	0,68	0,22	0,82	0,60
27	0,530	27,92	0,26	0,99	0,73	0,22	0,86	0,64
28	0,552	28,90	0,26	1,07	0,82	0,22	0,94	0,72
29	0,600	30,96	0,26	1,37	1,11	0,22	1,20	0,97

Interface Shear

Layer Number	Elevation	Depth	ΔW_w	$P_{AEH}(z)$	F_i	Sum of F_i	$S_i(z)$	$V_u(z)$	FS_{sc}
1	0,20	5,80	26,68	255,99	12,93	251,30	16,86	16,94	1,00
2	0,40	5,60	25,76	247,76	8,68	242,63	16,88	16,94	1,00

Table 4.2. Calculation of kc for H = 6 m, L = 4,2 m, Spacing = 0,2 m, Lw = 0,2 m, β = 3° (Continued)

3	0,60	5,40	24,84	239,48	8,72	233,91	16,90	16,94	1,00
4	0,80	5,20	23,92	231,16	8,76	225,15	16,93	16,94	1,00
5	1,00	5,00	23,00	222,80	8,80	216,35	16,95	16,94	1,00
6	1,20	4,80	22,08	214,40	8,84	207,50	16,97	16,94	1,00
7	1,40	4,60	21,16	205,95	8,89	198,62	16,99	16,94	1,00
8	1,60	4,40	20,24	197,33	8,93	189,69	16,87	16,94	1,00
9	1,80	4,20	19,32	188,80	8,97	180,72	16,89	16,94	1,00
10	2,00	4,00	18,40	180,23	9,01	171,71	16,91	16,94	1,00
11	2,20	3,80	17,48	171,56	9,05	162,66	16,87	16,93	1,00
12	2,40	3,60	16,56	162,38	9,07	153,59	16,32	16,35	1,00
13	2,60	3,40	15,64	153,21	9,09	144,51	15,80	15,78	1,00
14	2,80	3,20	14,72	143,88	9,10	135,41	15,14	15,20	1,00
15	3,00	3,00	13,80	134,67	9,11	126,30	14,61	14,63	1,00
16	3,20	2,80	12,88	125,49	9,12	117,18	14,12	14,05	1,00
17	3,40	2,60	11,96	116,18	9,12	108,06	13,50	13,48	1,00
18	3,60	2,40	11,04	106,88	9,11	98,94	12,89	12,90	1,00
19	3,80	2,20	10,12	97,66	9,11	89,83	12,35	12,33	1,00
20	4,00	2,00	9,20	88,39	9,09	80,74	11,74	11,75	1,00
21	4,20	1,80	8,28	79,18	9,07	71,67	11,19	11,18	1,00
22	4,40	1,60	7,36	69,99	9,04	62,62	10,62	10,60	1,00
23	4,60	1,40	6,44	60,84	9,01	53,62	10,06	10,03	1,00
24	4,80	1,20	5,52	51,71	8,95	44,67	9,46	9,45	1,00
25	5,00	1,00	4,60	42,69	8,88	35,78	8,90	8,87	1,00
26	5,20	0,80	3,68	33,70	8,79	27,00	8,30	8,30	1,00
27	5,40	0,60	2,76	24,87	8,66	18,33	7,71	7,72	1,00
28	5,60	0,40	1,84	16,20	8,48	9,85	7,12	7,15	1,00
29	5,80	0,20	0,92	6,23	9,85	0,00	6,56	6,57	1,00

Layer Number	k_c	θ	K_A	K_{AE}	ΔK_{dyn}	K_{AH}	K_{AEH}	ΔK_{dynH}
1	0,456	24,53	0,26	0,77	0,52	0,24	0,73	0,49
2	0,456	24,53	0,26	0,77	0,52	0,24	0,73	0,49
3	0,456	24,53	0,26	0,77	0,52	0,24	0,73	0,49
4	0,456	24,53	0,26	0,77	0,52	0,24	0,73	0,49
5	0,456	24,53	0,26	0,77	0,52	0,24	0,73	0,49
6	0,456	24,53	0,26	0,77	0,52	0,24	0,73	0,49
7	0,456	24,53	0,26	0,77	0,52	0,24	0,73	0,49
8	0,456	24,52	0,26	0,77	0,52	0,24	0,73	0,49
9	0,456	24,52	0,26	0,77	0,52	0,24	0,73	0,49
10	0,456	24,52	0,26	0,77	0,52	0,24	0,73	0,49
11	0,456	24,51	0,26	0,77	0,52	0,24	0,73	0,49
12	0,455	24,47	0,26	0,77	0,52	0,24	0,73	0,49
13	0,454	24,43	0,26	0,77	0,51	0,24	0,73	0,49
14	0,453	24,37	0,26	0,77	0,51	0,24	0,73	0,48
15	0,452	24,32	0,26	0,76	0,51	0,24	0,72	0,48
16	0,451	24,28	0,26	0,76	0,51	0,24	0,72	0,48
17	0,450	24,21	0,26	0,76	0,50	0,24	0,72	0,48
18	0,448	24,15	0,26	0,75	0,50	0,24	0,72	0,47
19	0,447	24,08	0,26	0,75	0,50	0,24	0,71	0,47
20	0,445	24,01	0,26	0,75	0,49	0,24	0,71	0,47
21	0,444	23,93	0,26	0,74	0,49	0,24	0,71	0,47
22	0,442	23,85	0,26	0,74	0,49	0,24	0,70	0,46
23	0,440	23,75	0,26	0,74	0,48	0,24	0,70	0,46
24	0,438	23,63	0,26	0,73	0,48	0,24	0,69	0,45
25	0,435	23,51	0,26	0,73	0,47	0,24	0,69	0,45
26	0,432	23,35	0,26	0,72	0,46	0,24	0,68	0,44
27	0,428	23,15	0,26	0,71	0,46	0,24	0,67	0,43
28	0,422	22,88	0,26	0,70	0,44	0,24	0,66	0,42
29	0,362	19,90	0,26	0,60	0,34	0,24	0,57	0,32

Layer Number	Elevation	Depth	S_{vi}	Z_{vi}	ΔWwi	F_{stai}	F_{dyni}
1	0,20	5,80	0,30	5,85	1,38	8,50	3,81
2	0,40	5,60	0,20	5,60	0,92	5,42	2,83
3	0,60	5,40	0,20	5,40	0,92	5,23	3,07

Table 4.2. Calculation of kc for H = 6 m, L = 4,2 m, Spacing = 0,2 m, Lw = 0,2 m, β = 3° (Continued)

4	0,80	5,20	0,20	5,20	0,92	5,04	3,30
5	1,00	5,00	0,20	5,00	0,92	4,84	3,54
6	1,20	4,80	0,20	4,80	0,92	4,65	3,78
7	1,40	4,60	0,20	4,60	0,92	4,45	4,01
8	1,60	4,40	0,20	4,40	0,92	4,26	4,24
9	1,80	4,20	0,20	4,20	0,92	4,07	4,48
10	2,00	4,00	0,20	4,00	0,92	3,87	4,72
11	2,20	3,80	0,20	3,80	0,92	3,68	4,95
12	2,40	3,60	0,20	3,60	0,92	3,49	5,17
13	2,60	3,40	0,20	3,40	0,92	3,29	5,38
14	2,80	3,20	0,20	3,20	0,92	3,10	5,58
15	3,00	3,00	0,20	3,00	0,92	2,91	5,79
16	3,20	2,80	0,20	2,80	0,92	2,71	5,99
17	3,40	2,60	0,20	2,60	0,92	2,52	6,19
18	3,60	2,40	0,20	2,40	0,92	2,32	6,38
19	3,80	2,20	0,20	2,20	0,92	2,13	6,57
20	4,00	2,00	0,20	2,00	0,92	1,94	6,75
21	4,20	1,80	0,20	1,80	0,92	1,74	6,92
22	4,40	1,60	0,20	1,60	0,92	1,55	7,09
23	4,60	1,40	0,20	1,40	0,92	1,36	7,25
24	4,80	1,20	0,20	1,20	0,92	1,16	7,39
25	5,00	1,00	0,20	1,00	0,92	0,97	7,52
26	5,20	0,80	0,20	0,80	0,92	0,77	7,62
27	5,40	0,60	0,20	0,60	0,92	0,58	7,69
28	5,60	0,40	0,20	0,40	0,92	0,39	7,70
29	5,80	0,20	0,30	0,15	1,38	0,22	9,14

Table 4.3. Calculation of Displacement for H = 6 m, L = 4,2 m, Spacing = 0,2 m, Lw = 0,2 m, β = 3°

External Base Sliding

	k_c	k_m	k_c/k_m	v_m (cm/sn)	d (Newmark) (cm)	d (Bathurst and Cai) (cm)
	0,426	0,63	0,68	27,70	0,44	0,47

Internal Sliding

Layer	k_c	k_m	k_c/k_m	v_m (cm/sn)	d (Newmark) (cm)	d (Bathurst and Cai) (cm)
1	0,444	0,63	0,71	27,70	0,37	0,38
2	0,444	0,63	0,71	27,70	0,37	0,38
3	0,448	0,63	0,71	27,70	0,35	0,36
4	0,452	0,63	0,72	27,70	0,34	0,34
5	0,454	0,63	0,72	27,70	0,33	0,33
6	0,456	0,63	0,73	27,70	0,32	0,33
7	0,458	0,63	0,73	27,70	0,32	0,32
8	0,460	0,63	0,73	27,70	0,31	0,31
9	0,462	0,63	0,74	27,70	0,30	0,30
10	0,466	0,63	0,74	27,70	0,29	0,29
11	0,468	0,63	0,75	27,70	0,29	0,28
12	0,470	0,63	0,75	27,70	0,28	0,28
13	0,472	0,63	0,75	27,70	0,27	0,27
14	0,474	0,63	0,75	27,70	0,27	0,26
15	0,476	0,63	0,76	27,70	0,26	0,26
16	0,478	0,63	0,76	27,70	0,26	0,25
17	0,480	0,63	0,76	27,70	0,25	0,25
18	0,482	0,63	0,77	27,70	0,25	0,24
19	0,484	0,63	0,77	27,70	0,24	0,23
20	0,486	0,63	0,77	27,70	0,24	0,23
21	0,490	0,63	0,78	27,70	0,22	0,22
22	0,494	0,63	0,79	27,70	0,21	0,21
23	0,498	0,63	0,79	27,70	0,20	0,20
24	0,502	0,63	0,80	27,70	0,20	0,19
25	0,508	0,63	0,81	27,70	0,18	0,18
26	0,516	0,63	0,82	27,70	0,16	0,16
27	0,530	0,63	0,84	27,70	0,14	0,14
28	0,552	0,63	0,88	27,70	0,10	0,11
29	0,600	0,63	0,96	27,70	0,03	0,06

Interface Shear

Layer	k_c	k_m	k_c/k_m	v_m (cm/sn)	d (Newmark) (cm)	d (Bathurst and Cai) (cm)
1	0,456	0,63	0,73	27,70	0,32	0,32
2	0,456	0,63	0,73	27,70	0,32	0,32
3	0,456	0,63	0,73	27,70	0,32	0,32

Table 4.3. Calculation of Displacement for H = 6 m, L = 4,2 m, Spacing = 0,2 m, Lw = 0,2 m, β = 3° (Continued)

4	0,456	0,63	0,73	27,70	0,32	0,32
5	0,456	0,63	0,73	27,70	0,32	0,32
6	0,456	0,63	0,73	27,70	0,32	0,32
7	0,456	0,63	0,73	27,70	0,32	0,32
8	0,456	0,63	0,73	27,70	0,32	0,33
9	0,456	0,63	0,73	27,70	0,32	0,33
10	0,456	0,63	0,73	27,70	0,32	0,33
11	0,456	0,63	0,73	27,70	0,32	0,33
12	0,455	0,63	0,72	27,70	0,33	0,33
13	0,454	0,63	0,72	27,70	0,33	0,33
14	0,453	0,63	0,72	27,70	0,33	0,34
15	0,452	0,63	0,72	27,70	0,34	0,34
16	0,451	0,63	0,72	27,70	0,34	0,35
17	0,450	0,63	0,72	27,70	0,34	0,35
18	0,448	0,63	0,71	27,70	0,35	0,36
19	0,447	0,63	0,71	27,70	0,35	0,36
20	0,445	0,63	0,71	27,70	0,36	0,37
21	0,444	0,63	0,71	27,70	0,37	0,38
22	0,442	0,63	0,70	27,70	0,37	0,38
23	0,440	0,63	0,70	27,70	0,38	0,39
24	0,438	0,63	0,70	27,70	0,39	0,41
25	0,435	0,63	0,69	27,70	0,40	0,42
26	0,432	0,63	0,69	27,70	0,41	0,44
27	0,428	0,63	0,68	27,70	0,43	0,46
28	0,422	0,63	0,67	27,70	0,45	0,49
29	0,362	0,63	0,58	27,70	0,79	1,00

Total	d (Newmark) (cm)	d (Bathurst and Cai) (cm)
Base Sliding	0,44	0,47
1	0,80	0,84
2	1,17	1,22
3	1,52	1,58
4	1,85	1,92
5	2,18	2,25
6	2,51	2,58
7	2,83	2,90
8	3,15	3,23
9	3,48	3,55
10	3,80	3,88
11	4,12	4,20
12	4,45	4,53
13	4,78	4,87
14	5,11	5,20
15	5,45	5,55

Table 4.3. Calculation of Displacement for H = 6 m, L = 4,2 m, Spacing = 0,2 m, Lw = 0,2 m, β = 3° (Continued)

16	5,79	5,89
17	6,13	6,24
18	6,48	6,60
19	6,84	6,96
20	7,20	7,33
21	7,56	7,71
22	7,94	8,09
23	8,32	8,49
24	8,70	8,89
25	9,10	9,31
26	9,52	9,75
27	9,94	10,20
28	10,40	10,69
29	11,19	11,69

Table 4.4. Distribution of Displacements by Percentage

	Newmark	Bathurst
Base Sliding	4%	4%
Internal Sliding	19%	18%
Interface Shear	77%	78%

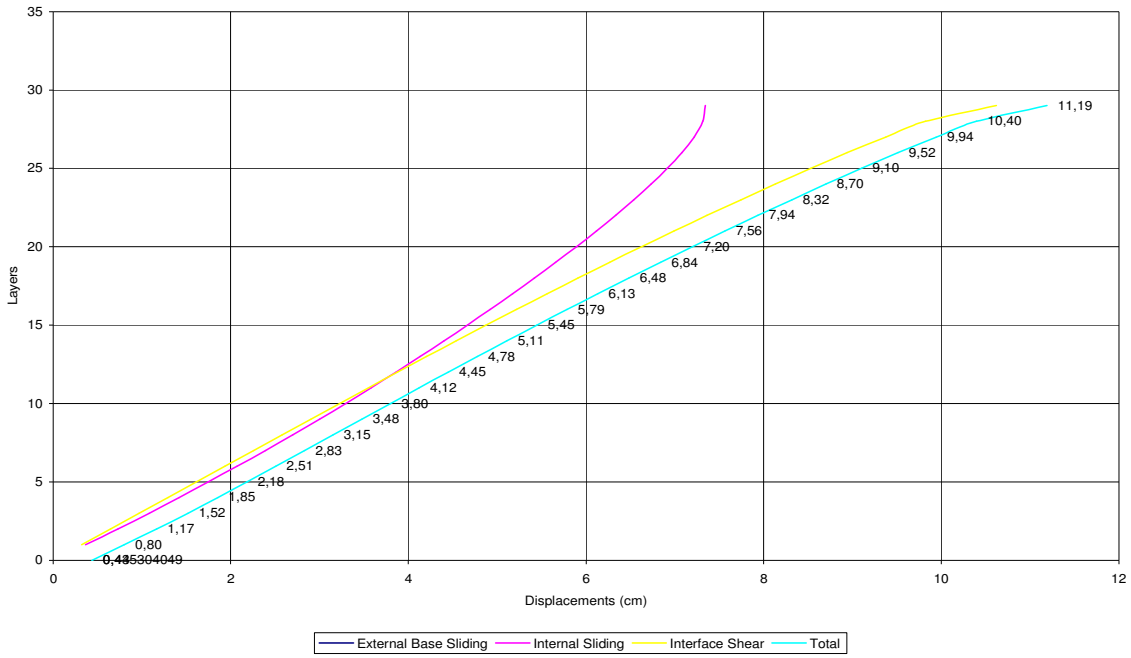

Figure 4.2. Displacement Distribution of H = 6 m, L = 4,2 m, Spacing = 0,2 m, Lw = 0,2 m, β = 3° Newmark

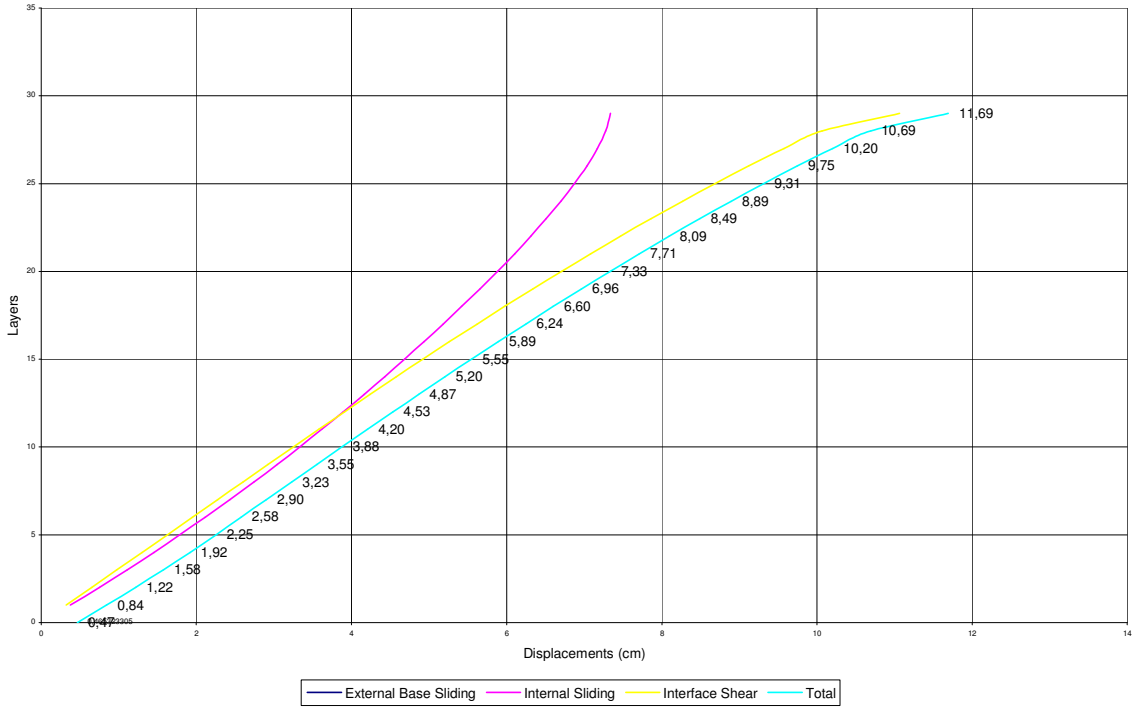

Figure 4.3. Displacement Distribution of H = 6 m, L = 4,2 m, Spacing = 0,2 m, Lw = 0,2 m, β = 3° Bathurst

5. RESULTS

The comparisons of the methods used, reinforcement length, reinforcement spacing, inclination angle, and block widths are shown in the following figures.

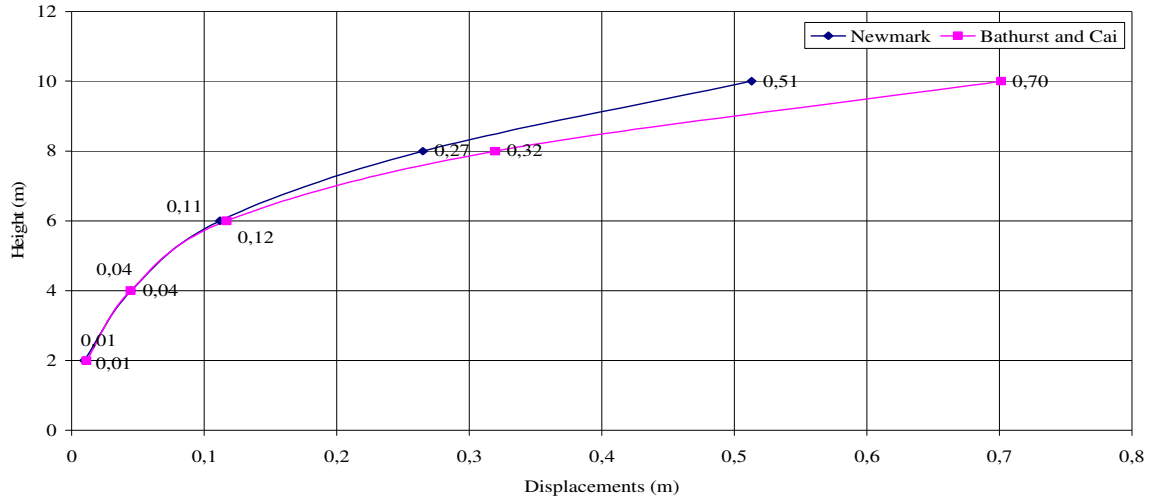

Figure 5.1. Total Displacement Change According to Newmark and Bathurst, L/H= 0,7, Spacing = 0,2, Lw = 0,2 m, β = 3°

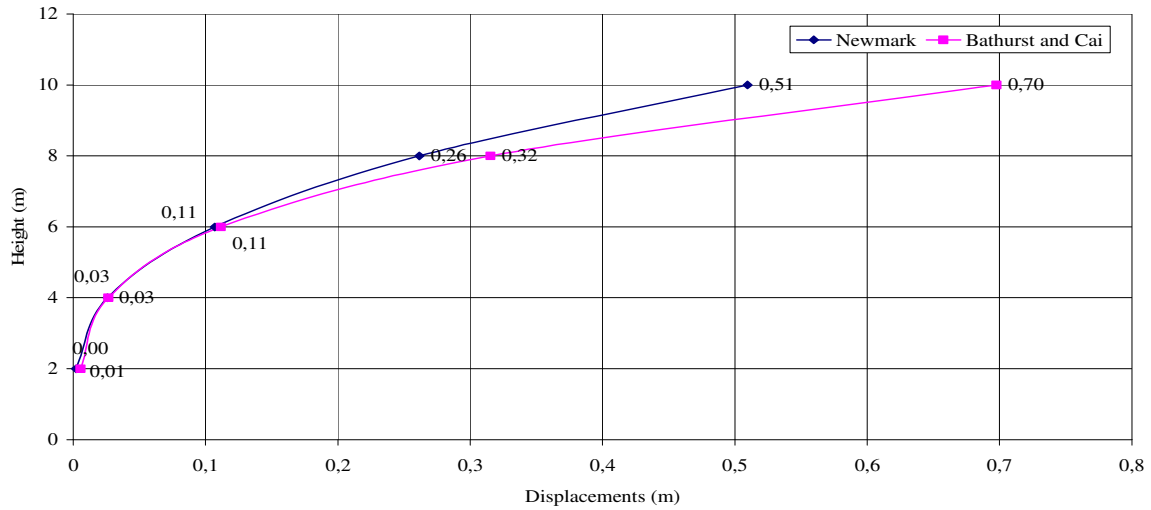

Figure 5.2. Total Displacement Change According to Newmark and Bathurst, L/H= 1,0, Spacing = 0,2, Lw = 0,2 m, β = 3°

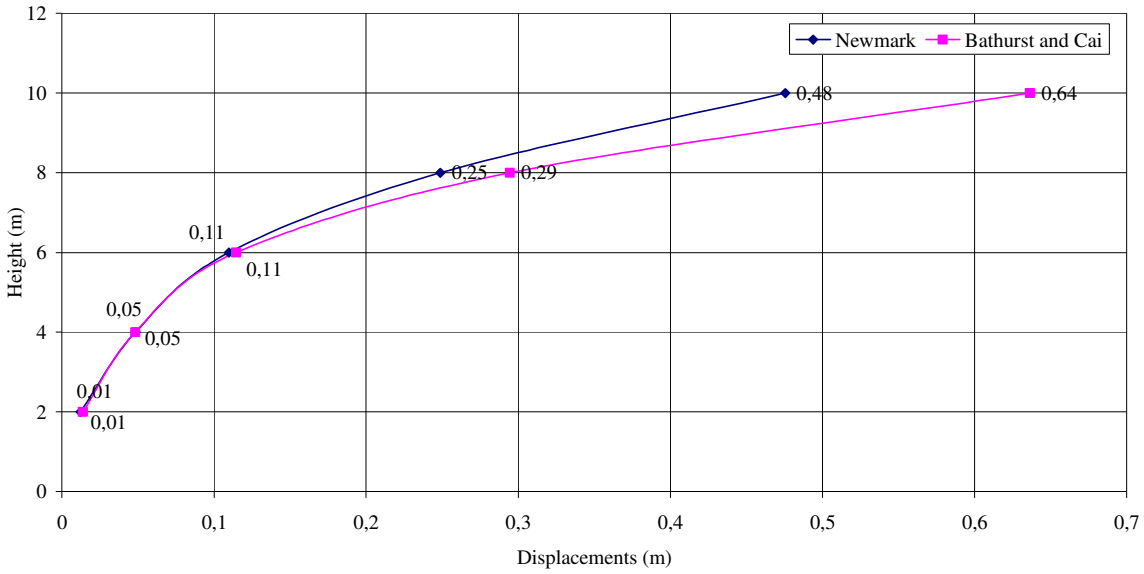

Figure 5.3. Total Displacement Change According to Newmark and Bathurst, L/H= 0,7, Spacing = 0,2, Lw = 0,2 m, β = 0°

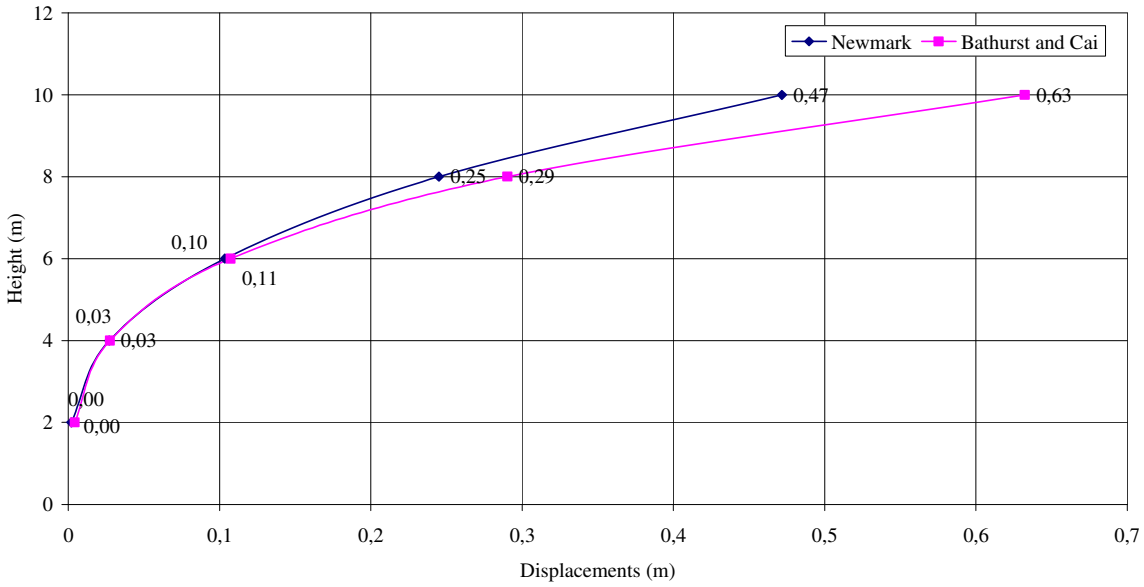

Figure 5.4. Total Displacement Change According to Newmark and Bathurst, L/H= 1,0, Spacing = 0,2, Lw = 0,2 m, β = 0°

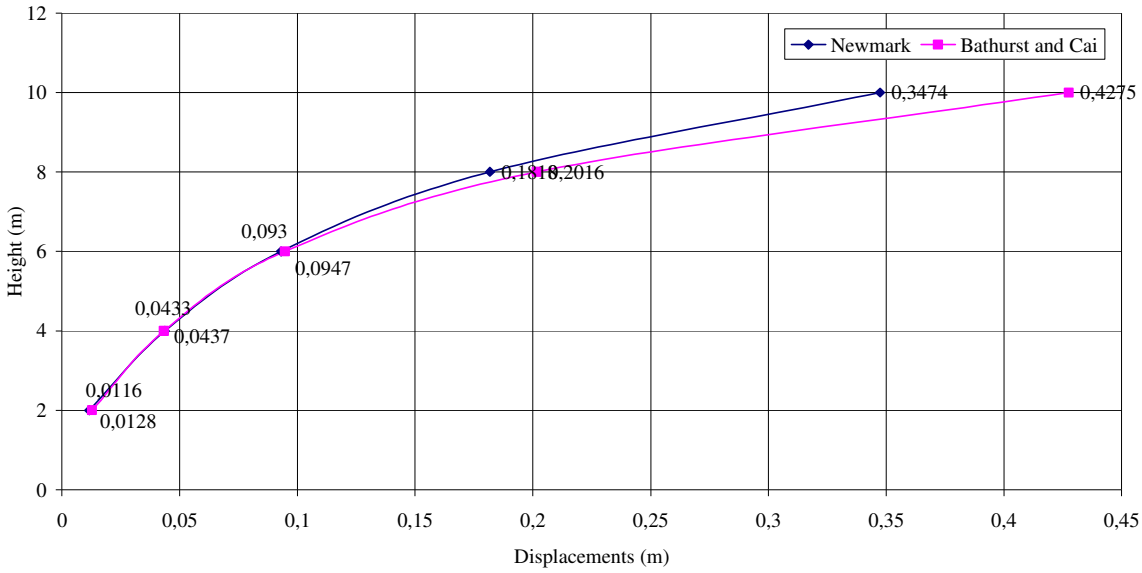

Figure 5.5. Total Displacement Change According to Newmark and Bathurst, L/H= 0,7, Spacing = 0,2, Lw = 0,4 m, β = 3°

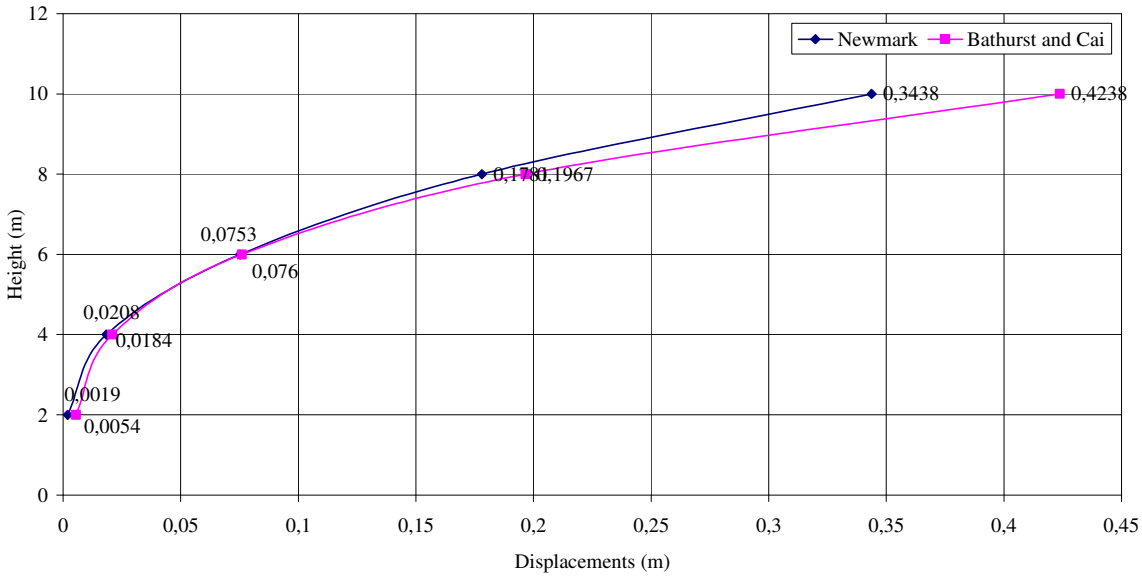

Figure 5.6. Total Displacement Change According to Newmark and Bathurst, L/H= 1,0, Spacing = 0,2, Lw = 0,4 m, β = 3°

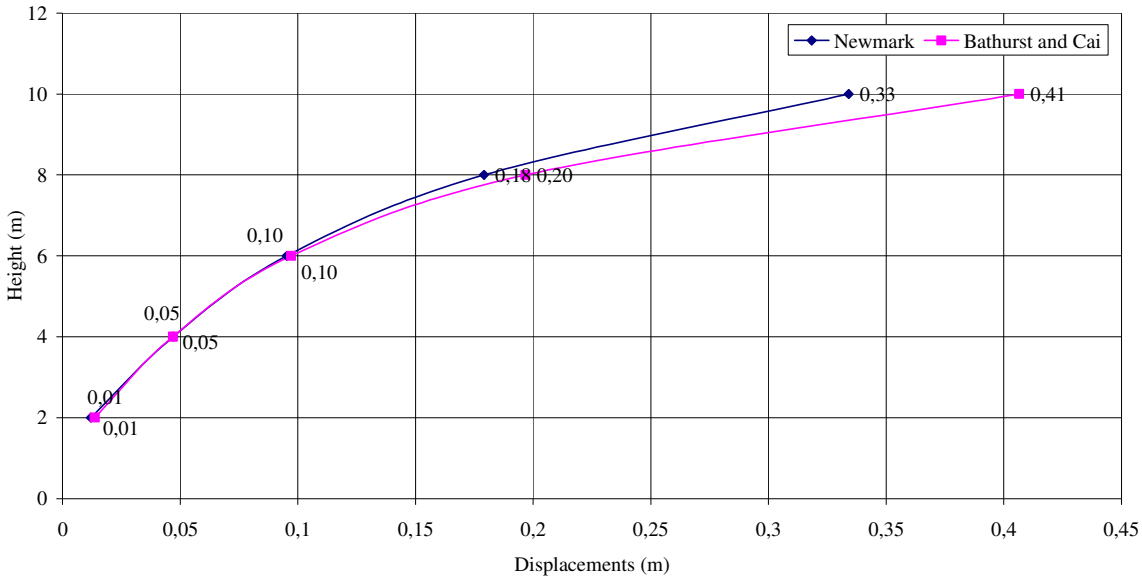

Figure 5.7. Total Displacement Change According to Newmark and Bathurst,L/H= 0,7, Spacing = 0,2, Lw = 0,4 m, β = 0°

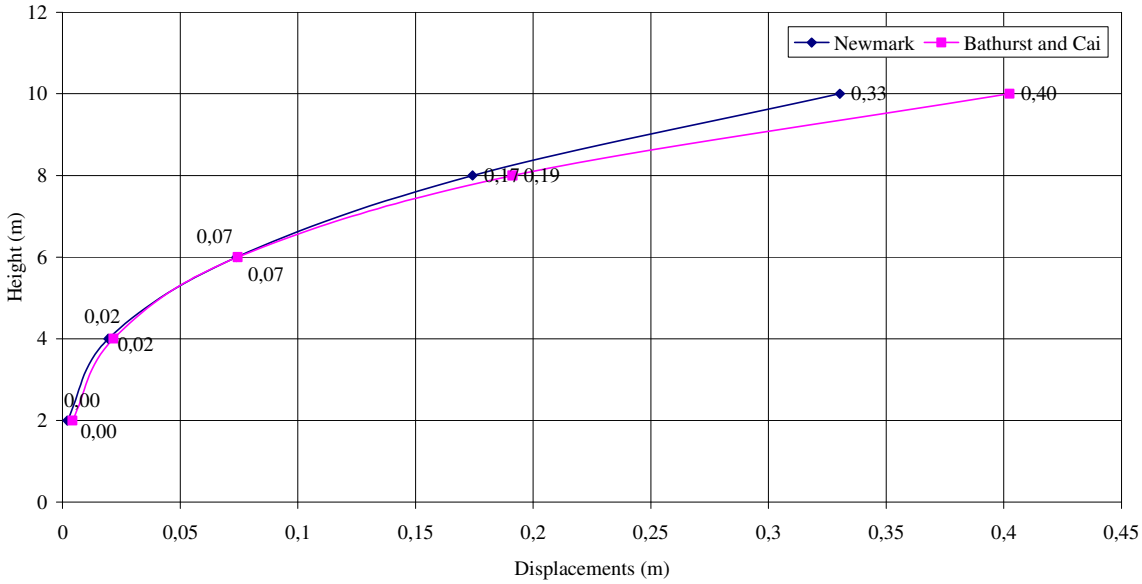

Figure 5.8. Total Displacement Change According to Newmark and Bathurst, L/H= 1,0, Spacing = 0,2, Lw = 0,4 m, β = 0°

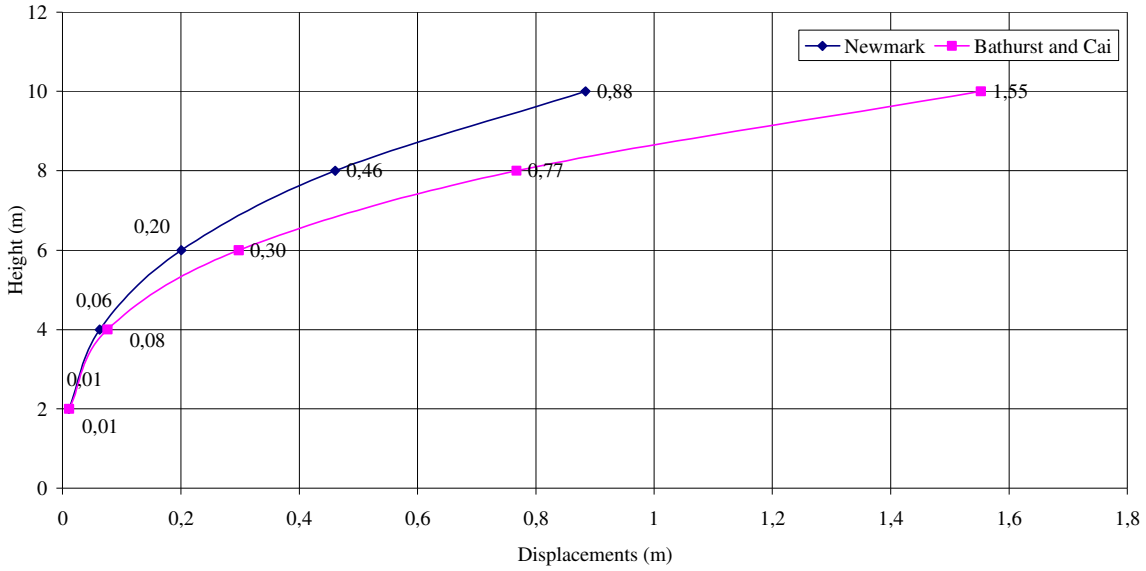

Figure 5.9. Total Displacement Change According to Newmark and Bathurst, L/H= 0,7, Spacing = 0,4, Lw = 0,2 m, β = 3°

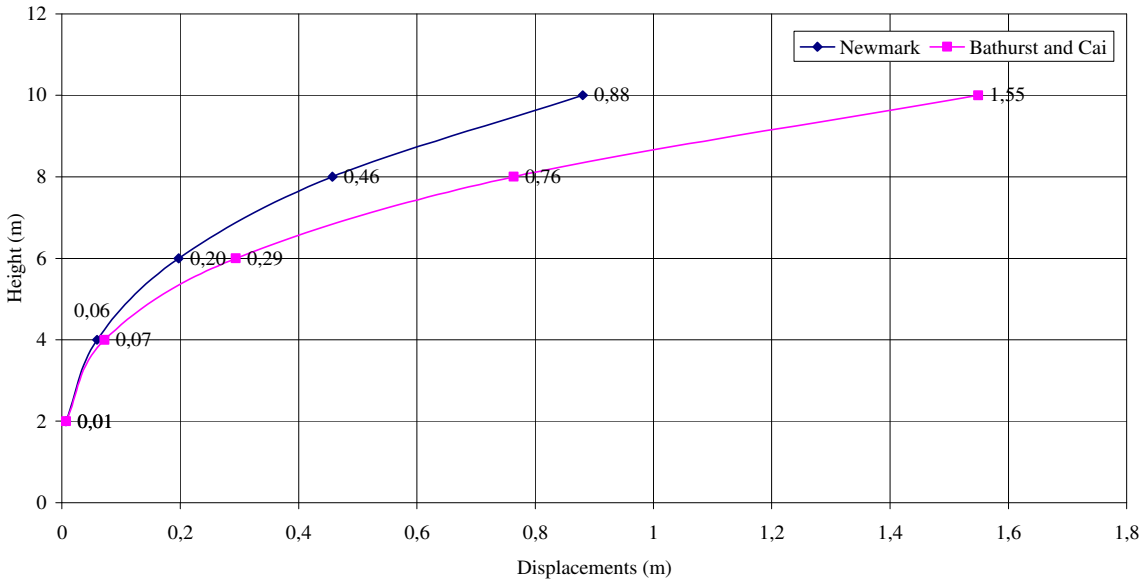

Figure 5.10. Total Displacement Change According to Newmark and Bathurst, L/H= 1,0, Spacing = 0,4, Lw = 0,2 m, β = 3°

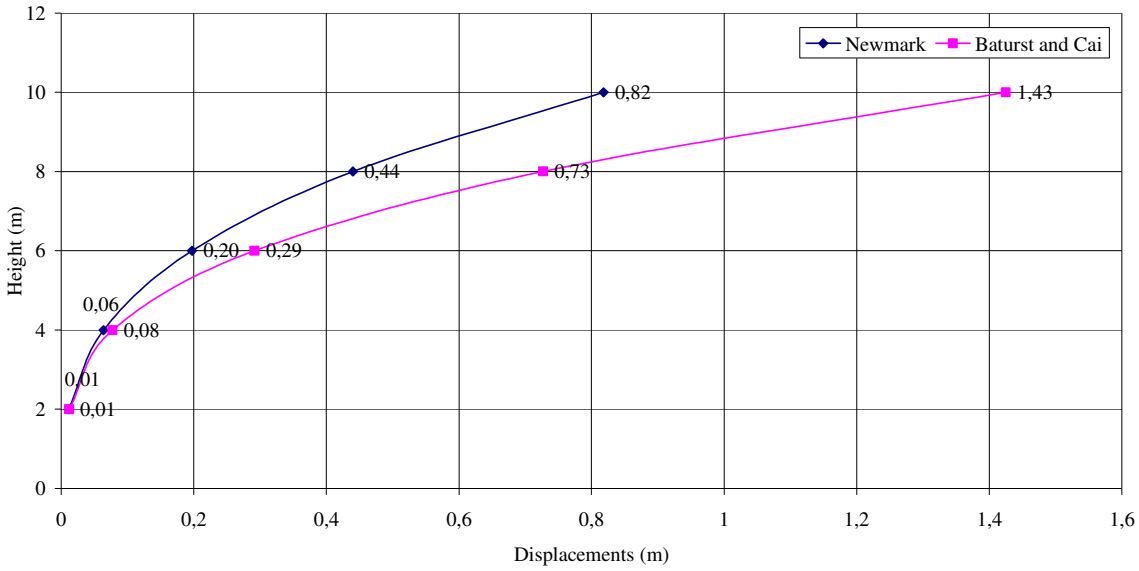

Figure 5.11. Total Displacement Change According to Newmark and Bathurst, L/H= 0,7, Spacing = 0,4, Lw = 0,2 m, β = 0°

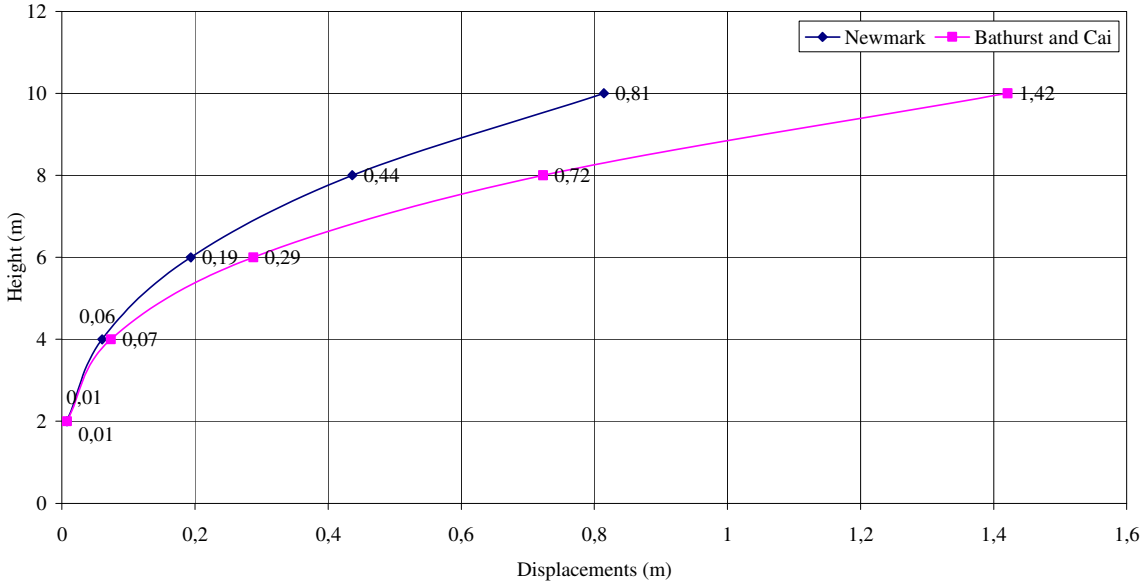

Figure 5.12. Total Displacement Change According to Newmark and Bathurst, L/H= 1,0, Spacing = 0,4, Lw = 0,2 m, β = 0°

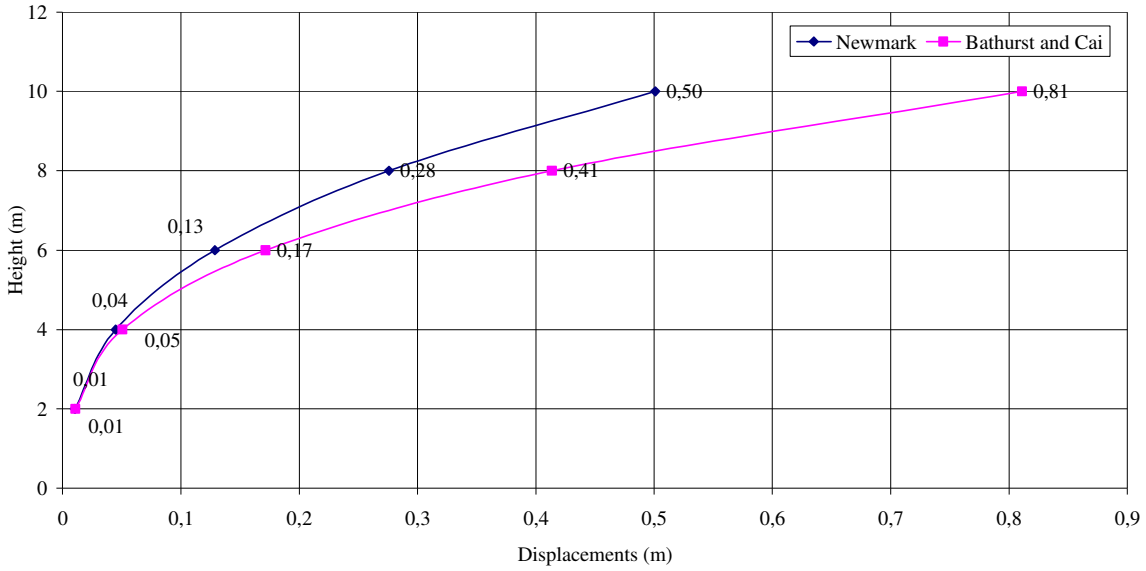

Figure 5.13. Total Displacement Change According to Newmark and Bathurst, L/H= 0,7, Spacing = 0,4, Lw = 0,4 m, β = 3°

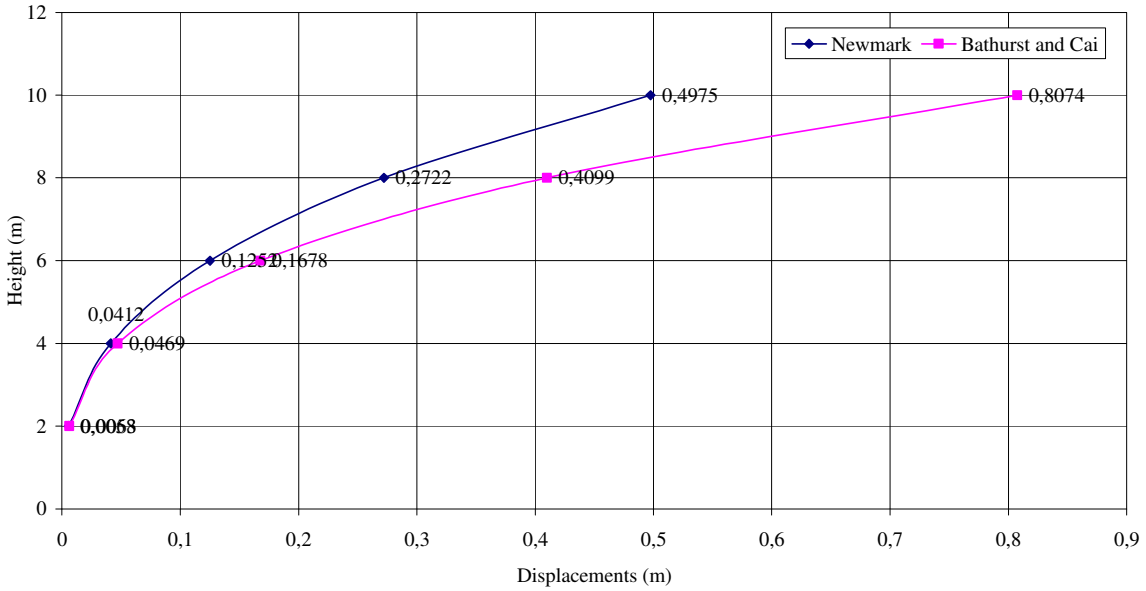

Figure 5.14. Total Displacement Change According to Newmark and Bathurst, L/H= 1,0, Spacing = 0,4, Lw = 0,4 m, β = 3°

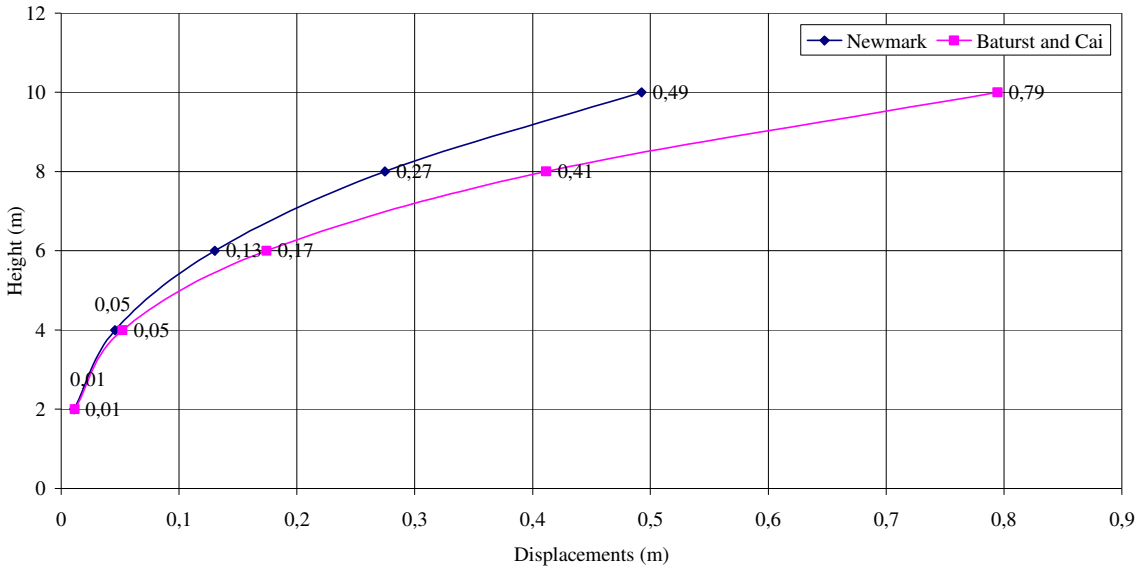

Figure 5.15. Total Displacement Change According to Newmark and Bathurst, L/H= 0,7, Spacing = 0,4, Lw = 0,4 m, β = 0°

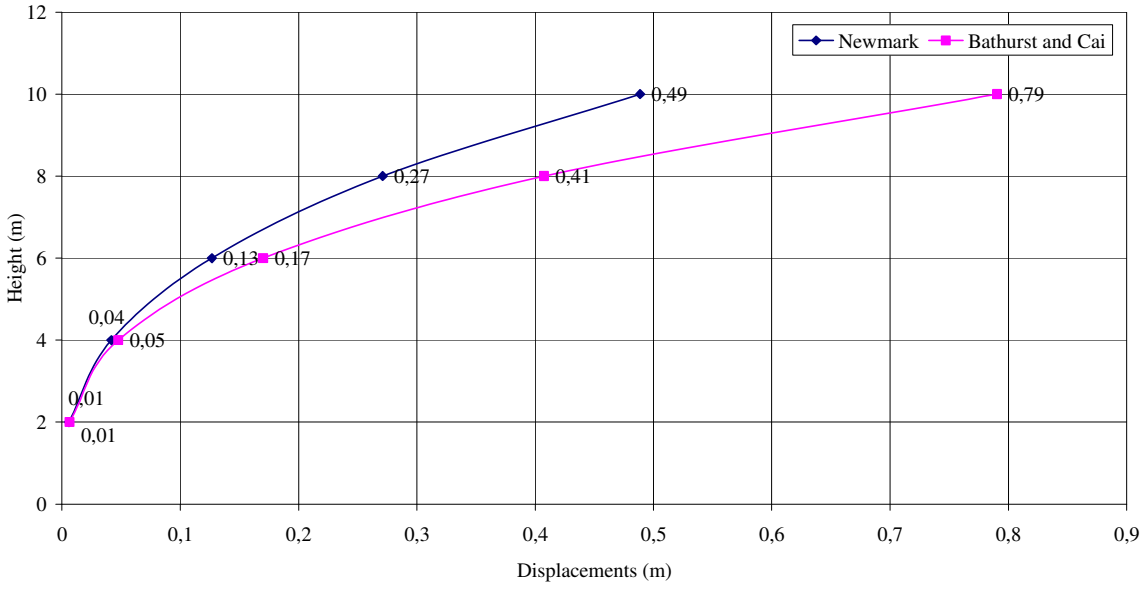

Figure 5.16. Total Displacement Change According to Newmark and Bathurst, L/H= 1,0, Spacing = 0,4, Lw = 0,4 m, β = 0°

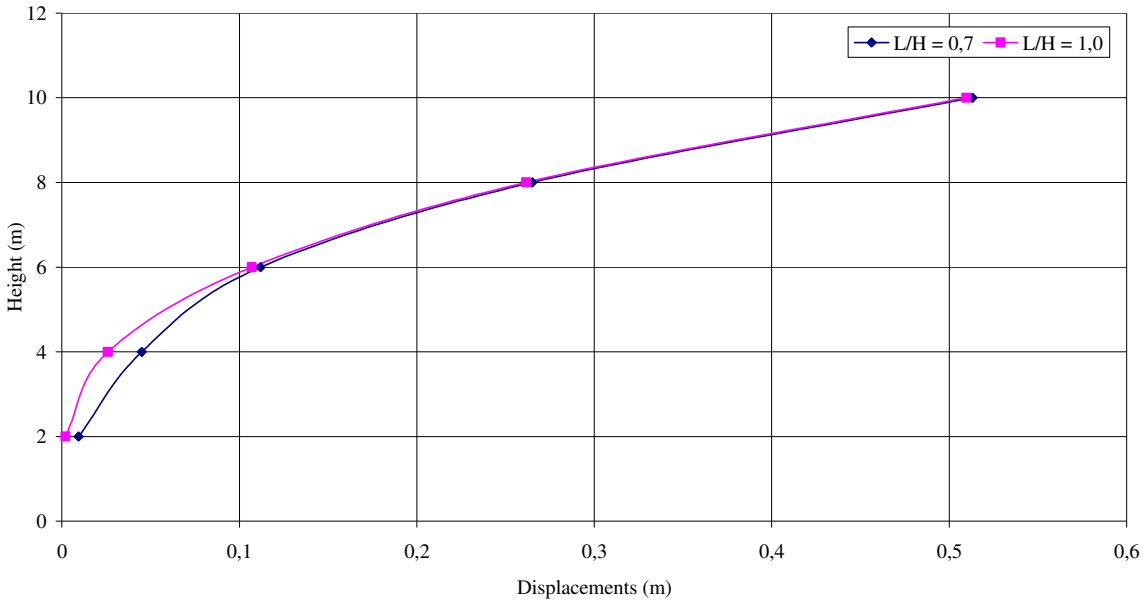

Figure 5.17. Total Displacement Change According to L/H, Spacing = 0,2, Lw = 0,2 m, β = 3° Newmark

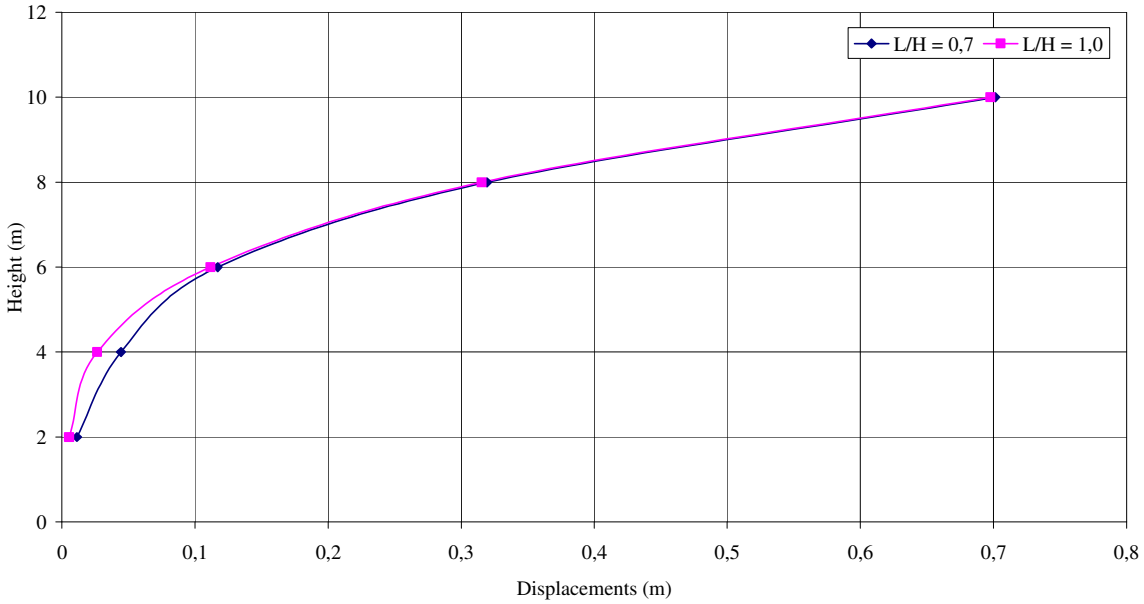

Figure 5.18. Total Displacement Change According to L/H, Spacing = 0,2, Lw = 0,2 m, β = 3° Bathurst

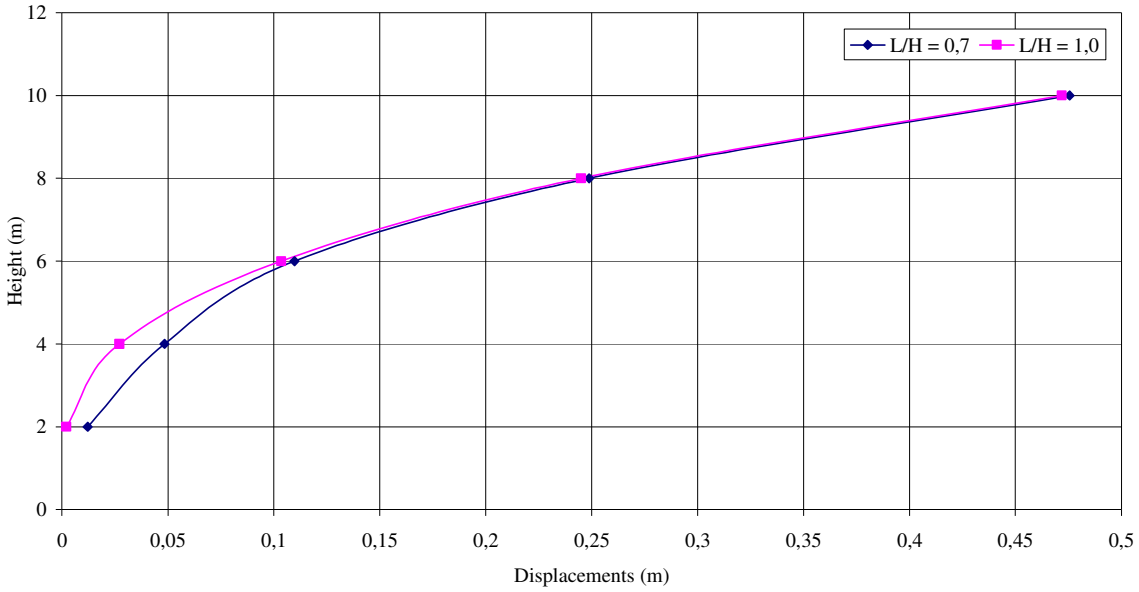

Figure 5.19. Total Displacement Change According to L/H, Spacing = 0,2, Lw = 0,2 m, β = 0° Newmark

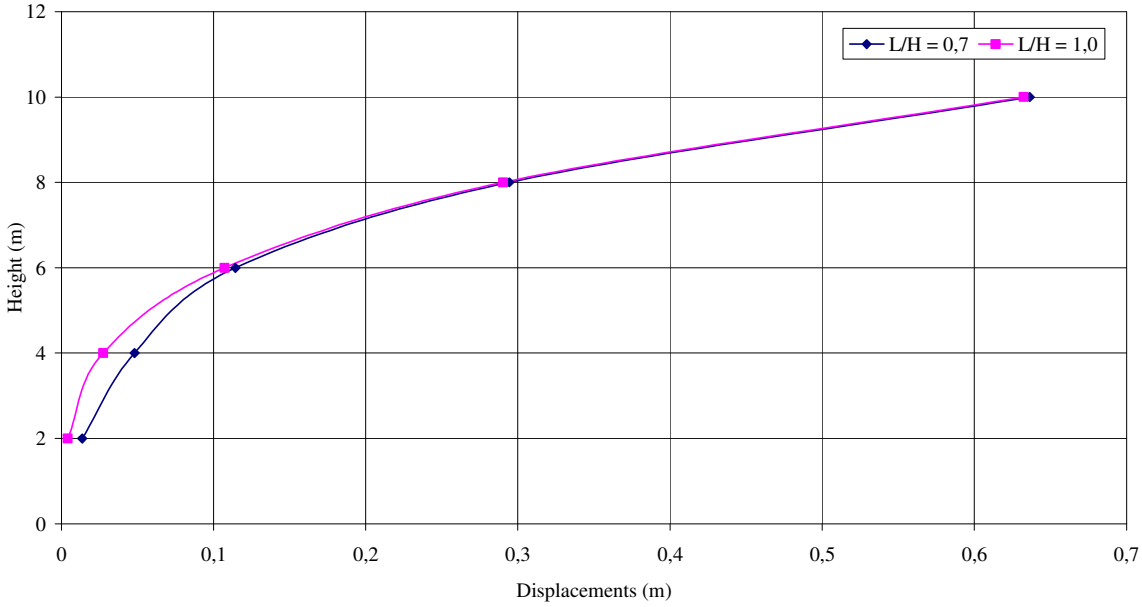

Figure 5.20. Total Displacement Change According to L/H, Spacing = 0,2, Lw = 0,2 m, β = 0° Bathurst

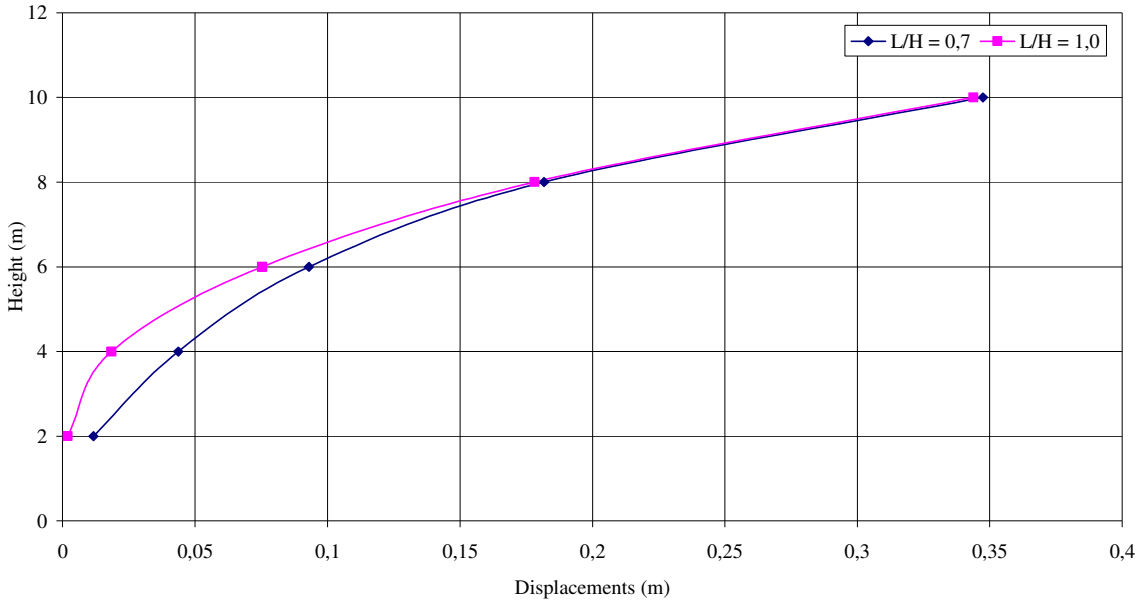

Figure 5.21. Total Displacement Change According to L/H, Spacing = 0,2, Lw = 0,4 m, β = 3° Newmark

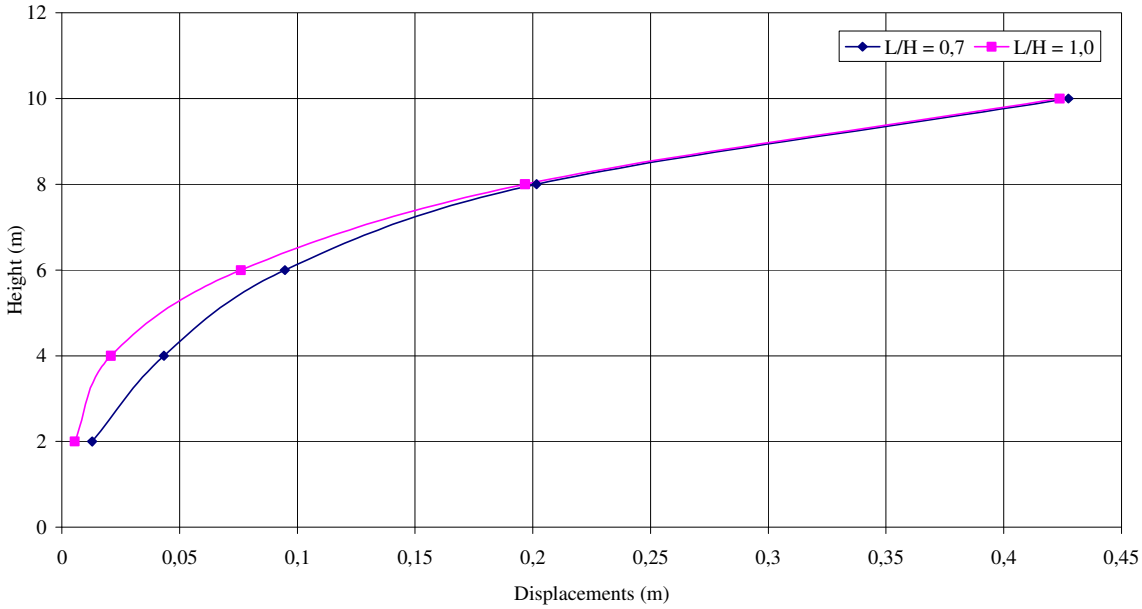

Figure 5.22. Total Displacement Change According to L/H, Spacing = 0,2, Lw = 0,4 m, β = 3° Bathurst

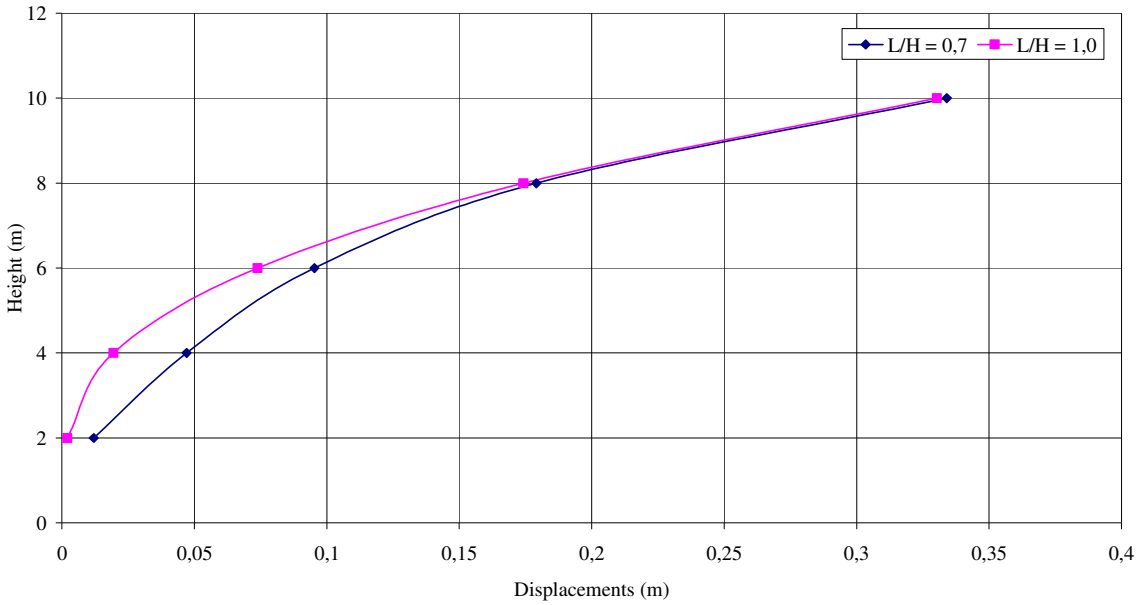

Figure 5.23. Total Displacement Change According to L/H, Spacing = 0,2, Lw = 0,4 m, β = 0° Newmark

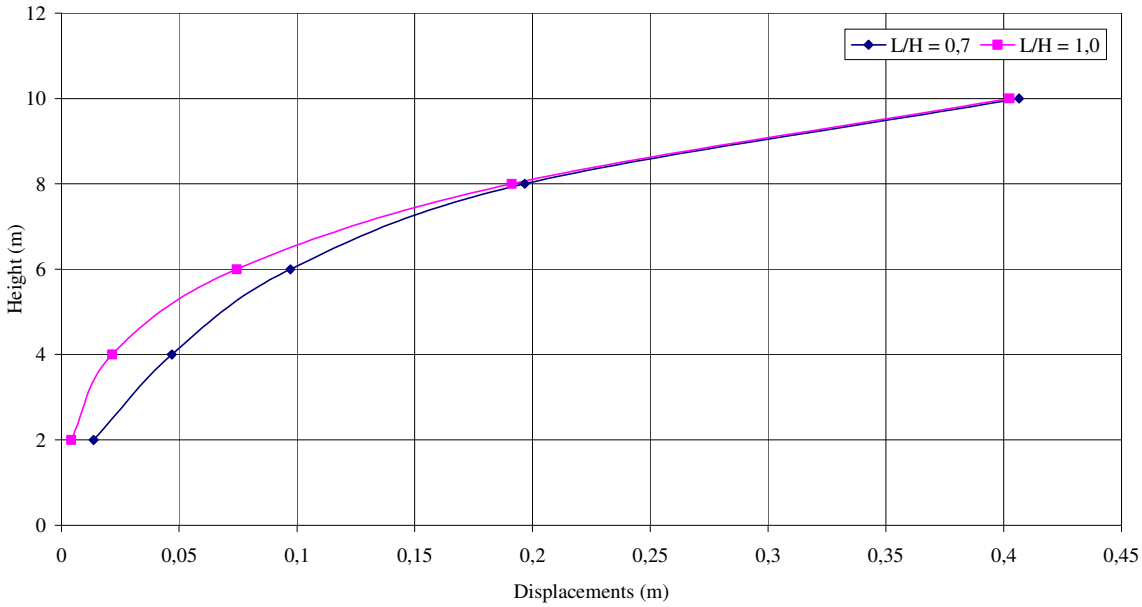

Figure 5.24. Total Displacement Change According to L/H, Spacing = 0,2, Lw = 0,4 m, β = 0° Bathurst

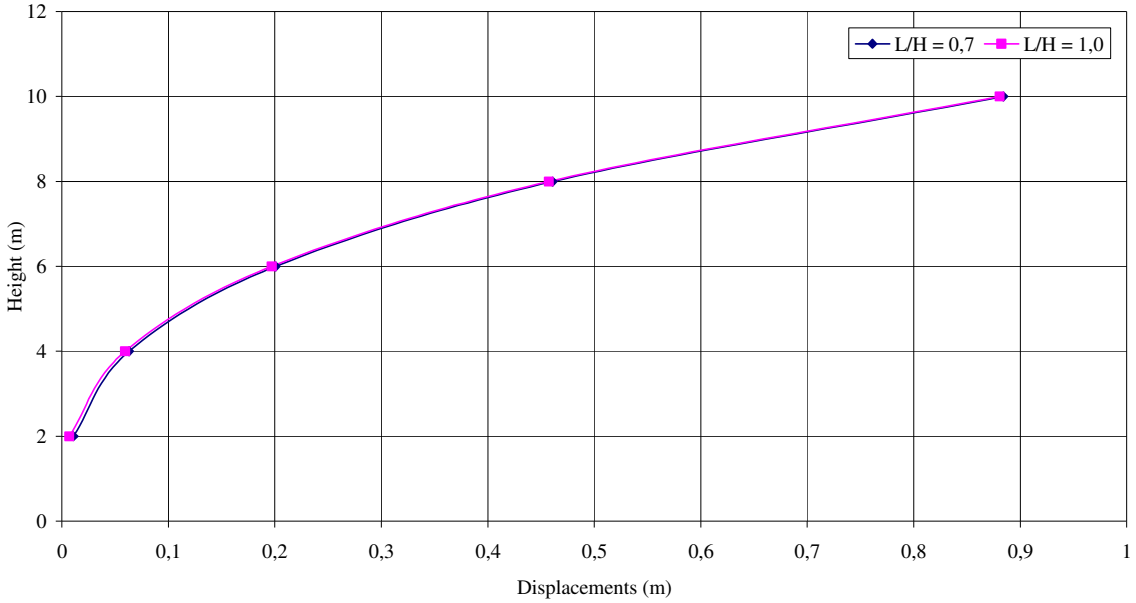

Figure 5.25. Total Displacement Change According to L/H, Spacing = 0,4, Lw = 0,2 m, β = 3° Newmark

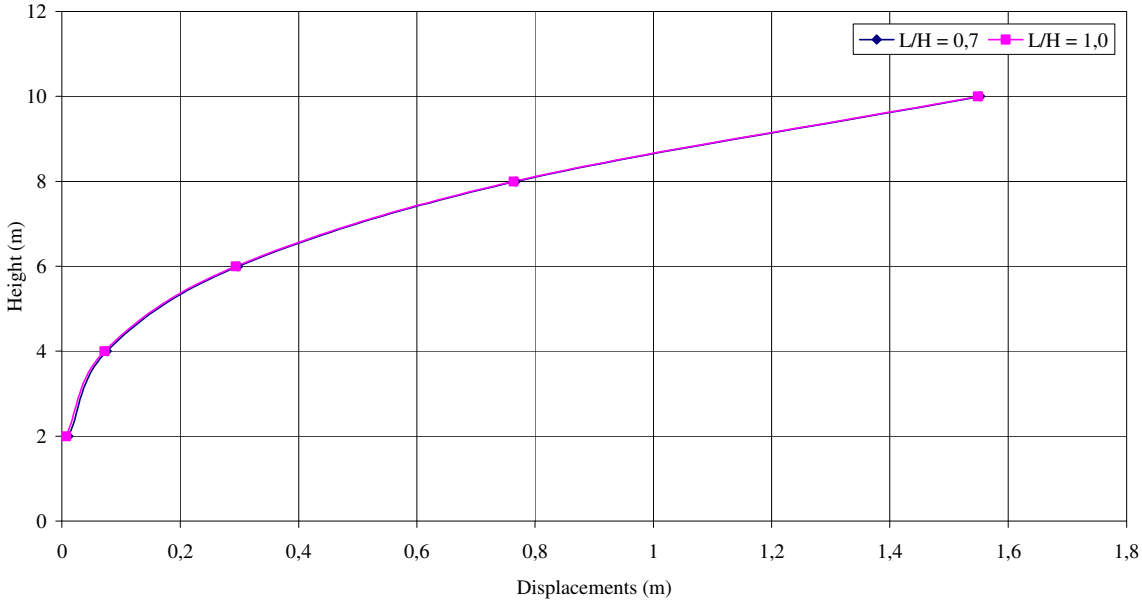

Figure 5.26. Total Displacement Change According to L/H, Spacing = 0,4, Lw = 0,2 m, β = 3° Bathurst

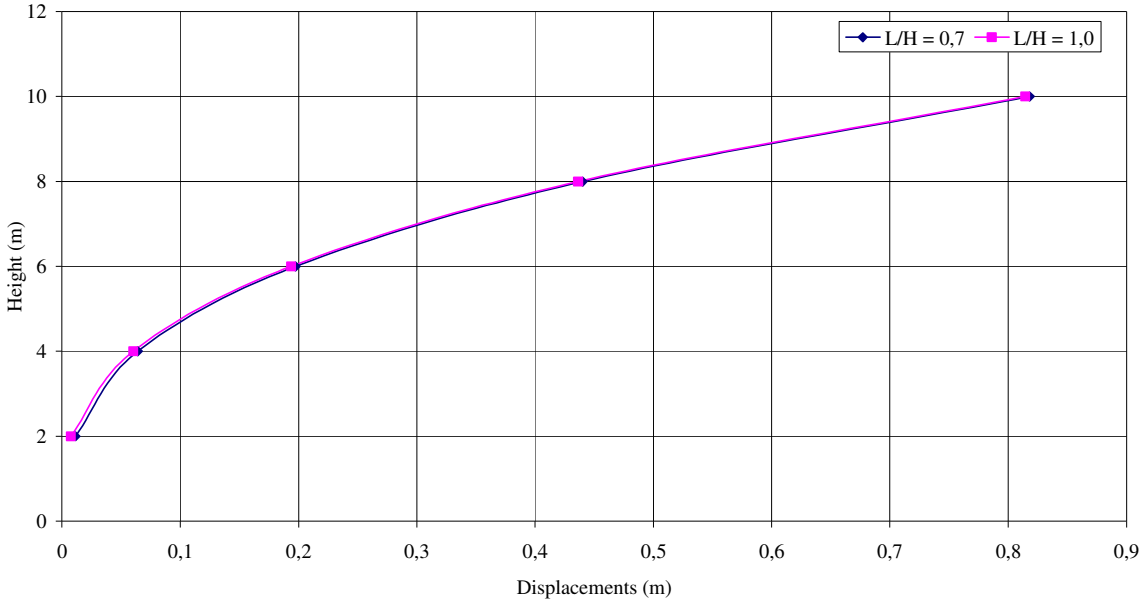

Figure 5.27. Total Displacement Change According to L/H, Spacing = 0,4, Lw = 0,2 m, β = 0° Newmark

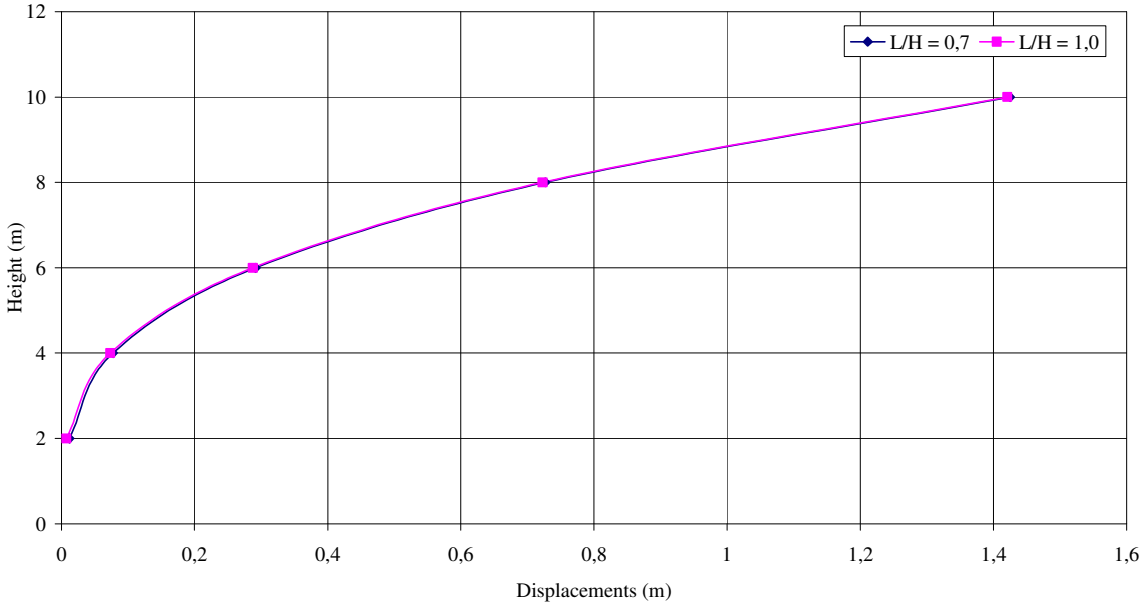

Figure 5.28. Total Displacement Change According to L/H, Spacing = 0,4, Lw = 0,2 m, β = 0° Bathurst

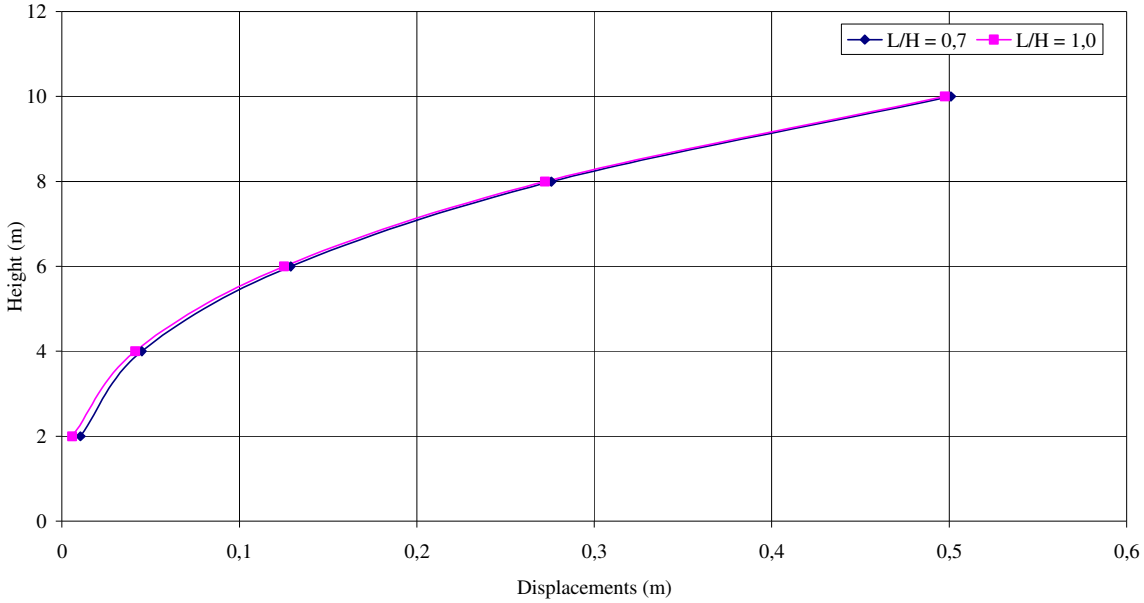

Figure 5.29. Total Displacement Change According to L/H, Spacing = 0,4, Lw = 0,4 m, β = 3° Newmark

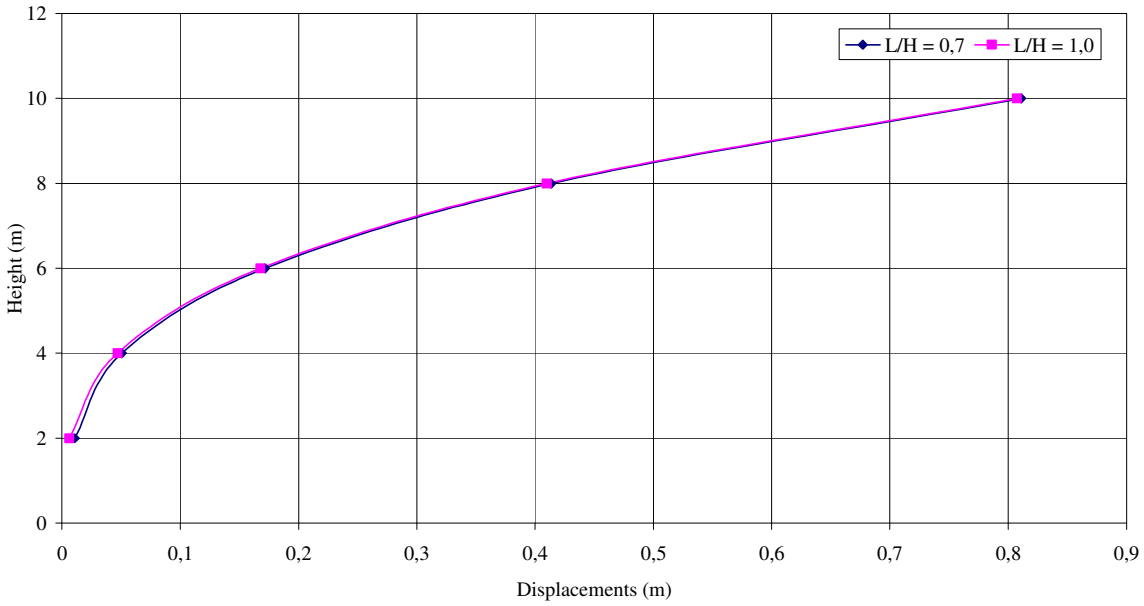

Figure 5.30. Total Displacement Change According to L/H, Spacing = 0,4, Lw = 0,4 m, β = 3° Bathurst

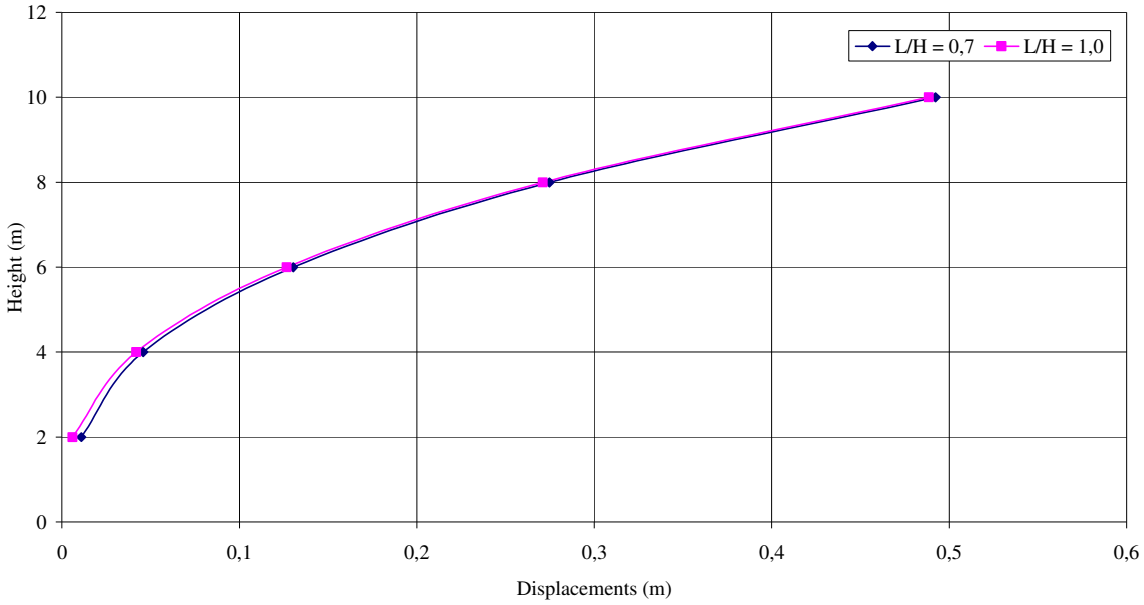

Figure 5.31. Total Displacement Change According to L/H, Spacing = 0,4, Lw = 0,4 m, β = 0° Newmark

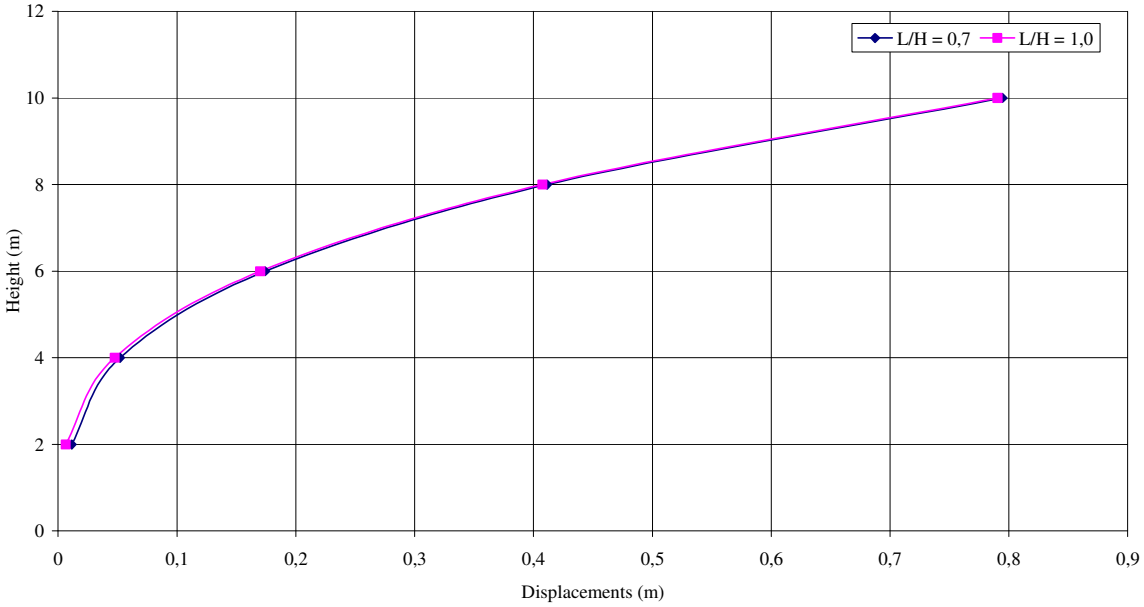

Figure 5.32. Total Displacement Change According to L/H, Spacing = 0,4, Lw = 0,4 m, β = 0° Bathurst

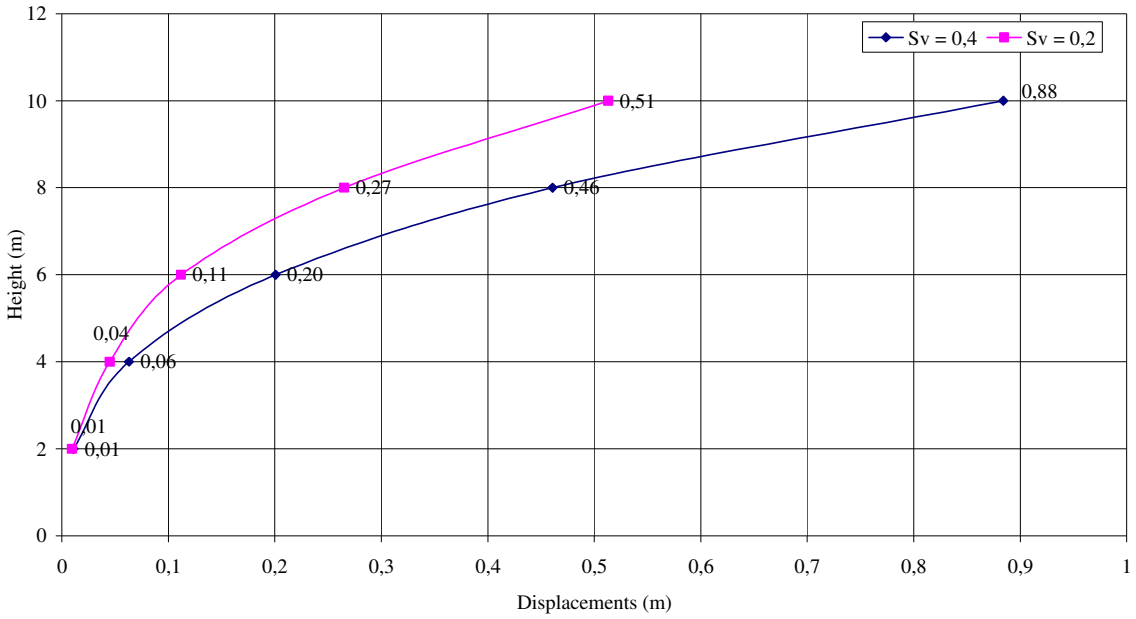

Figure 5.33. Total Displacement Change According to Spacing, L/H= 0,7, Lw = 0,2, β = 3° Newmark

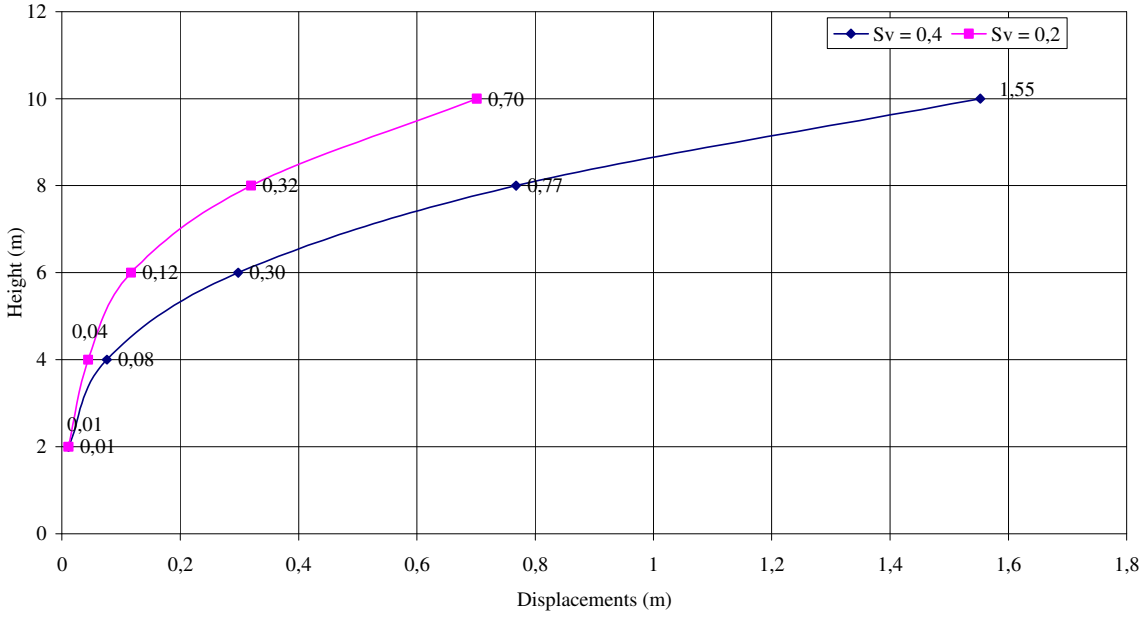

Figure 5.34. Total Displacement Change According to Spacing, L/H= 0,7, Lw = 0,2, β = 3° Bathurst

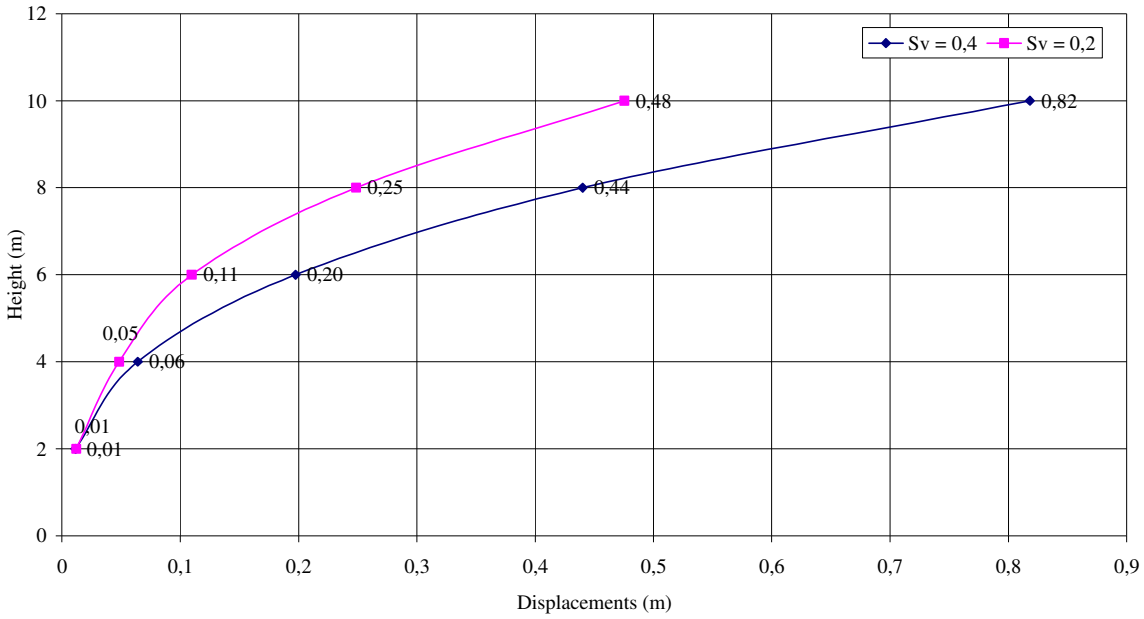

Figure 5.35. Total Displacement Change According to Spacing, L/H= 0,7, Lw = 0,2, β = 0° Newmark

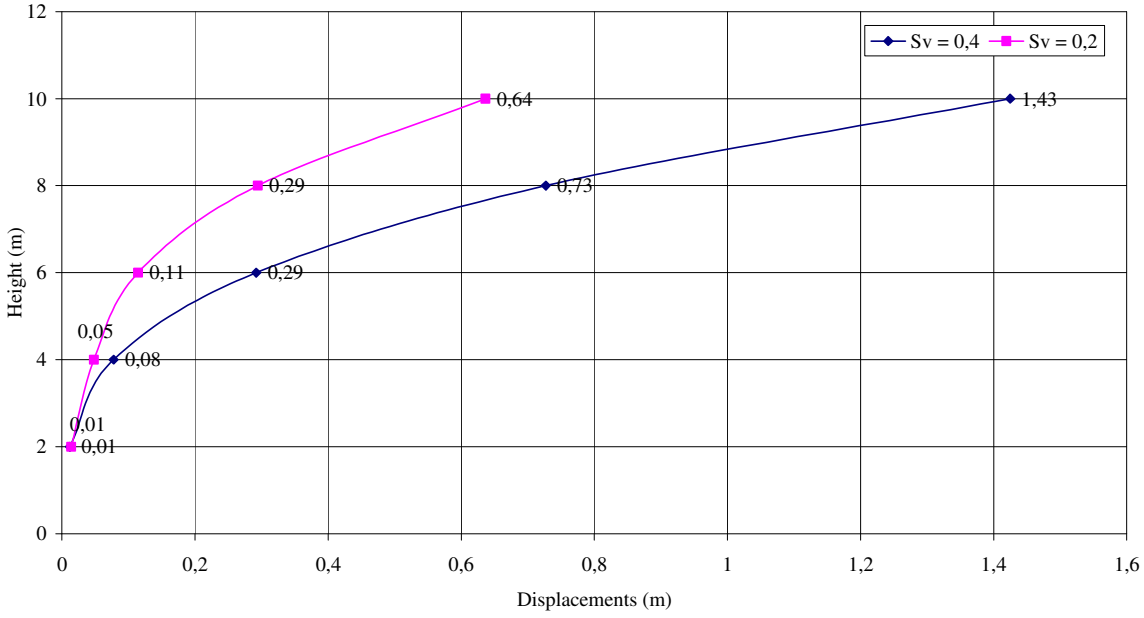

Figure 5.36. Total Displacement Change According to Spacing, L/H= 0,7, Lw = 0,2, β = 0° Bathurst

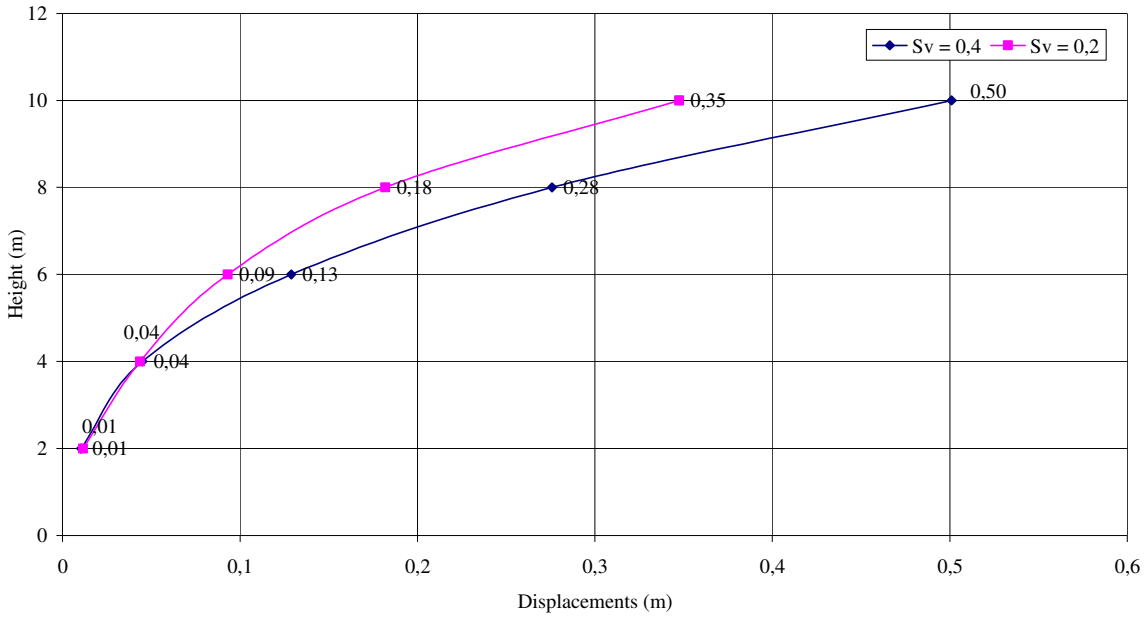

Figure 5.37. Total Displacement Change According to Spacing, L/H= 0,7, Lw = 0,4, β = 3° Newmark

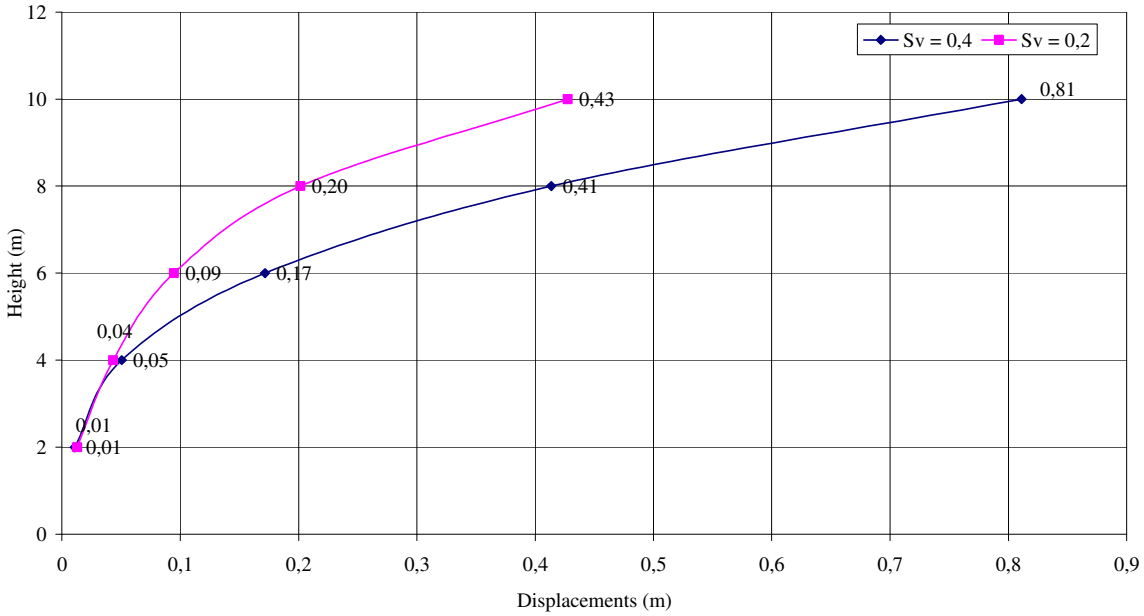

Figure 5.38. Total Displacement Change According to Spacing, L/H= 0,7, Lw = 0,4, β = 3° Bathurst

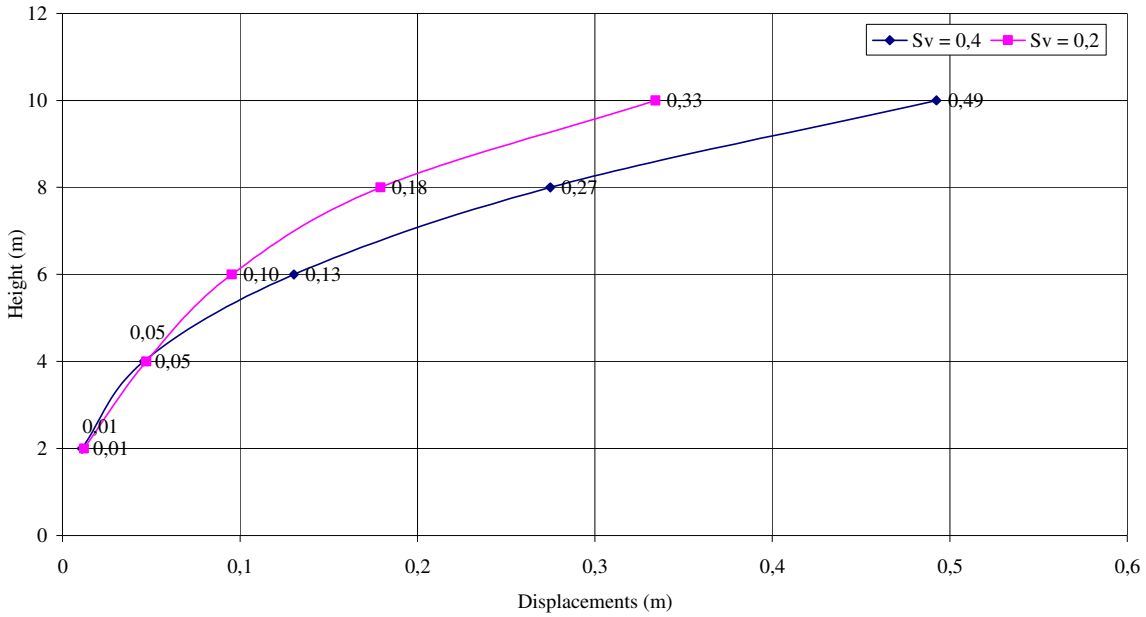

Figure 5.39. Total Displacement Change According to Spacing, L/H= 0,7, Lw = 0,4, β = 0° Newmark

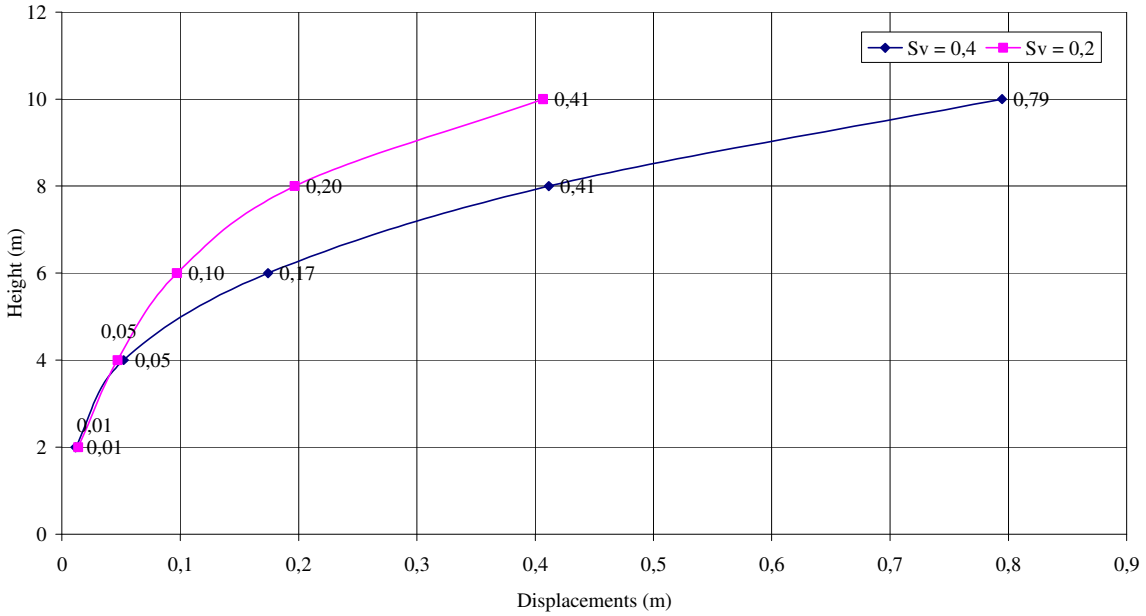

Figure 5.40. Total Displacement Change According to Spacing, L/H= 0,7, Lw = 0,4, β = 0° Bathurst

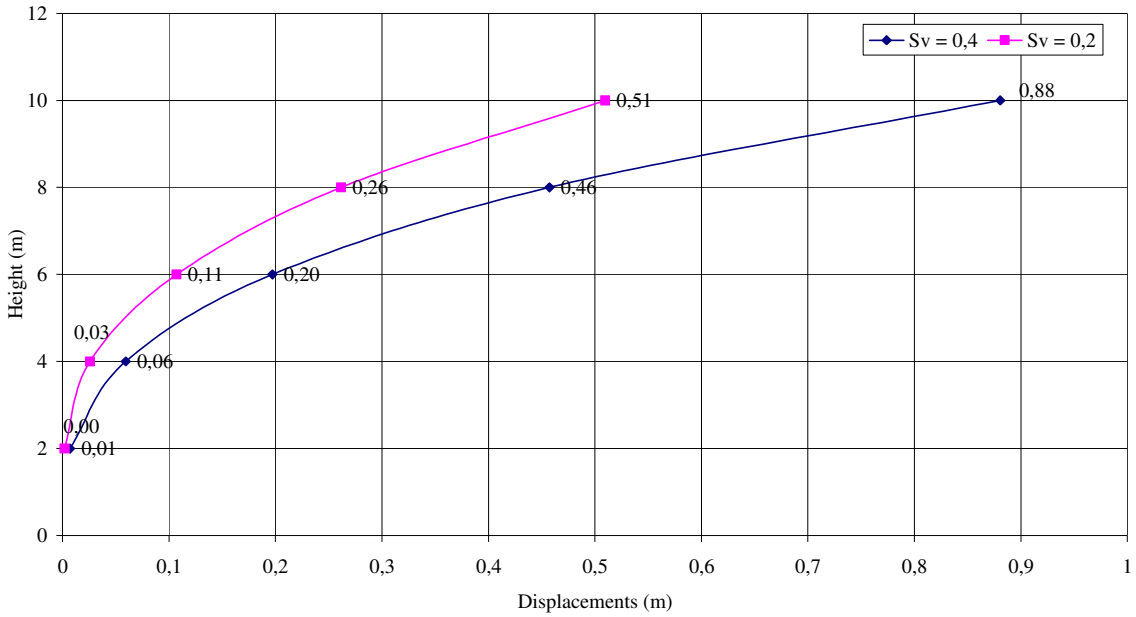

Figure 5.41. Total Displacement Change According to Spacing, L/H= 1,0, Lw = 0,2, β = 3° Newmark

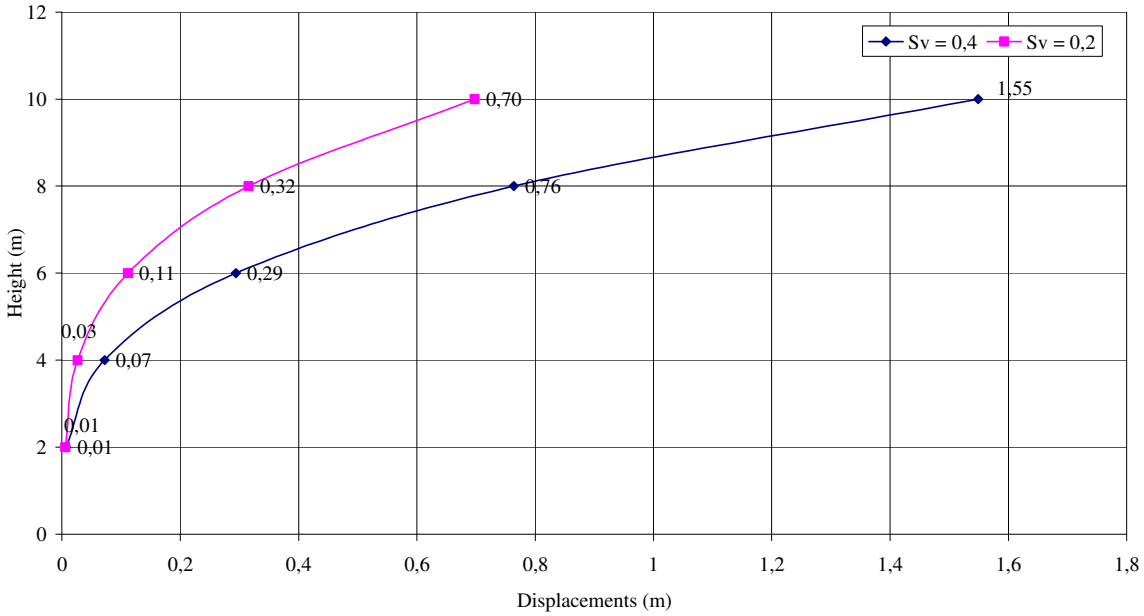

Figure 5.42. Total Displacement Change According to Spacing, L/H= 1,0, Lw = 0,2, β = 3° Bathurst

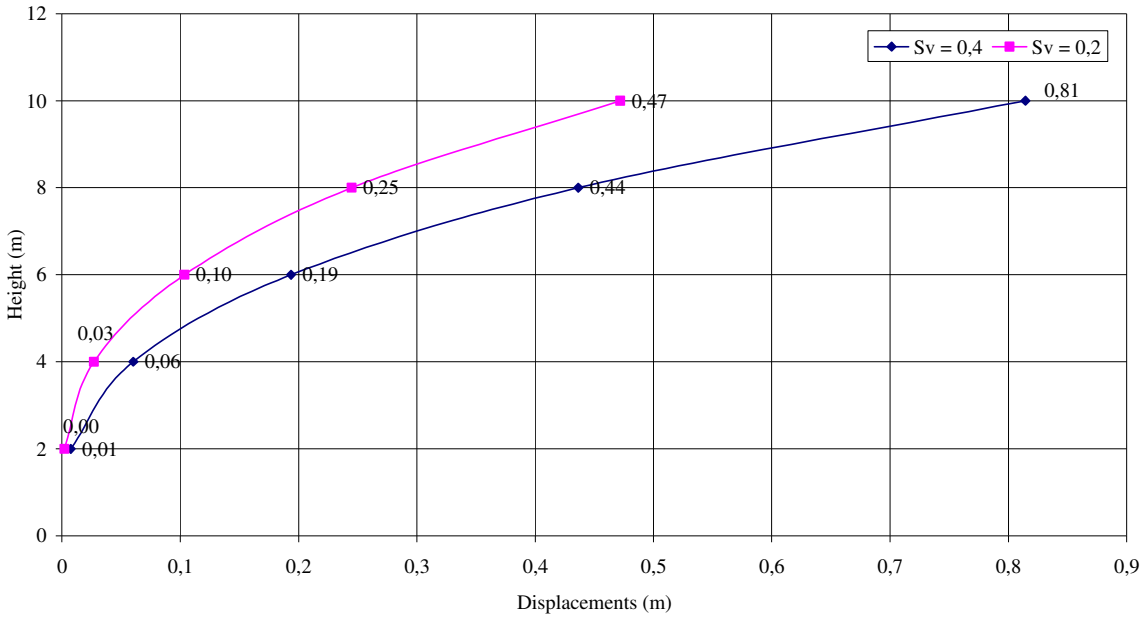

Figure 5.43. Total Displacement Change According to Spacing, L/H= 1,0, Lw = 0,2, β = 0° Newmark

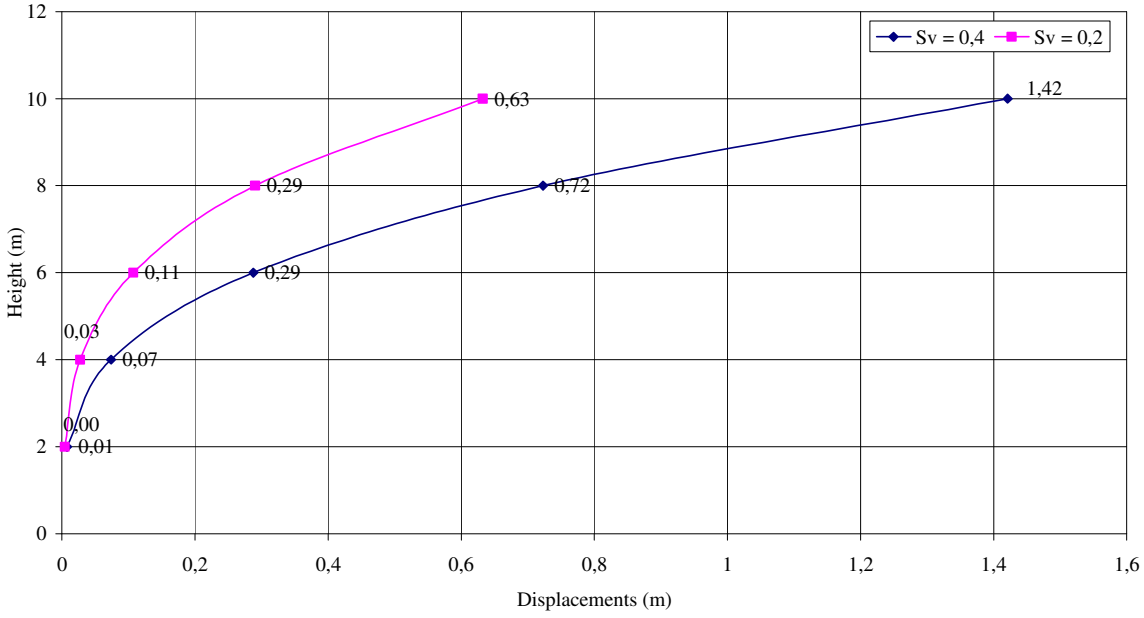

Figure 5.44. Total Displacement Change According to Spacing, L/H= 1,0, Lw = 0,2, β = 0° Bathurst

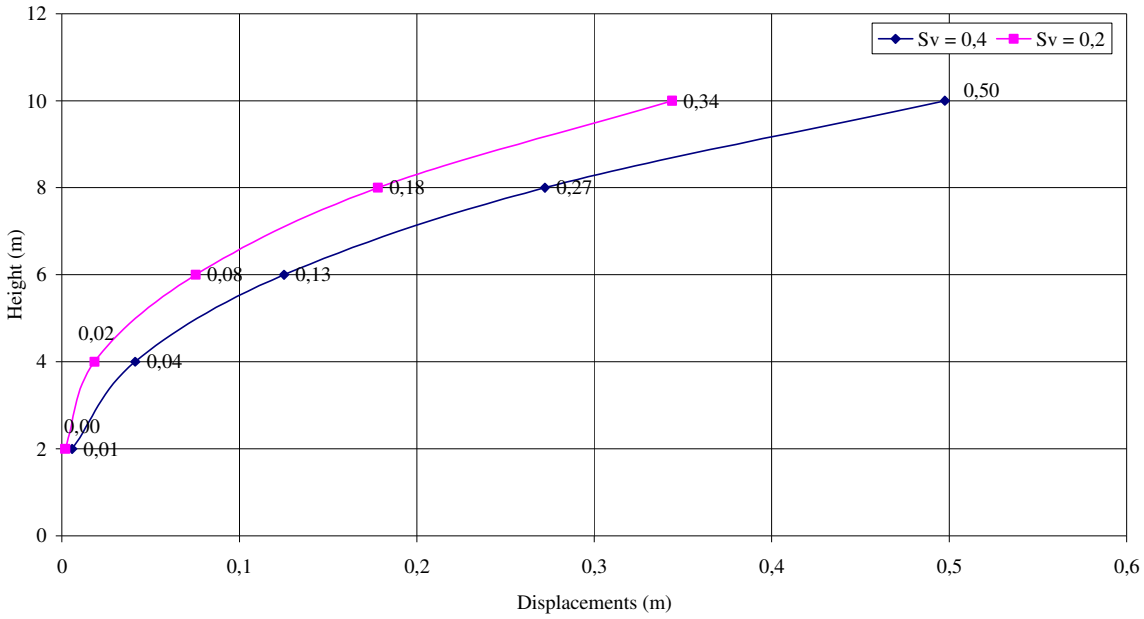

Figure 5.45. Total Displacement Change According to Spacing, L/H= 1,0, Lw = 0,4, β = 3° Newmark

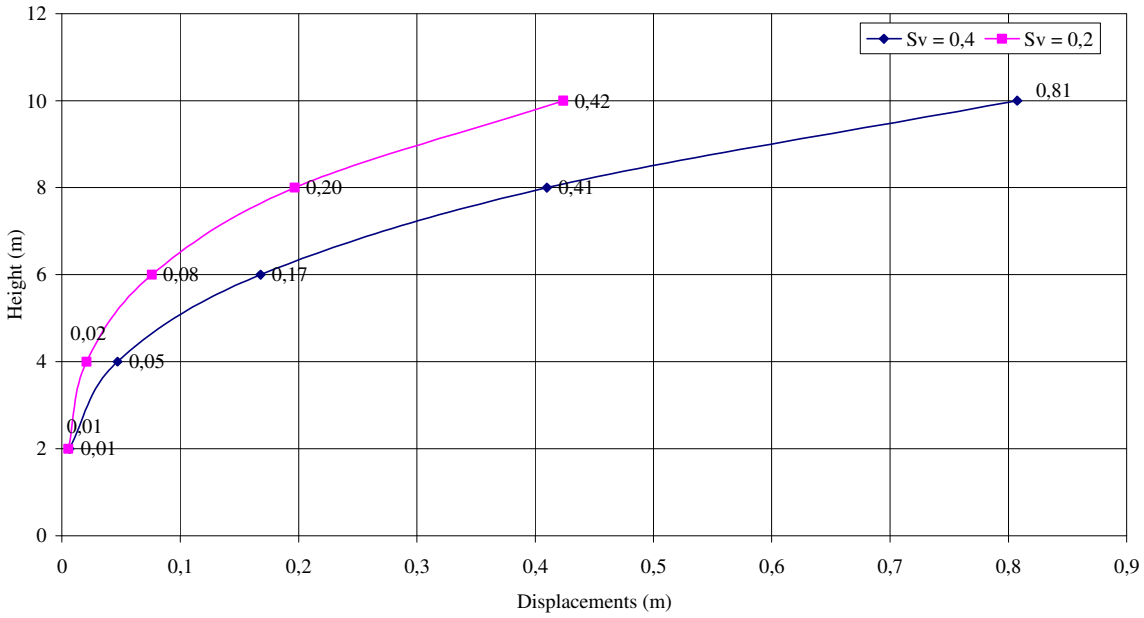

Figure 5.46. Total Displacement Change According to Spacing, L/H= 1,0, Lw = 0,4, β = 3° Bathurst

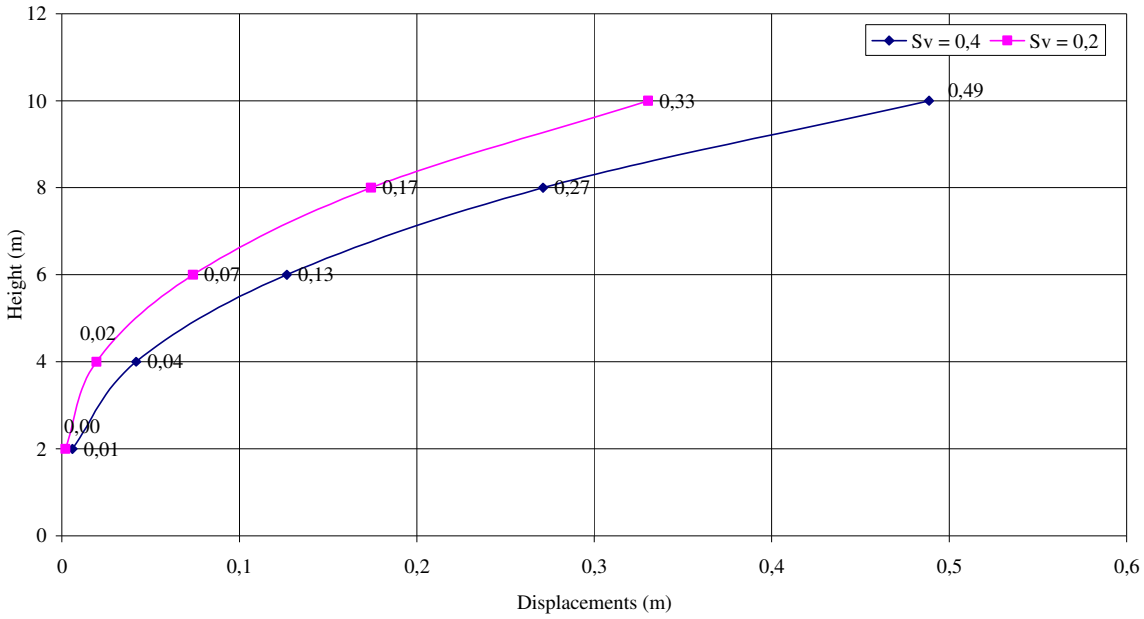

Figure 5.47. Total Displacement Change According to Spacing, L/H= 1,0, Lw = 0,4, β = 0° Newmark

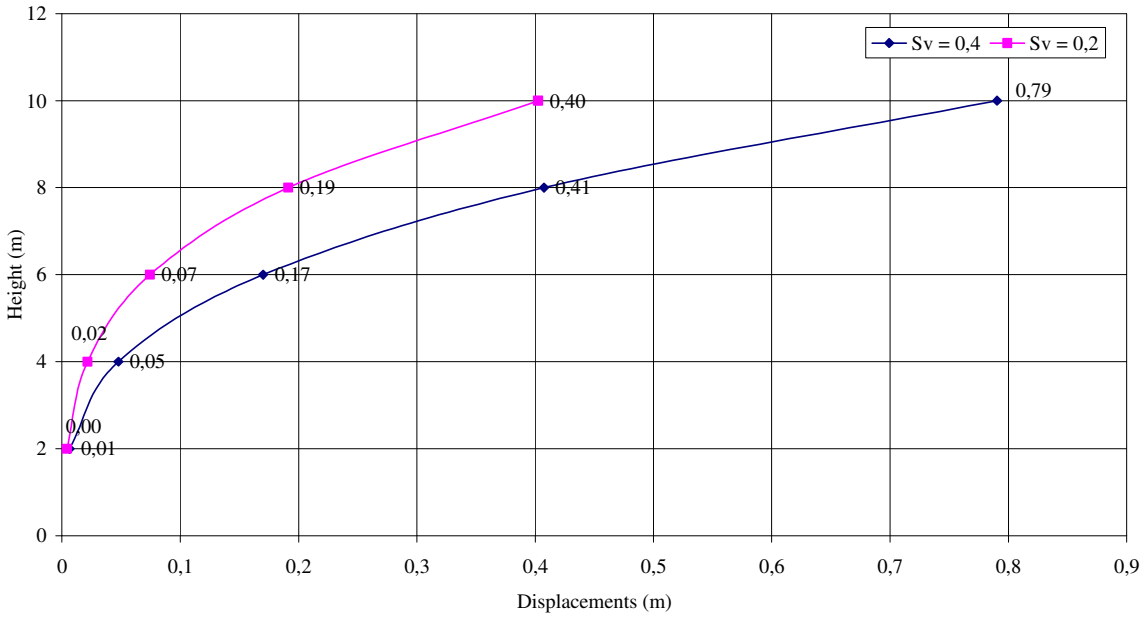

Figure 5.48. Total Displacement Change According to Spacing, L/H= 1,0, Lw = 0,4, β = 0° Bathurst

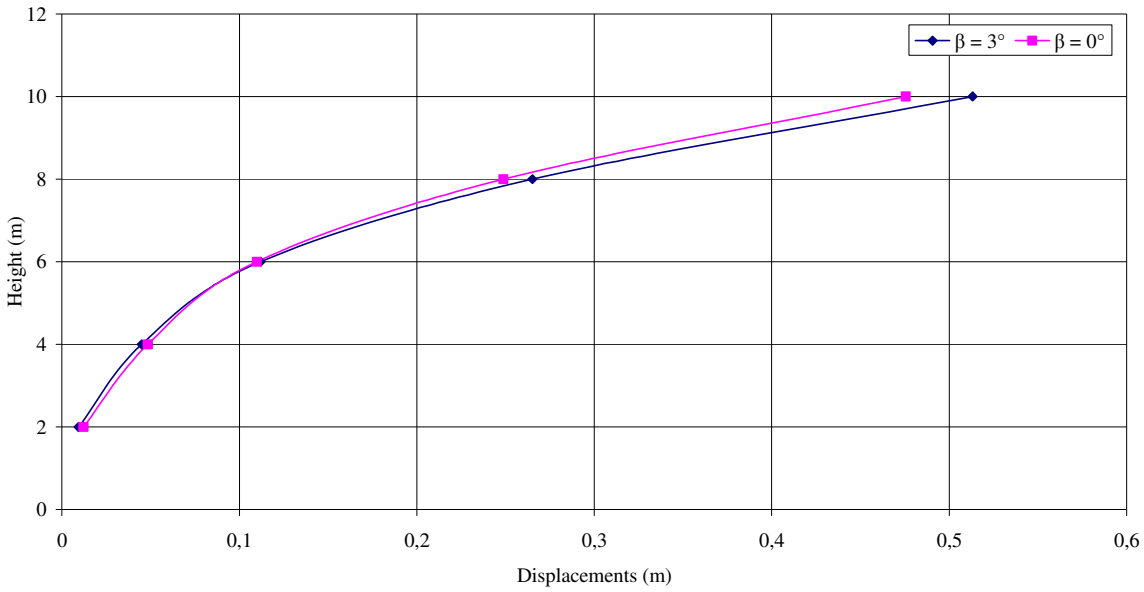

Figure 5.49. Total Displacement Change According to Wall Inclination, L/H= 0,7, Spacing = 0,2, Lw = 0,2 Newmark

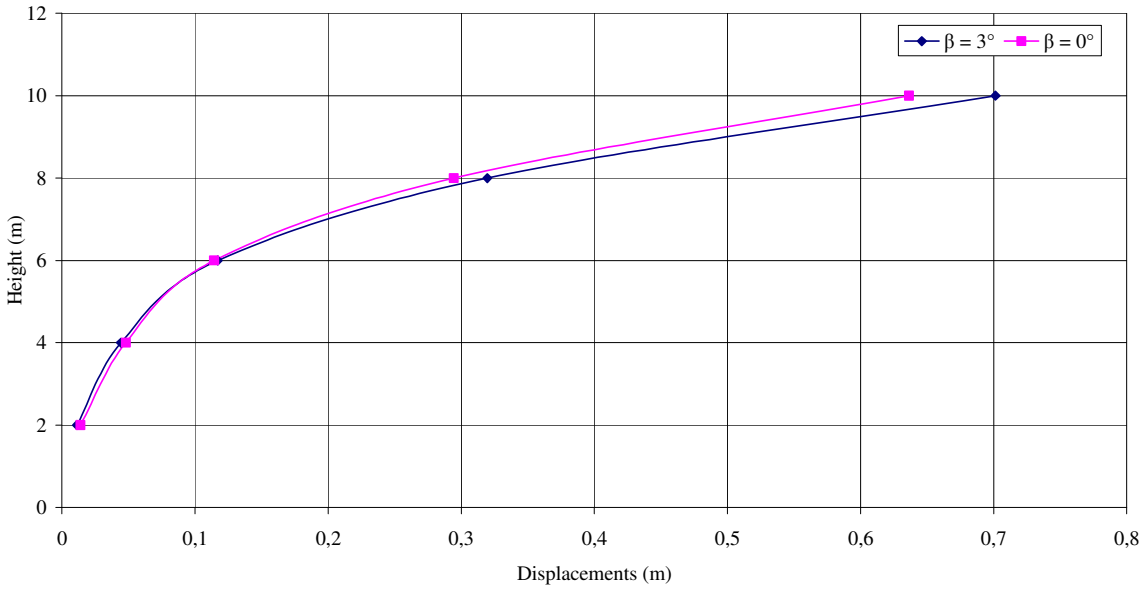

Figure 5.50. Total Displacement Change According to Wall Inclination, L/H= 0,7, Spacing = 0,2, Lw = 0,2 Bathurst

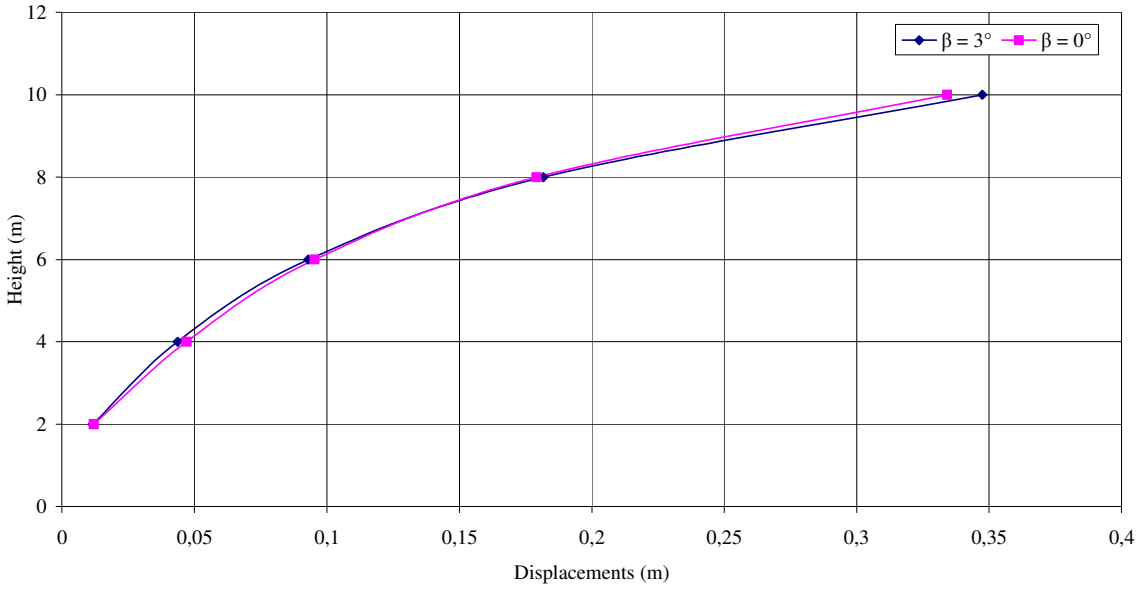

Figure 5.51. Total Displacement Change According to Wall Inclination, L/H= 0,7, Spacing = 0,2, Lw = 0,4 Newmark

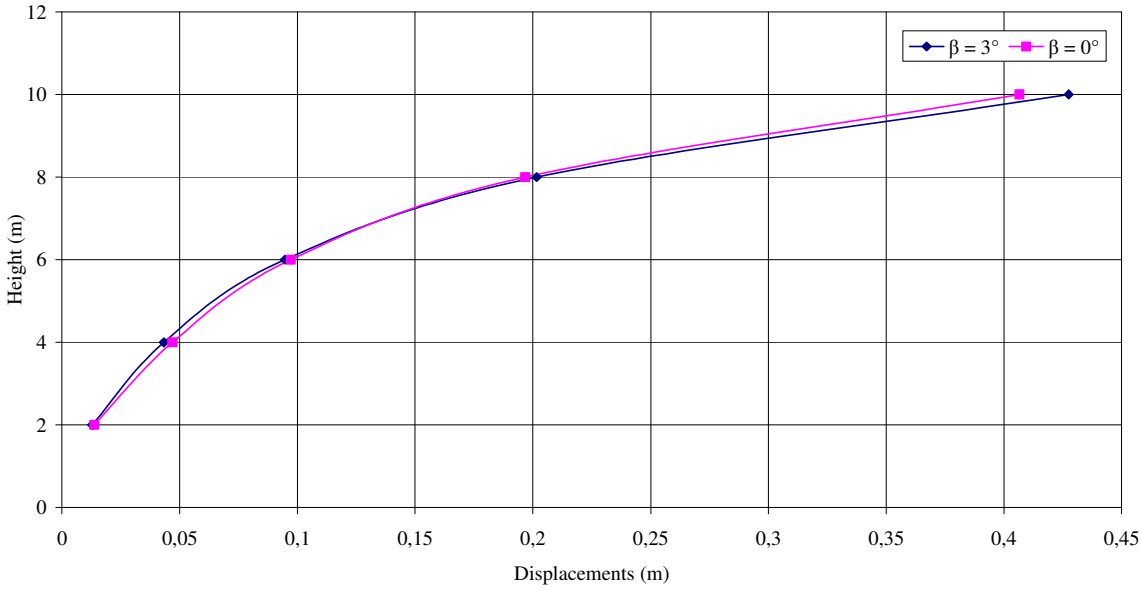

Figure 5.52. Total Displacement Change According to Wall Inclination, L/H= 0,7, Spacing = 0,2, Lw = 0,4 Bathurst

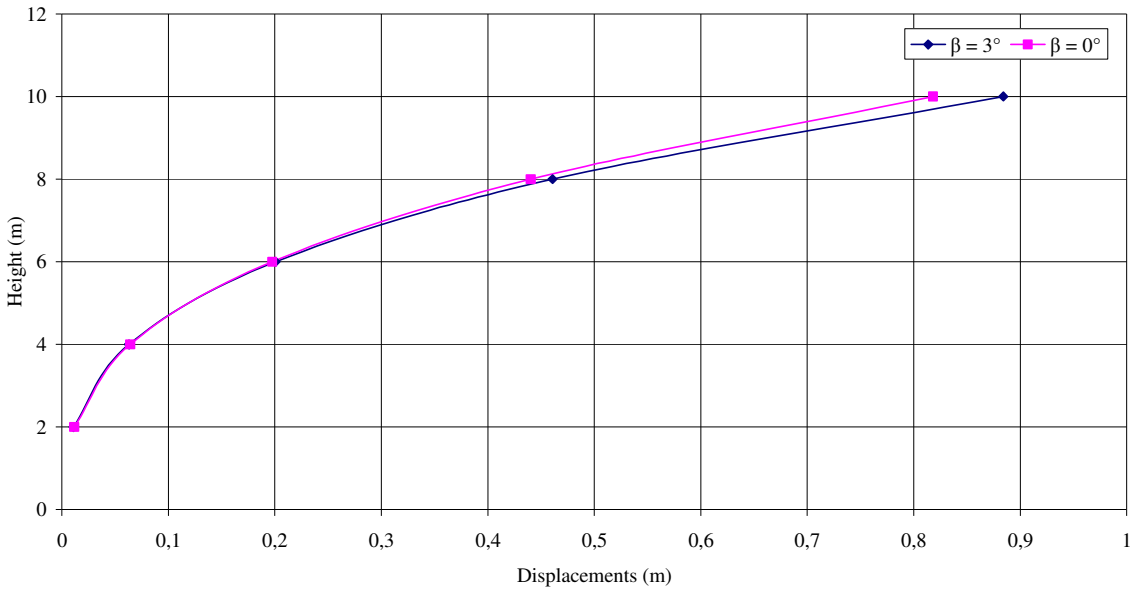

Figure 5.53. Total Displacement Change According to Wall Inclination, L/H= 0,7, Spacing = 0,4, Lw = 0,2 Newmark

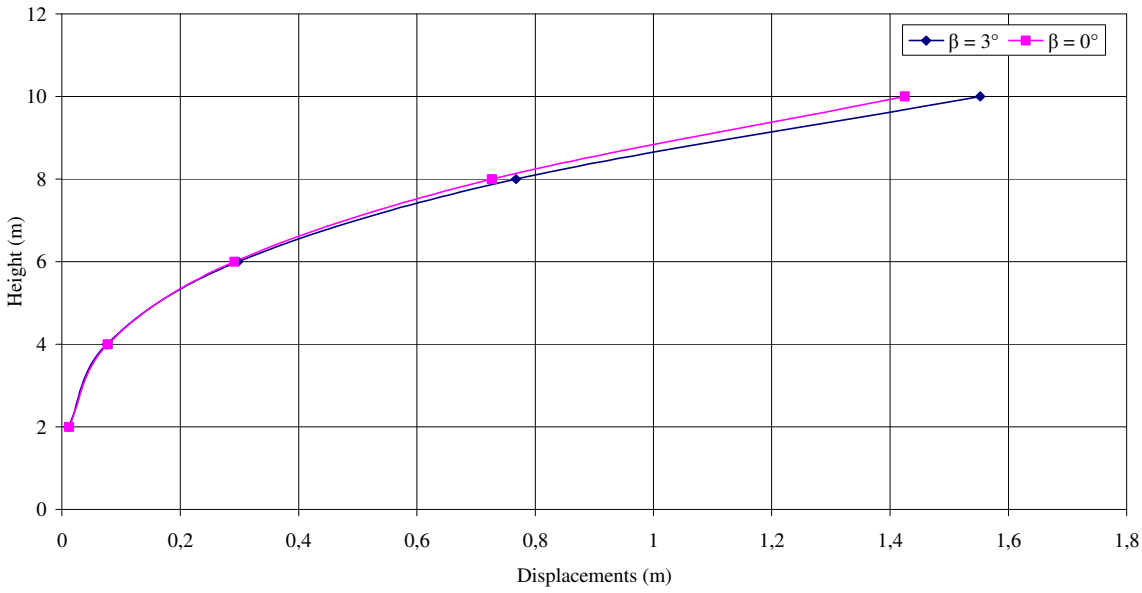

Figure 5.54. Total Displacement Change According to Wall Inclination, L/H= 0,7, Spacing = 0,4, Lw = 0,2 Bathurst

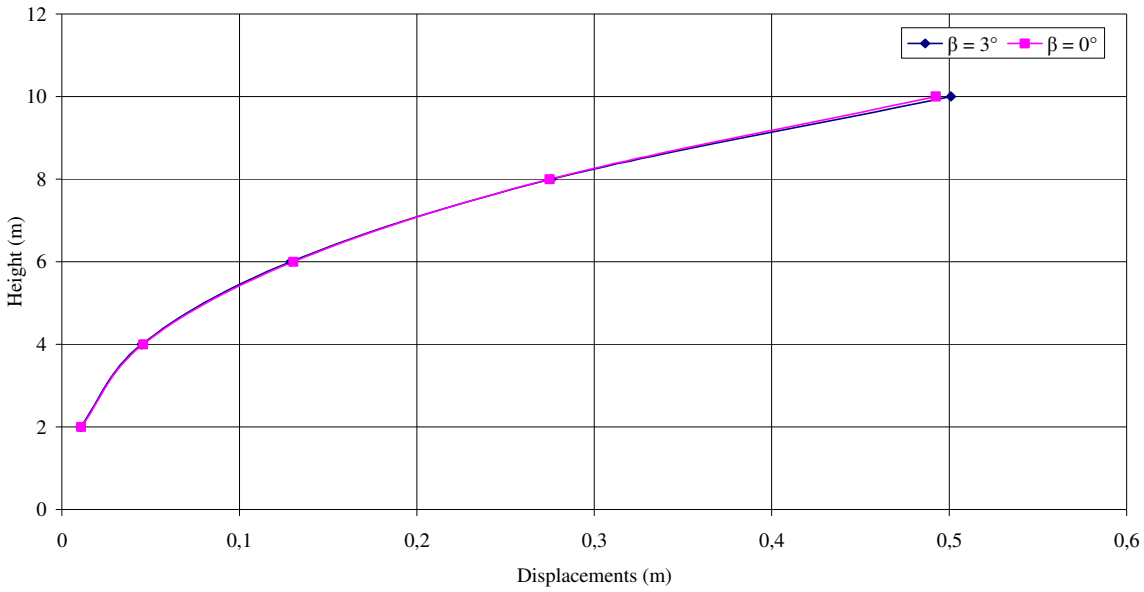

Figure 5.55. Total Displacement Change According to Wall Inclination, L/H= 0,7, Spacing = 0,4, Lw = 0,4 Newmark

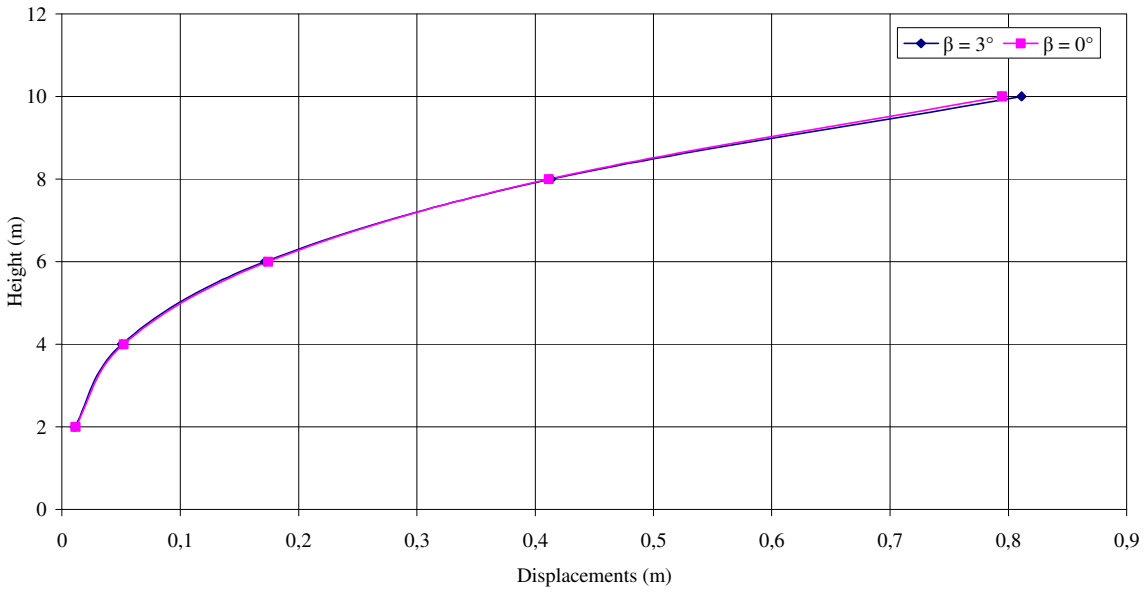

Figure 5.56. Total Displacement Change According to Wall Inclination, L/H= 0,7, Spacing = 0,4, Lw = 0,4 Bathurst

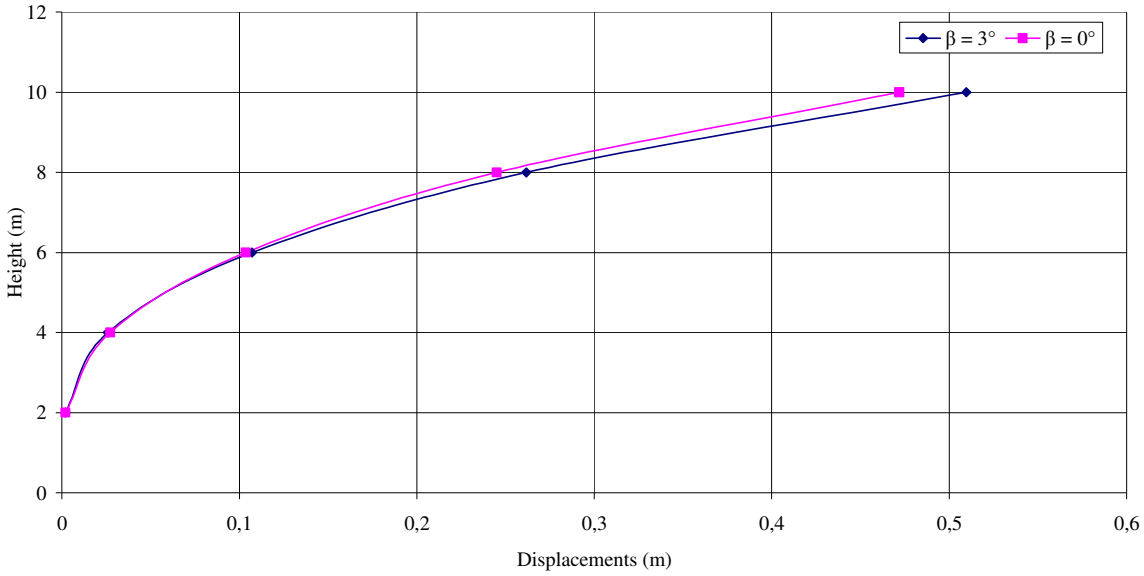

Figure 5.57. Total Displacement Change According to Wall Inclination, L/H= 1,0, Spacing = 0,2, Lw = 0,2 Newmark

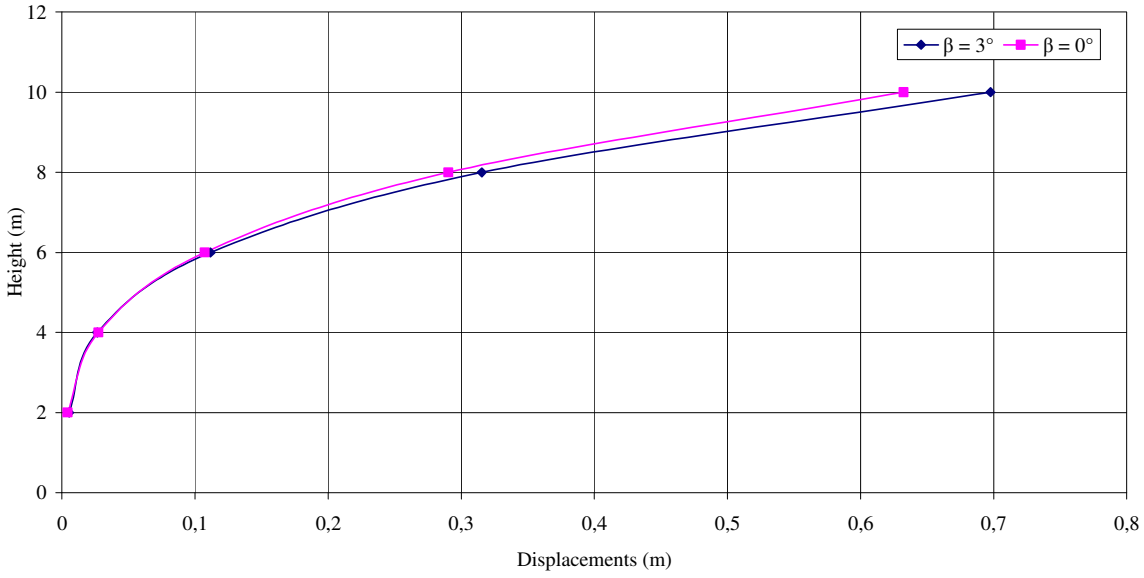

Figure 5.58. Total Displacement Change According to Wall Inclination, L/H= 1,0, Spacing = 0,2, Lw = 0,2 Bathurst

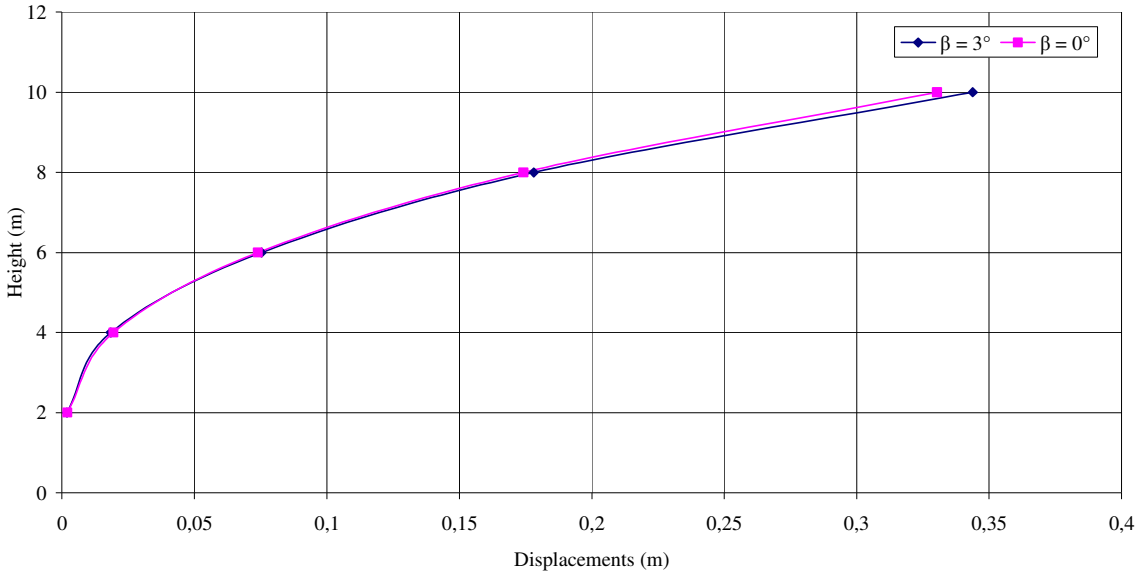

Figure 5.59. Total Displacement Change According to Wall Inclination, L/H= 1,0, Spacing = 0,2, Lw = 0,4 Newmark

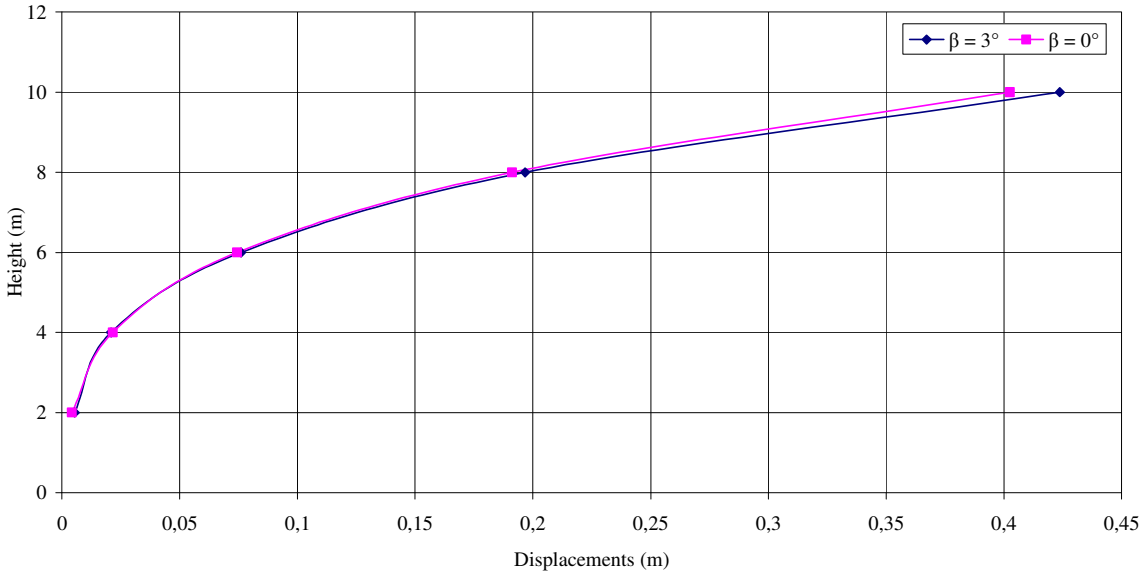

Figure 5.60. Total Displacement Change According to Wall Inclination, L/H= 1,0, Spacing = 0,2, Lw = 0,4 Bathurst

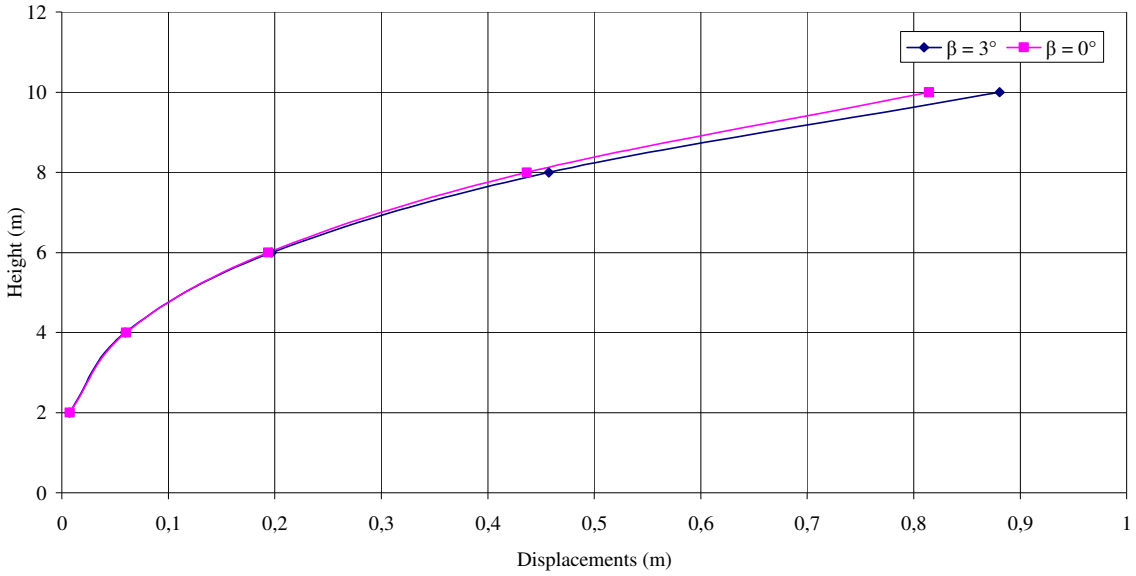

Figure 5.61. Total Displacement Change According to Wall Inclination, L/H= 1,0, Spacing = 0,4, Lw = 0,2 Newmark

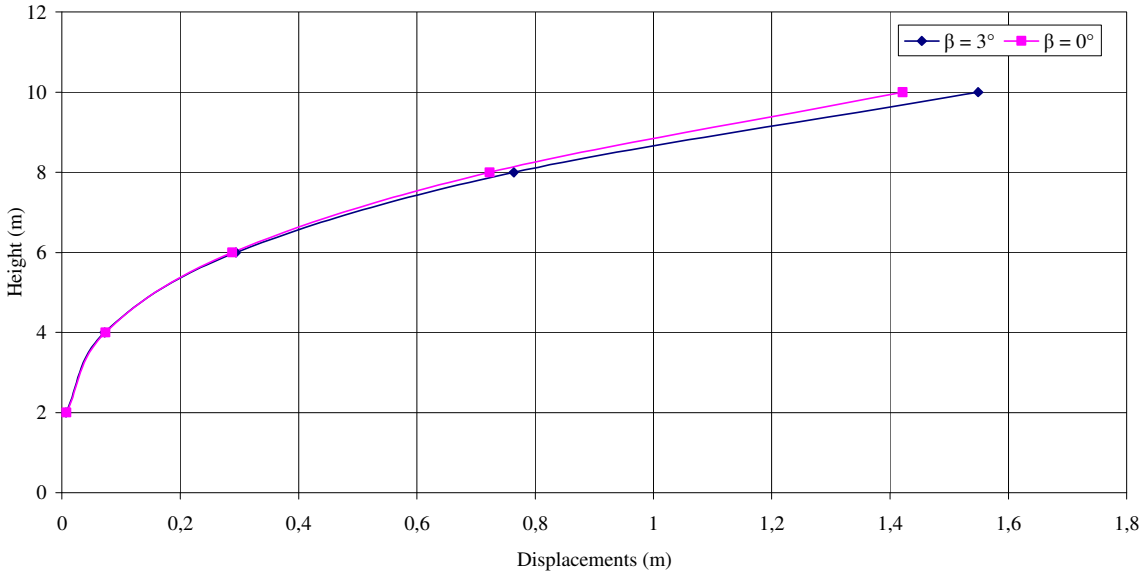

Figure 5.62. Total Displacement Change According to Wall Inclination, L/H= 1,0, Spacing = 0,4, Lw = 0,2 Bathurst

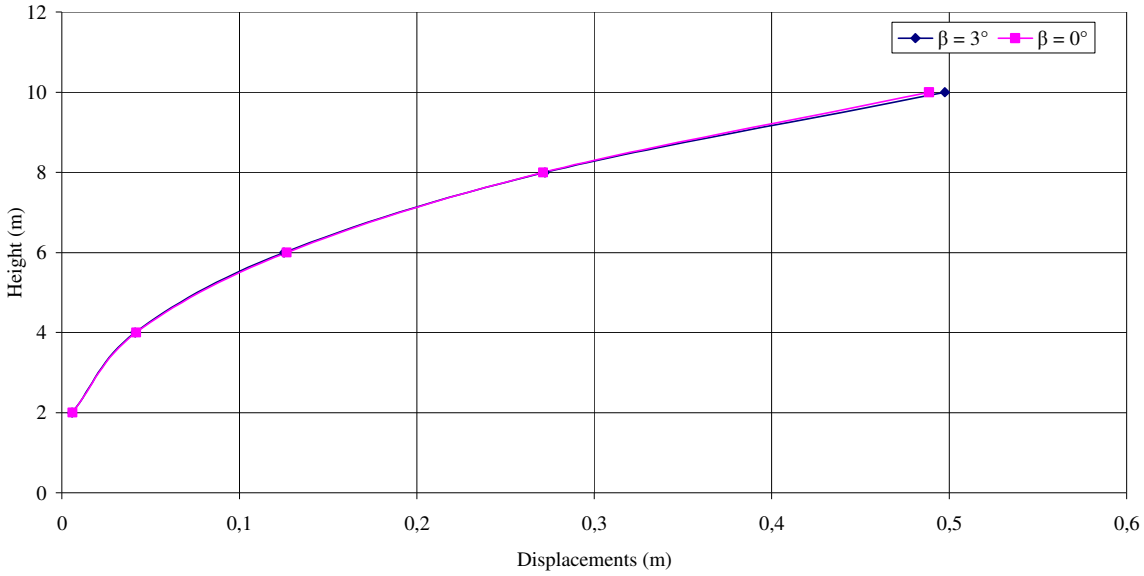

Figure 5.63. Total Displacement Change According to Wall Inclination, L/H= 1,0, Spacing = 0,4, Lw = 0,4 Newmark

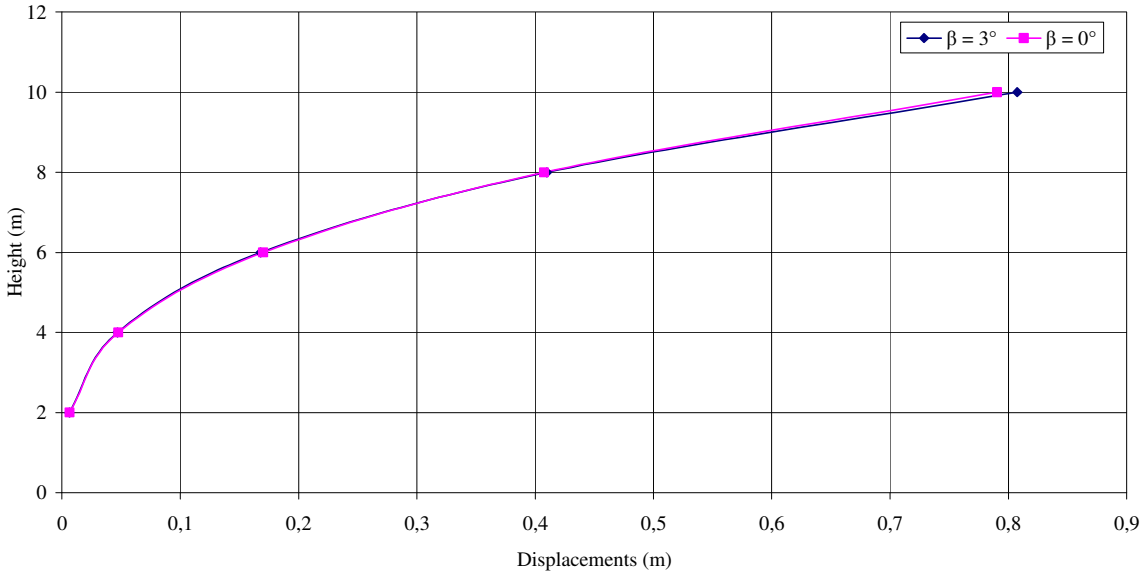

Figure 5.64. Total Displacement Change According to Wall Inclination, L/H= 1,0, Spacing = 0,4, Lw = 0,4 Bathurst

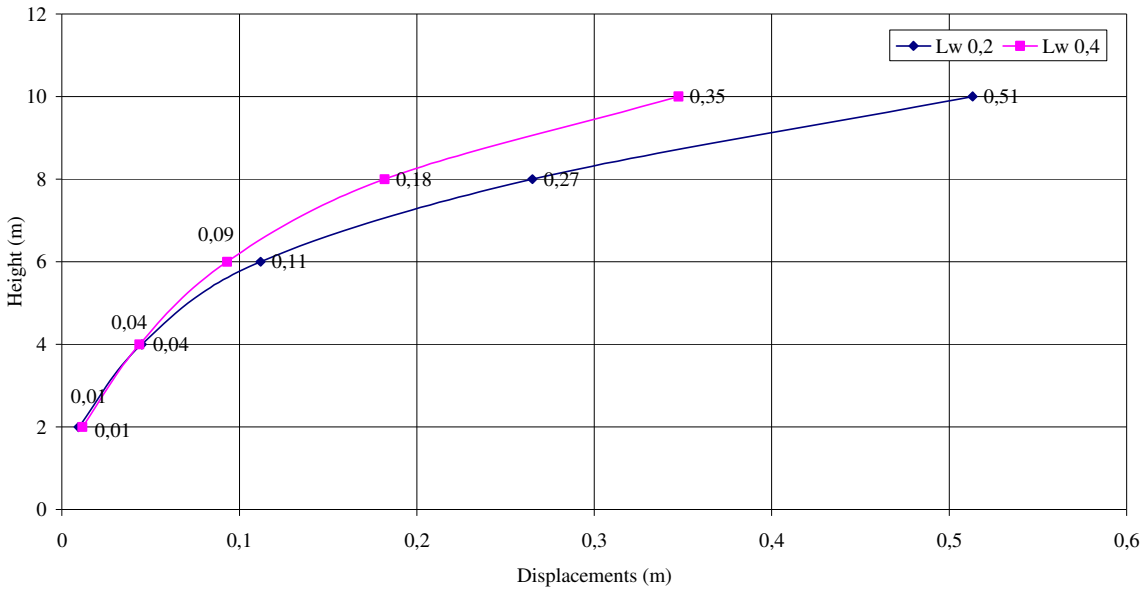

Figure 5.65. Total Displacement Change According to Block Width, L/H= 0,7, Spacing = 0,2, β = 3° Newmark

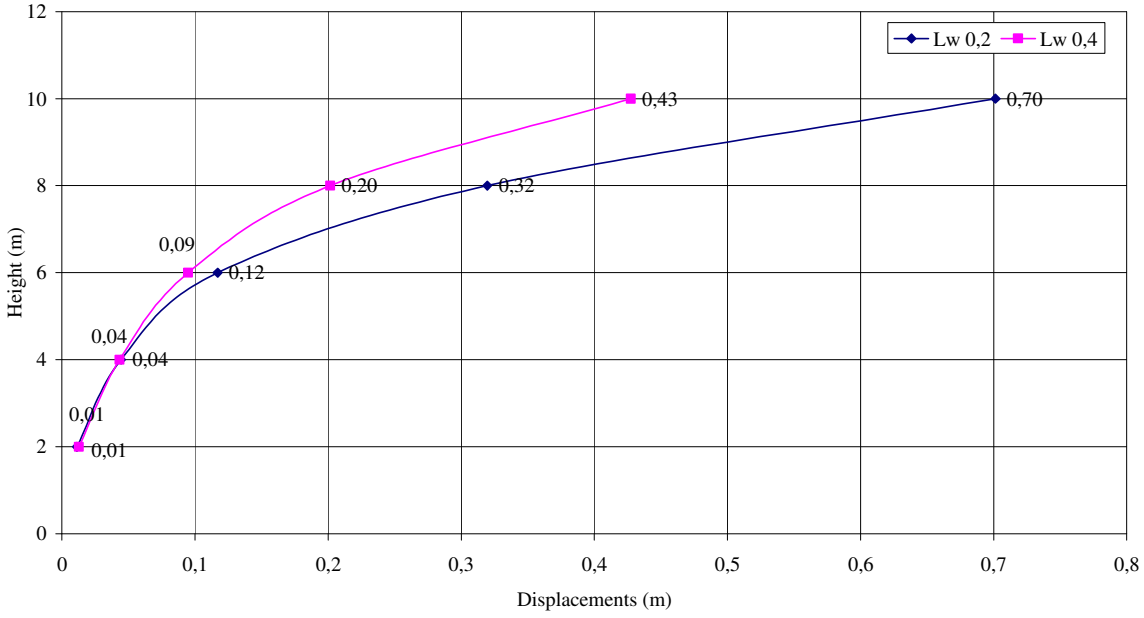

Figure 5.66. Total Displacement Change According to Block Width, L/H= 0,7, Spacing = 0,2, β = 3° Bathurst

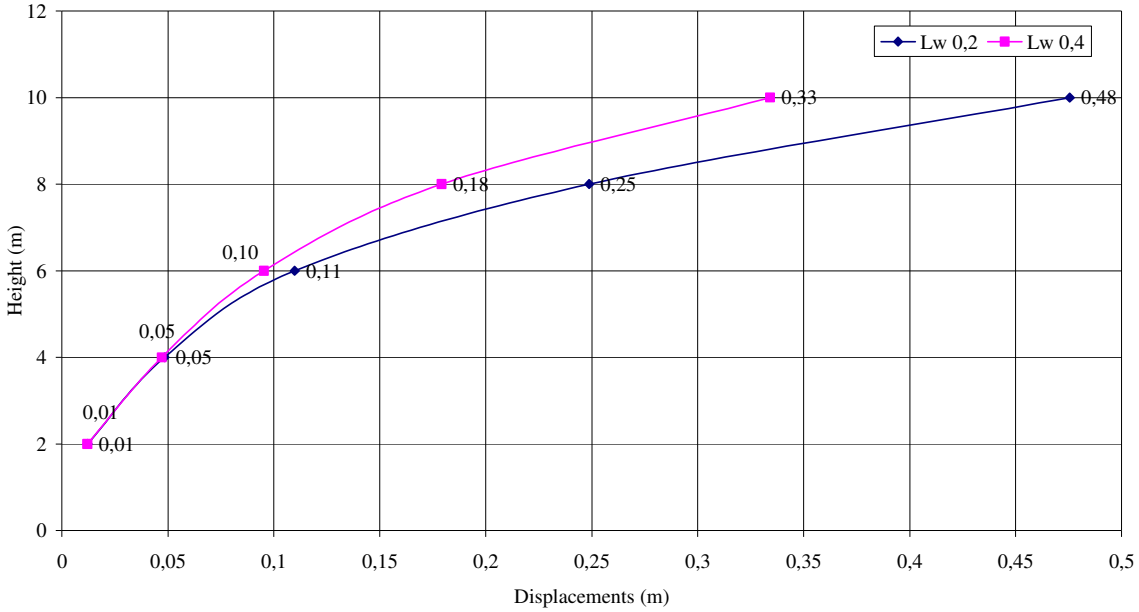

Figure 5.67. Total Displacement Change According to Block Width, L/H= 0,7, Spacing = 0,2, β = 0° Newmark

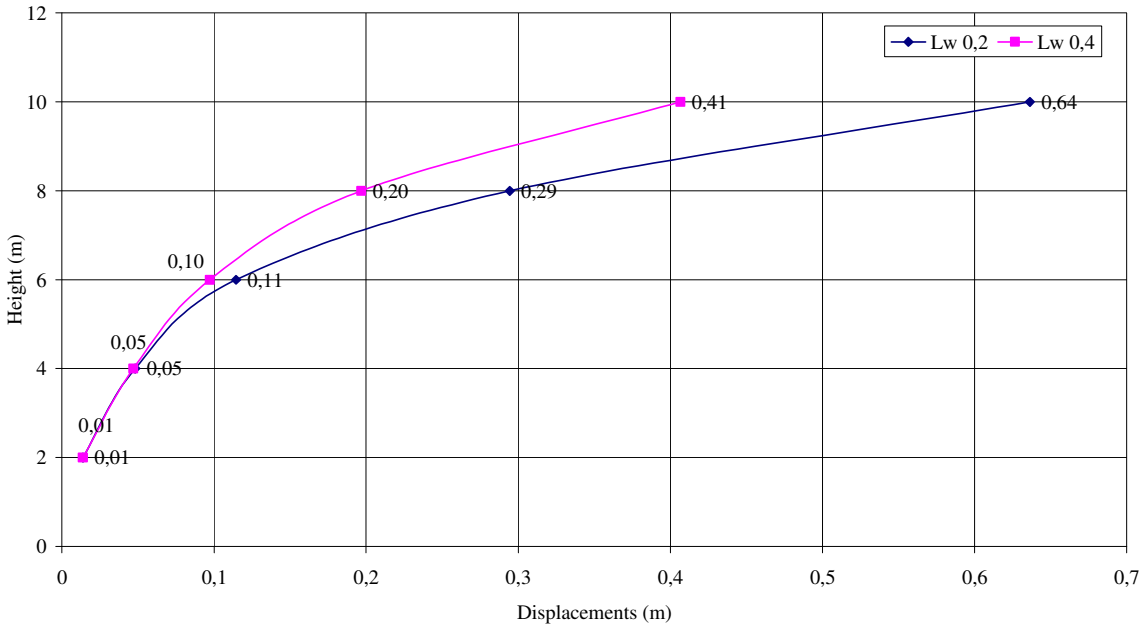

Figure 5.68. Total Displacement Change According to Block Width, L/H= 0,7, Spacing = 0,2, β = 0° Bathurst

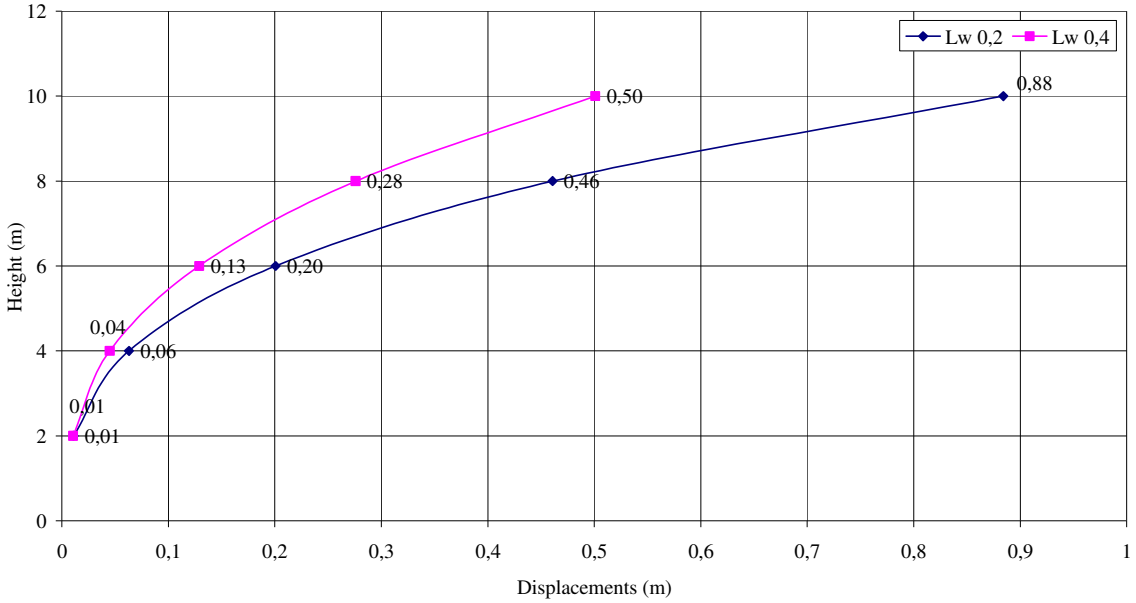

Figure 5.69. Total Displacement Change According to Block Width, L/H= 0,7, Spacing = 0,4, β = 3° Newmark

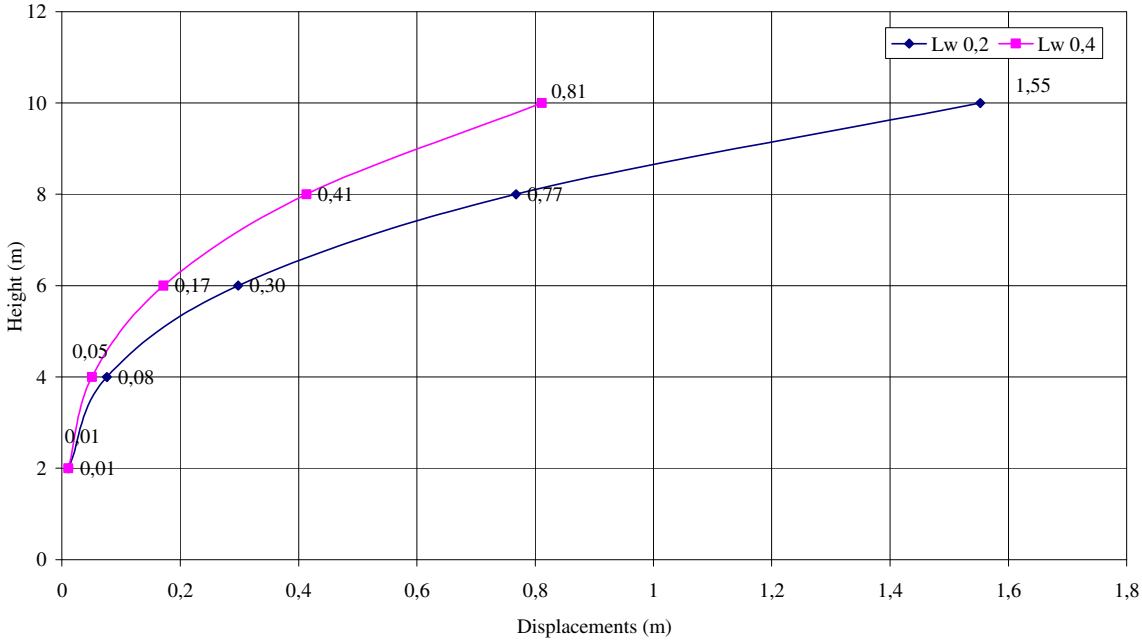

Figure 5.70. Total Displacement Change According to Block Width, L/H= 0,7, Spacing = 0,4, β = 3° Bathurst

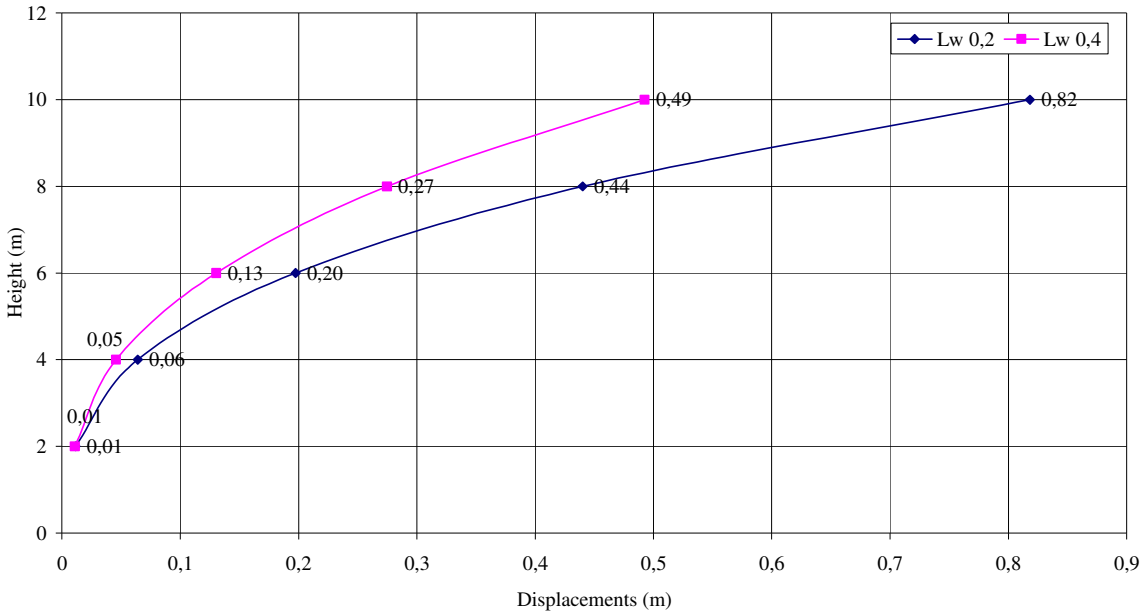

Figure 5.71. Total Displacement Change According to Block Width, L/H= 0,7, Spacing = 0,4, β = 0° Newmark

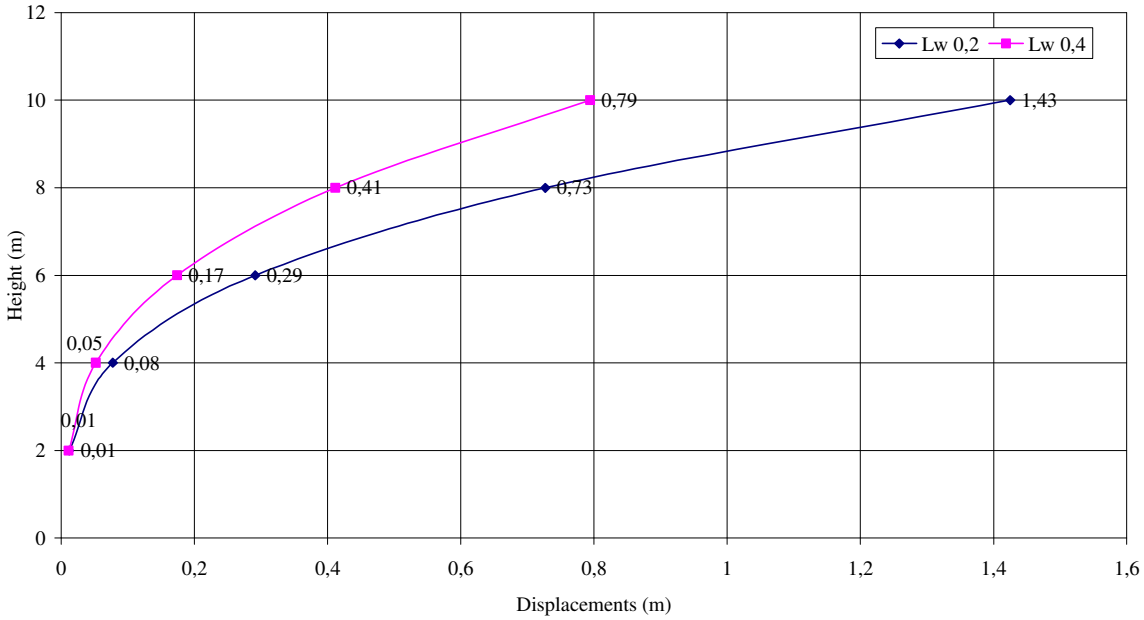

Figure 5.72. Total Displacement Change According to Block Width, L/H= 0,7, Spacing = 0,4, β = 0° Bathurst

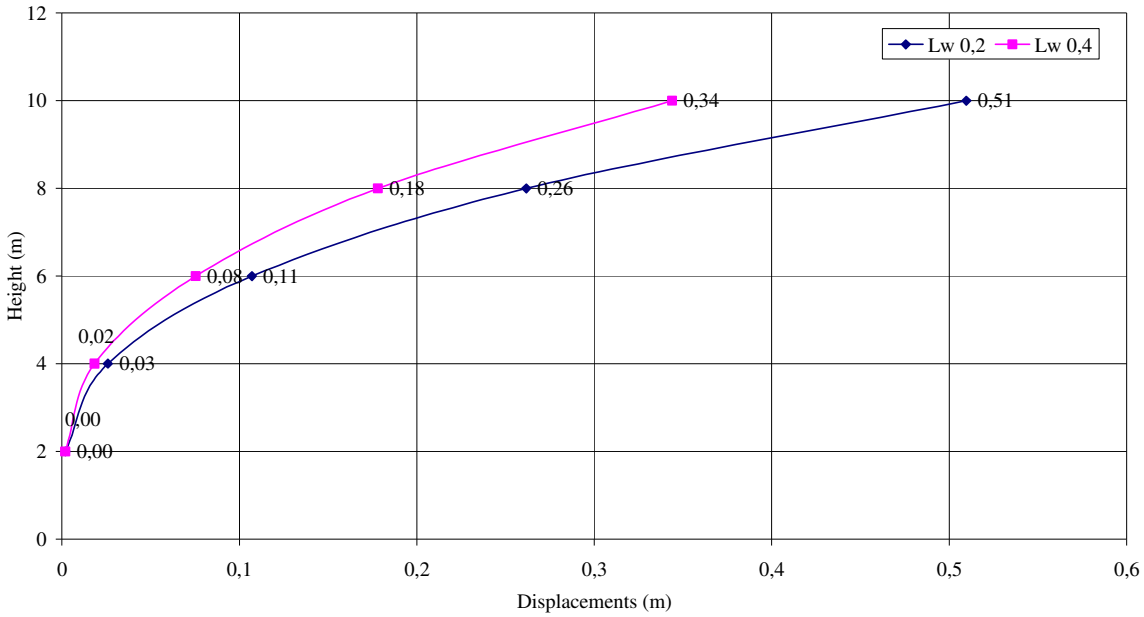

Figure 5.73. Total Displacement Change According to Block Width, L/H= 1,0, Spacing = 0,2, β = 3° Newmark

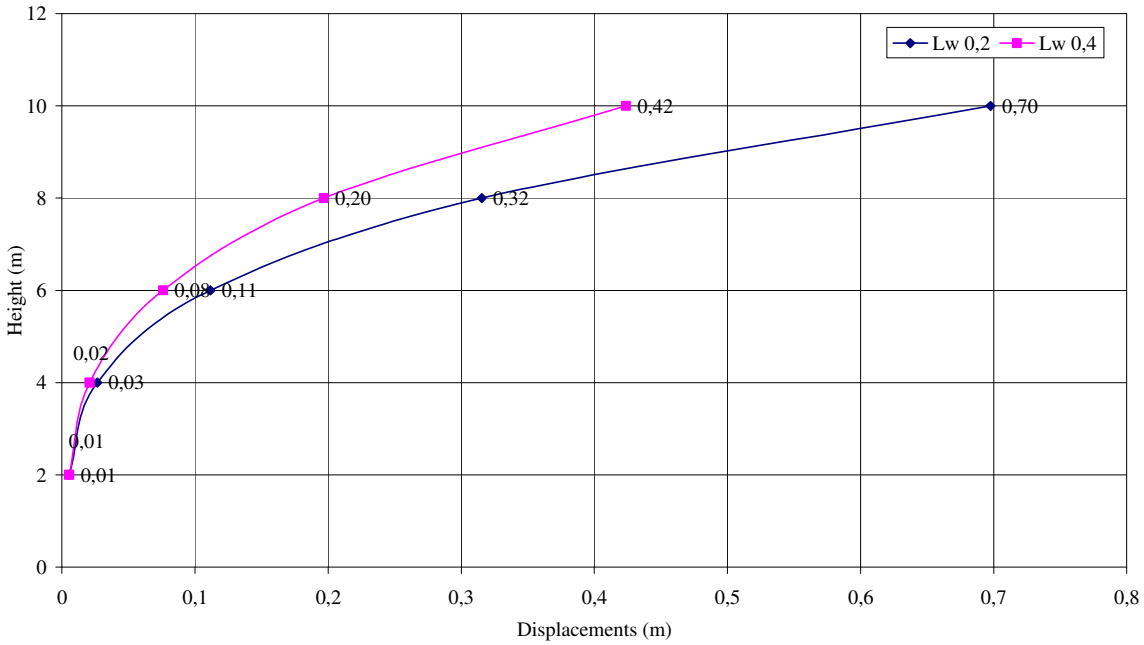

Figure 5.74. Total Displacement Change According to Block Width, L/H= 1,0, Spacing = 0,2, β = 3° Bathurst

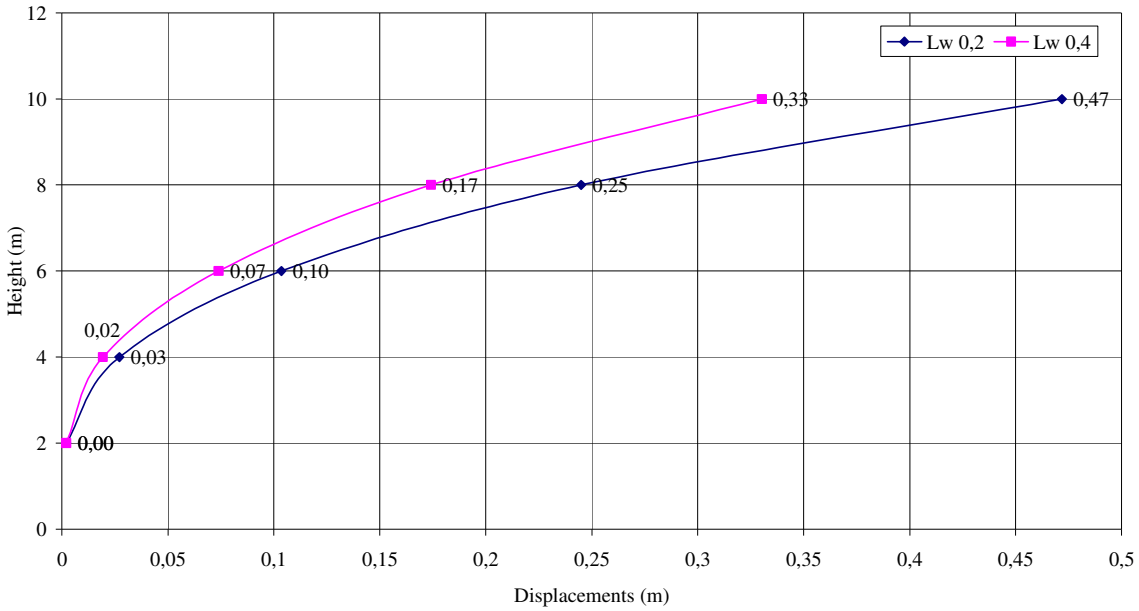

Figure 5.75. Total Displacement Change According to Block Width, L/H= 1,0, Spacing = 0,2, β = 0° Newmark

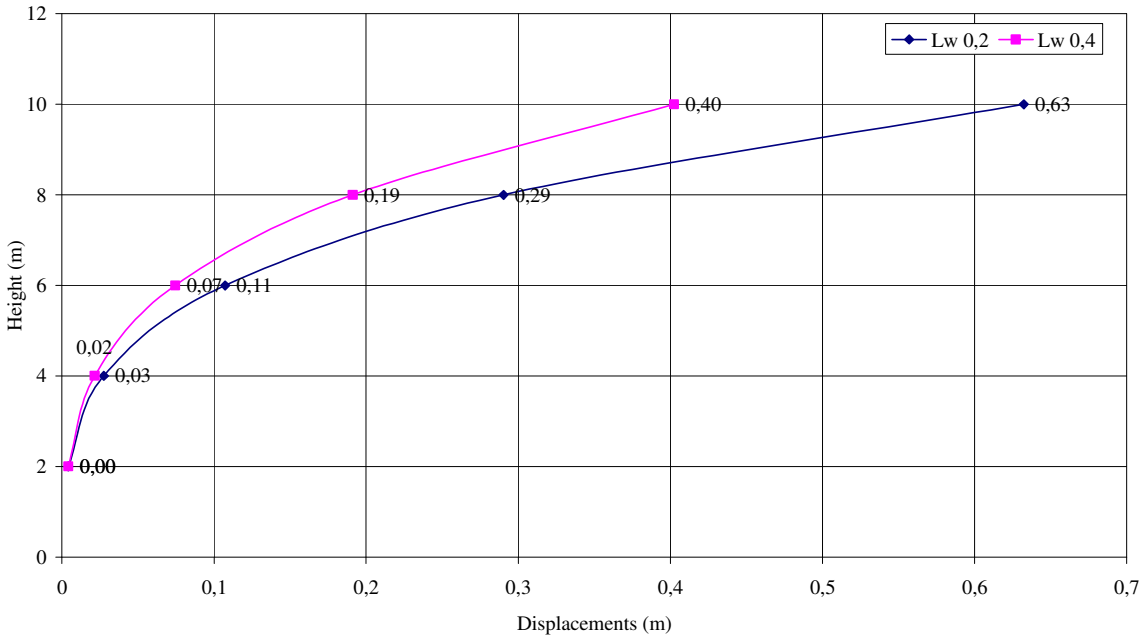

Figure 5.76. Total Displacement Change According to Block Width, L/H= 1,0, Spacing = 0,2, β = 0° Bathurst

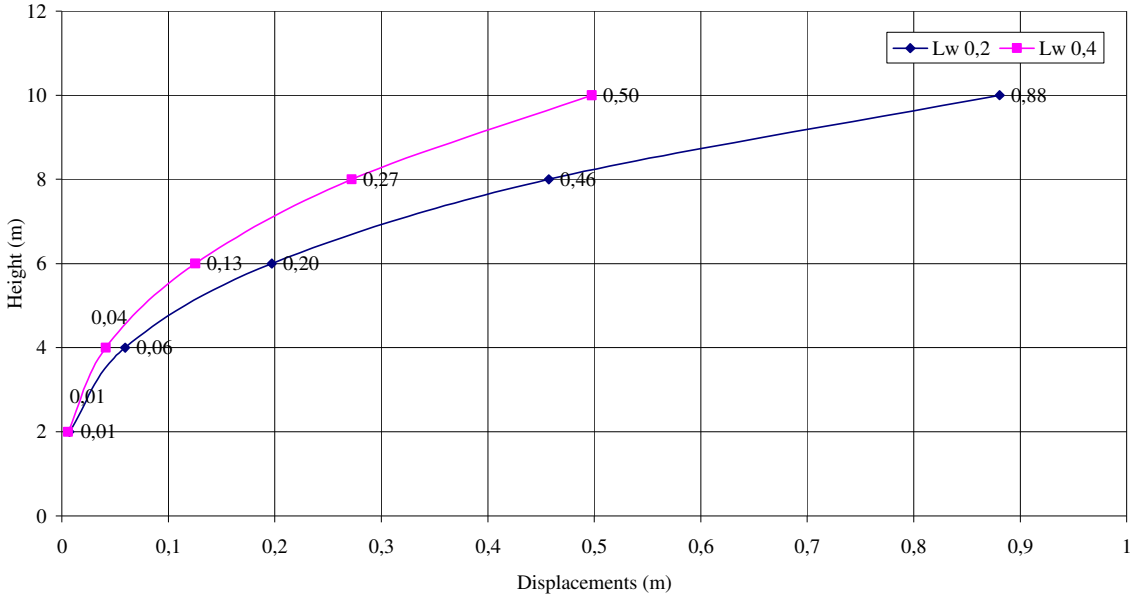

Figure 5.77. Total Displacement Change According to Block Width, L/H= 1,0, Spacing = 0,4, β = 3° Newmark

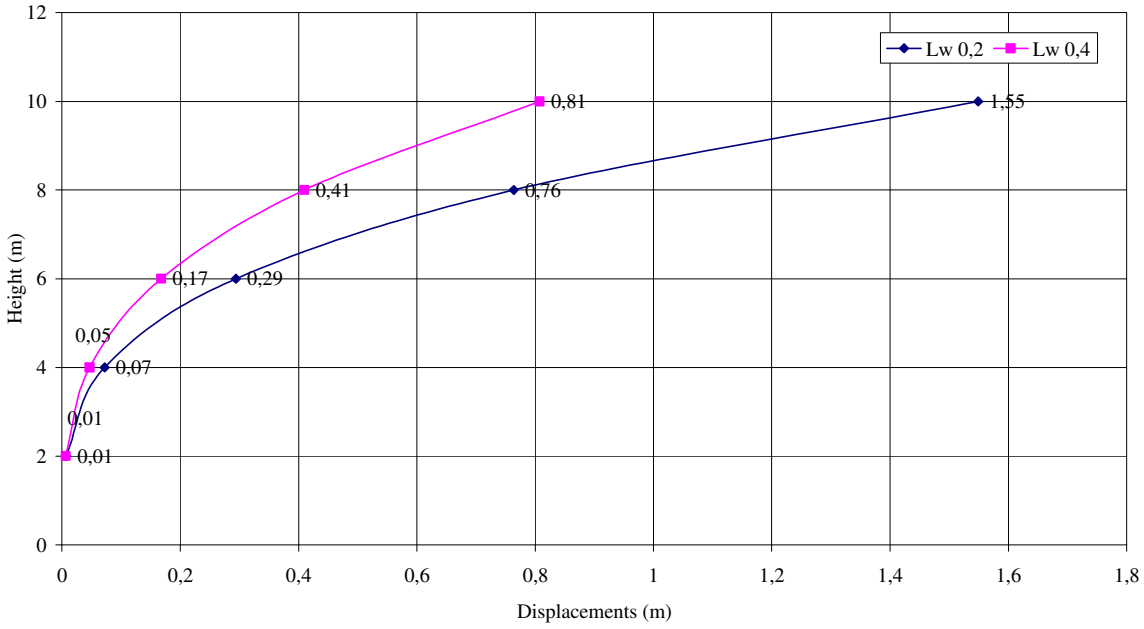

Figure 5.78. Total Displacement Change According to Block Width, L/H= 1,0, Spacing = 0,4, β = 3° Bathurst

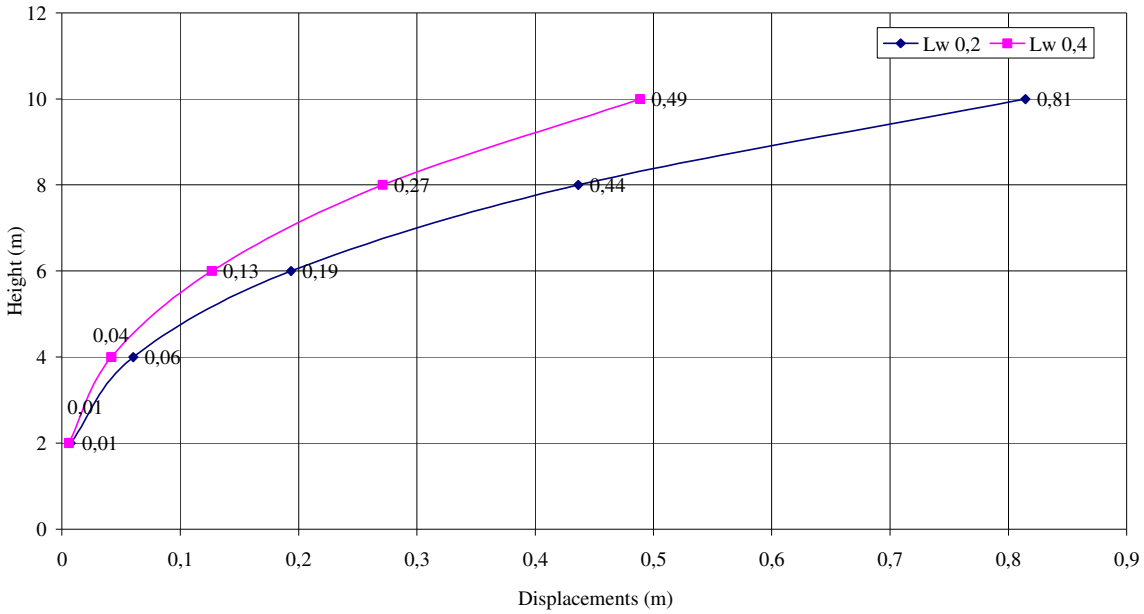

Figure 5.79. Total Displacement Change According to Block Width, L/H= 1,0, Spacing = 0,4, β = 0° Newmark

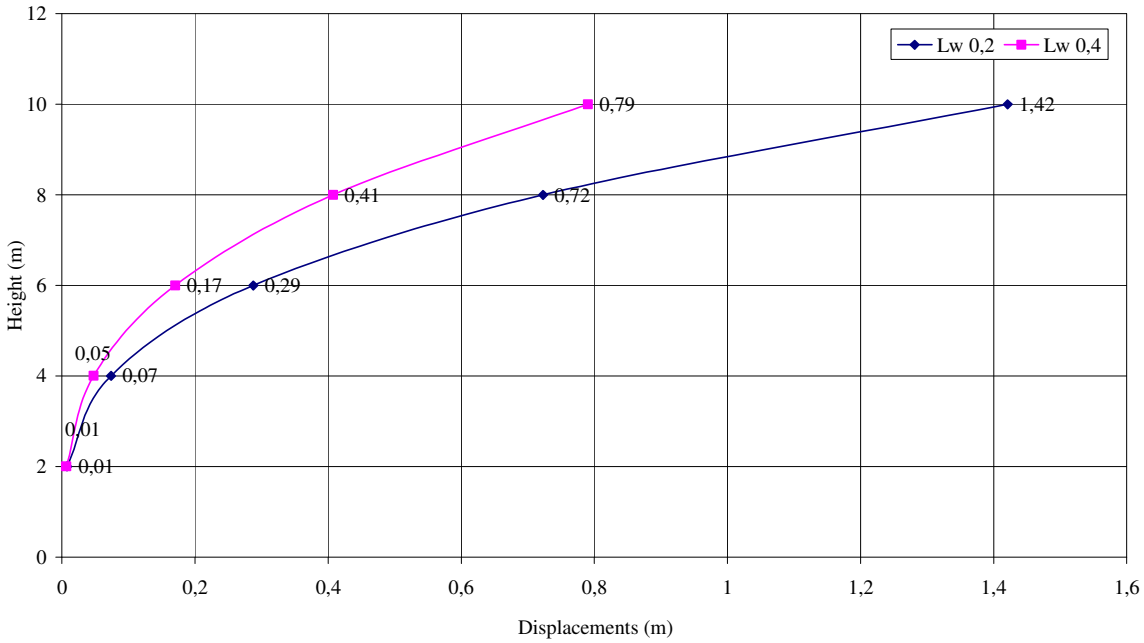

Figure 5.80. Total Displacement Change According to Block Width, L/H= 1,0, Spacing = 0,4, β = 0° Bathurst

6. VERIFICATION

6.1. Valencia Wall

The Valencia wall has a maximum height of 6.5 m and is located al a distance of 23 km from the epicenter of the Northridge Earthquake. Three landslides were reported to have occurred in the general area of the Valencia wall as a result of the earthquake. The foundation soils at the Valencia wall site are composed of a deep deposit of silty sand and clay. A cross-section of the wall is shown in Figure 5.1. The width of the reinforced mass measured from the toe of the wall is 5.5 m with the exception of the top 2.2 m of the structure where the reinforcement lengths were shortened to facilitate placement of subsurface utilities. Hence, this upper portion of the wall has a reinforced mass that is l.8 m wide measured from the wall face. Design data for the wall is limited but it appears that the wall was designed for k_h = 0.3 and k_v = 0 and the effect of the horizontal acceleration was treated as an additional uniform horizontal earth pressure distribution equal lo 104 kPa. No data is available to show how this distribution was used (if at all) in stability calculations related to internal and local facing modes of failure.

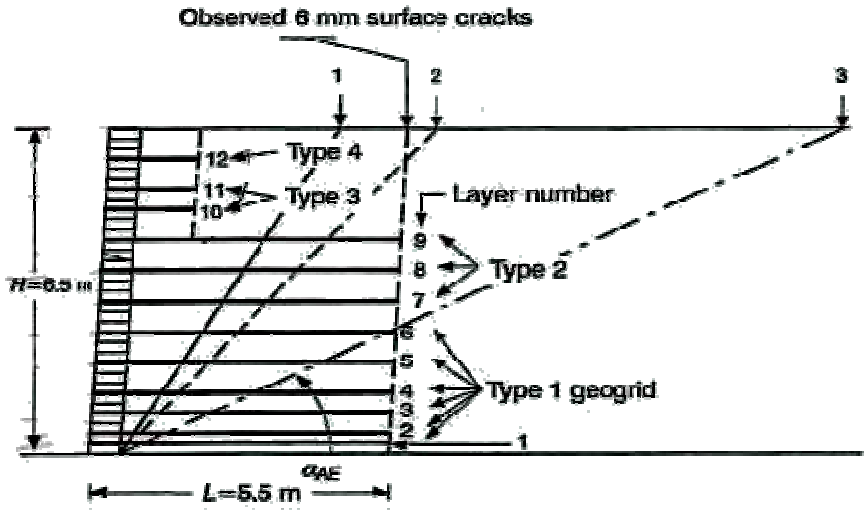

Figure 6.1.Cross-section view of Valencia Wall showing location and orientation of internal failure planes under static and dynamic loading conditions

The estimated peak horizontal ground accelerations in this site range from 0.19 and 0.5 g based on data from UCB/EERC (1994). The lower value is based on a mean estimate taken from a peak horizontal ground acceleration-epicentral distance attenuation curve for the Northridge earthquake. The maximum value is based on peak ground acceleration contours reported for the Northridge earthquake in the Los Angeles area. A simplifying assumption made by the writers is that the range of peak ground accelerations estimated for the site can be used as a conservative estimate of the range of k_h values for the backfill soils (i.e. would be conservative for design). This range of values also includes the value of k_h that was used in the original design. Application of Equation 2.28 to this range of peak ground acceleration values according to current FHWA guidelines would result in a mean value of $k_h = 0.23$ and a maximum value of $k_h = 0.48$. However, these adjustments do not influence the general conclusions that follow, and to simplify the analyses, values of $k_h = 0.19$ and $k_h = 0.5$ are used for demonstration purposes only. No site-specific vertical acceleration data is available and $k_v = 0$ was assumed by the Bathurst and Cai. Soil and reinforcement properties used in the stability analysis of the structure are given in Table 6.1.

The Coulomb failure wedge geometries calculated using Equation 2.6 for static, mean and maximum k_h values are illustrated in Figure 6.1. The results of static and dynamic stability analyses are given in Table 6.1 for the entire wall. In the actual wall, 6 mm surface crack was observed. For verification, Valencia Wall is calculated with the methodology used in this study and 7.6 mm for Newmark and 8.2 mm for Bathurst and Cai is calculated. Results compared with the actual displacement are very close. The critical acceleration coefficient and the permanent displacement of the Valencia wall are shown in the following Tables.

Table 6.1. Material Properties for Valenica Wall

	Properties	Values of Valencia Wall
Soil	Friction angle (Φ) (°)	33
	Unit Weight(γ) (Kn/m^3)	19.8
Geosynthetic Properties	Index Strength (ASTM D 4595) (Kn/m)	
	Type 1	125
	Type 2	100
	Type 3	49,5
	Type 4	35,5
Design Strength (T_{allow}) (Kn/m)	Type 1 and 2 Type 3 and 4	27 8,3
Segmental Block Properties	Width (toe to heel) (mm) Height (mm) Length (mm) Infilled Block Weight (kg)	600 200 450 117
Interface Shear	a_u (Kn/m)	32,7
	λ_u (°)	15
Connection Strength	Type 1 and 2	
	a_{cs} (Kn/m)	23,5
	λ_{cs} (°)	32
	$F_{c(max)}$ (Kn/m)	-
	Type 3 and 4	
	a_{cs} (Kn/m)	17
	λ_{cs} (°)	0
	$F_{c(max)}$ (Kn/m)	17

Table 6.2. Valencia Wall Calculation of kc

External Base Sliding

k_c	0,520
Θ	27,47
K_A	0,24
K_{AE}	1,12
ΔK_{dyn}	0,88

H	6,40
L	5,50
K_{AH}	0,21
K_{AEH}	0,98
ΔK_{dynH}	0,77

W_w	76,03
W_i	620,93
W_r	696,96

W_i'	329,47

R_S	453,02
P_{IR}	210,86
P_{AEH}	242,62
FS_{sl}	1,00

Internal Sliding

Layer Number	Elevation	Depth	S_{vi}	Z_{vi}	L_i	H
1	0,20	6,20	0,30	6,25	5,50	6,40
2	0,40	6,00	0,30	5,95	5,50	6,40
3	0,80	5,60	0,40	5,60	5,50	6,40
4	1,20	5,20	0,50	4,85	5,50	6,40
5	1,80	4,60	0,60	4,00	5,50	6,40
6	2,40	4,00	0,60	3,40	5,50	6,40
7	3,00	3,40	0,60	2,80	5,50	6,40
8	3,60	2,80	0,60	2,20	5,50	6,40
9	4,20	2,20	0,60	1,60	5,50	6,40
10	4,80	1,60	0,50	1,15	1,80	6,40
11	5,20	1,20	0,50	1,15	1,80	6,40
12	5,80	0,60	0,90	0,45	1,80	6,40

Layer Number	Elevation	Depth	ΔW_w	$\Delta W_i'$	$\Delta P_{IR}(z)$	h_{zi}	$P_{AEH}(z)$	$V_u(z)$	ΔWi	$R_S(z)$	FS_{sli}
1	0,20	6,20	80,61	349,32	230,87	6,20	212,43	54,30	601,52	444,69	1,00
2	0,40	6,00	78,01	338,05	224,67	6,00	207,30	53,61	582,12	431,40	1,00
3	0,80	5,60	72,81	315,52	210,86	5,60	195,15	52,21	543,31	404,82	1,00
4	1,20	5,20	67,61	292,98	196,52	5,20	182,32	50,82	504,50	378,24	1,00
5	1,80	4,60	59,81	259,17	175,12	4,60	163,49	48,73	446,29	338,37	1,00
6	2,40	4,00	52,01	225,37	153,39	4,00	144,34	46,64	388,08	298,50	1,00

Table 6.2. Valencia Wall Calculation of kc (Continued)

7	3,00	3,40	44,21	191,56	131,80	3,40	125,76	44,55	329,87	258,63	1,00
8	3,60	2,80	36,41	157,76	110,28	2,80	107,85	42,46	271,66	218,76	1,00
9	4,20	2,20	28,60	123,95	88,48	2,20	89,93	40,37	213,44	178,89	1,00
10	4,80	1,60	20,80	90,15	37,06	1,60	25,93	38,28	38,02	62,95	1,00
11	5,20	1,20	15,60	67,61	32,45	1,20	23,07	36,88	28,51	55,39	1,00
12	5,80	0,60	7,80	33,81	22,80	0,60	21,27	34,79	14,26	44,04	1,00

Layer Number	k_c	θ	K_A	K_{AE}	ΔK_{dyn}	K_{AH}	K_{AEH}	ΔK_{dynH}
1	0,537	28,24	0,24	1,00	0,76	0,21	0,87	0,66
2	0,540	28,37	0,24	1,01	0,77	0,21	0,88	0,67
3	0,543	28,50	0,24	1,02	0,78	0,21	0,89	0,68
4	0,545	28,59	0,24	1,03	0,79	0,21	0,90	0,69
5	0,549	28,77	0,24	1,05	0,81	0,21	0,91	0,70
6	0,553	28,94	0,24	1,06	0,82	0,21	0,93	0,72
7	0,559	29,21	0,24	1,09	0,85	0,21	0,95	0,74
8	0,568	29,60	0,24	1,13	0,89	0,21	0,98	0,77
9	0,580	30,11	0,24	1,18	0,94	0,21	1,03	0,82
10	0,334	18,47	0,24	0,56	0,32	0,21	0,49	0,28
11	0,390	21,31	0,24	0,65	0,41	0,21	0,56	0,36
12	0,548	28,72	0,24	1,04	0,80	0,21	0,91	0,70

Interface Shear

Layer Number	Elevation	Depth	ΔW_w	$P_{AEH}(z)$	F_i	Sum of F_i	$S_i(z)$	$V_u(z)$	FS_{sc}
1	0,20	6,20	80,61	421,87	17,48	413,54	54,06	54,30	1,00
2	0,40	6,00	78,01	405,37	17,81	395,72	53,61	53,61	1,00
3	0,80	5,60	72,81	382,65	24,43	371,30	52,32	52,21	1,00
4	1,20	5,20	67,61	352,49	31,96	339,34	50,81	50,82	1,00
5	1,80	4,60	59,81	314,42	40,44	298,90	48,64	48,73	1,00
6	2,40	4,00	52,01	275,41	41,70	257,20	46,85	46,64	1,00
7	3,00	3,40	44,21	234,79	42,74	214,45	44,50	44,55	1,00
8	3,60	2,80	36,41	193,49	43,63	170,82	42,41	42,46	1,00
9	4,20	2,20	28,60	151,40	44,26	126,56	40,20	40,37	1,00
10	4,80	1,60	20,80	114,84	38,66	87,90	38,23	38,28	1,00
11	5,20	1,20	15,60	80,65	36,02	51,88	36,96	36,88	1,00
12	5,80	0,60	7,80	31,15	51,88	0,00	34,73	34,79	1,00

Layer Number	k_c	θ	K_A	K_{AE}	ΔK_{dyn}	K_{AH}	K_{AEH}	ΔK_{dynH}
1	0,567	29,56	0,24	1,12	0,88	0,23	1,07	0,84
2	0,564	29,40	0,24	1,11	0,87	0,23	1,05	0,82
3	0,563	29,36	0,24	1,10	0,86	0,23	1,05	0,82
4	0,557	29,11	0,24	1,08	0,84	0,23	1,02	0,80

Table 6.2. Valencia Wall Calculation of kc (Continued)

5	0,554	28,97	0,24	1,07	0,83	0,23	1,01	0,78
6	0,551	28,83	0,24	1,05	0,81	0,23	1,00	0,77
7	0,547	28,66	0,24	1,04	0,80	0,23	0,98	0,76
8	0,542	28,47	0,24	1,02	0,78	0,23	0,97	0,74
9	0,537	28,24	0,24	1,00	0,76	0,23	0,95	0,72
10	0,543	28,48	0,24	1,02	0,78	0,23	0,97	0,74
11	0,525	27,70	0,24	0,96	0,72	0,23	0,91	0,68
12	0,460	24,70	0,24	0,78	0,54	0,23	0,74	0,52

Layer Number	Elevation	Depth	S_{vi}	Z_{vi}	ΔWwi	F_{stai}	F_{dyni}
1	0,20	6,20	0,30	6,25	3,90	8,45	6,82
2	0,40	6,00	0,30	5,95	3,90	8,05	7,57
3	0,80	5,60	0,40	5,60	5,20	10,10	11,40
4	1,20	5,20	0,50	4,85	6,50	10,93	17,40
5	1,80	4,60	0,60	4,00	7,80	10,82	25,30
6	2,40	4,00	0,60	3,40	7,80	9,20	28,21
7	3,00	3,40	0,60	2,80	7,80	7,58	30,91
8	3,60	2,80	0,60	2,20	7,80	5,95	33,45
9	4,20	2,20	0,60	1,60	7,80	4,33	35,74
10	4,80	1,60	0,50	1,15	6,50	2,59	32,54
11	5,20	1,20	0,50	1,15	6,50	2,59	30,01
12	5,80	0,60	0,90	0,45	11,70	1,83	44,67

Table 6.3. Valencia Wall Displacement Calculation

External Base Sliding

	k_c	k_m	k_c/k_m	v_m (cm/sn)	d (Newmark) (cm)	d (Bathurst and Cai) (cm)
	0,520	0,50	1,04	25,00	0,00	0,00

Internal Sliding

Layer	k_c	k_m	k_c/k_m	v_m (cm/sn)	d (Newmark) (cm)	d (Bathurst and Cai) (cm)
1	0,537	0,50	1,07	25,00	0,00	0,00
2	0,540	0,50	1,08	25,00	0,00	0,00
3	0,543	0,50	1,09	25,00	0,00	0,00
4	0,545	0,50	1,09	25,00	0,00	0,00
5	0,549	0,50	1,10	25,00	0,00	0,00
6	0,553	0,50	1,11	25,00	0,00	0,00
7	0,559	0,50	1,12	25,00	0,00	0,00
8	0,568	0,50	1,14	25,00	0,00	0,00
9	0,580	0,50	1,16	25,00	0,00	0,00
10	0,334	0,50	0,67	25,00	0,47	0,51
11	0,390	0,50	0,78	25,00	0,23	0,22
12	0,548	0,50	1,10	25,00	0,00	0,00

Interface Shear

Layer	k_c	k_m	k_c/k_m	v_m (cm/sn)	d (Newmark) (cm)	d (Bathurst and Cai) (cm)
1	0,567	0,50	1,13	25,00	0,00	0,00
2	0,564	0,50	1,13	25,00	0,00	0,00
3	0,563	0,50	1,13	25,00	0,00	0,00
4	0,557	0,50	1,11	25,00	0,00	0,00
5	0,554	0,50	1,11	25,00	0,00	0,00
6	0,551	0,50	1,10	25,00	0,00	0,00
7	0,547	0,50	1,09	25,00	0,00	0,00
8	0,542	0,50	1,08	25,00	0,00	0,00
9	0,537	0,50	1,07	25,00	0,00	0,00
10	0,543	0,50	1,09	25,00	0,00	0,00
11	0,525	0,50	1,05	25,00	0,00	0,00
12	0,460	0,50	0,92	25,00	0,06	0,08

Total	d (Newmark) (cm)	d (Bathurst and Cai) (cm)
Base Sliding	0,00	0,00
1	0,00	0,00
2	0,00	0,00
3	0,00	0,00
4	0,00	0,00
5	0,00	0,00
6	0,00	0,00
7	0,00	0,00
8	0,00	0,00
9	0,00	0,00
10	0,47	0,51
11	0,70	0,74
12	0,76	0,82

7. CONCLUSION AND REMARKS

This study deals with only the calculation of permanent displacements of reinforced segmental retaining walls related to external sliding, internal sliding, and block interface shear failure. These are only mechanisms that can be treated using conventional sliding-block methods. The remaining failure mechanisms can be evaluated using a pseudo-static limit-equilibrium approach. However, pseudo-static methods adapted to segmental retaining wall structures can only be used to estimate factors of safety against collapse. An important assumption in this study is that the base acceleration at each geosynthetic elevation is the same as the ground acceleration.

The comparisons of the methods used, reinforcement length, reinforcement spacing, inclination angle, and block widths are shown in Chapter 5. And following results are observed.

- Newmark's method (1965) and the empirical approach (Bathurst and Cai (1996)) give similar results for small displacements but for large displacements the difference between two methods gets larger for three displacement mechanisms. (Figure 5.1 – 5.16)

- Permanent displacement increases as the height of the wall increases. For the reinforcement spacing of 0.2 m and reinforcement length over height ratio (L/H) of 0.7; for walls shorter than 6 m, internal sliding and interface shear governs the displacements but, for walls higher than 6 m, base sliding and interface shear governs the displacements. For L/H = 1.0; for walls shorter than 2 m height wall base sliding, internal sliding and interface shear governs the displacements but, for walls higher than 2 m height wall base sliding and interface shear governs the displacements. So, this means that longer reinforcement reduces internal sliding. For the reinforcement spacing of 0.4 m and L/H = 0.7 and block width (L_w) of 0.2; for walls shorter than 2 m height wall base sliding, internal sliding and interface shear governs the displacements but, for walls higher than 2 m height wall base sliding and interface shear governs the displacements. For the

reinforcement spacing of 0.4 m and L/H = 0.7 and block width (L_w) of 0.4; for walls higher than 4 m height wall base sliding, internal sliding and interface shear governs the displacements, for walls higher than 4 m height wall base sliding and interface shear governs the displacements. This fact shows that also the size of the facing element reduces internal sliding. For the reinforcement spacing of 0.4 m and L/H = 1.0; for walls higher than 2 m height wall base sliding, internal sliding and interface shear governs the displacements but, for walls higher than 2 m height wall base sliding and interface shear governs the displacements. (Table 7.1 – 7.2)

Table 7.1. Calculation of Displacement for H = 2 m, L = 1,4 m, Spacing = 0,2 m, Lw = 0,2 m, β = 3°

External Base Sliding

	k_c	k_m	k_c/k_m	v_m (cm/sn)	d (Newmark) (cm)	d (Bathurst and Cai) (cm)
	0,426	0,63	0,68	27,70	0,44	0,47

Internal Sliding

Layer	k_c	k_m	k_c/k_m	v_m (cm/sn)	d (Newmark) (cm)	d (Bathurst and Cai) (cm)
1	0,555	0,63	0,88	27,70	0,09	0,10
2	0,559	0,63	0,89	27,70	0,09	0,10
3	0,564	0,63	0,90	27,70	0,08	0,09
4	0,569	0,63	0,91	27,70	0,07	0,09
5	0,578	0,63	0,92	27,70	0,06	0,08
6	0,591	0,63	0,94	27,70	0,04	0,07
7	0,607	0,63	0,97	27,70	0,02	0,06
8	0,624	0,63	0,99	27,70	0,00	0,00
9	0,624	0,63	0,99	27,70	0,00	0,00

Interface Shear

Layer	k_c	k_m	k_c/k_m	v_m (cm/sn)	d (Newmark) (cm)	d (Bathurst and Cai) (cm)
1	0,625	0,63	0,99	27,70	0,00	0,00
2	0,625	0,63	0,99	27,70	0,00	0,00
3	0,624	0,63	0,99	27,70	0,00	0,00
4	0,624	0,63	0,99	27,70	0,00	0,00
5	0,623	0,63	0,99	27,70	0,00	0,00
6	0,623	0,63	0,99	27,70	0,01	0,05
7	0,621	0,63	0,99	27,70	0,01	0,05
8	0,619	0,63	0,99	27,70	0,01	0,05
9	0,587	0,63	0,93	27,70	0,05	0,07

Total	d (Newmark) (cm)	d (Bathurst and Cai) (cm)
Base Sliding	0,44	0,47
1	0,53	0,57
2	0,62	0,67
3	0,70	0,76

Table 7.1. Calculation of Displacement for H = 2 m, L = 1,4 m, Spacing = 0,2 m, Lw = 0,2 m, β = 3° (Continued)

4	0,77	0,85
5	0,83	0,92
6	0,87	0,99
7	0,89	1,05
8	0,90	1,05
9	0,94	1,12

Table 7.2. Calculation of Displacement for H = 4 m, L = 2,8 m, Spacing = 0,2 m, Lw = 0,2 m, β = 3°

External Base Sliding

	k_c	k_m	k_c/k_m	v_m (cm/sn)	d (Newmark) (cm)	d (Bathurst and Cai) (cm)
	0,425	0,63	0,68	27,70	0,44	0,47

Internal Sliding

Layer	k_c	k_m	k_c/k_m	v_m (cm/sn)	d (Newmark) (cm)	d (Bathurst and Cai) (cm)
1	0,470	0,63	0,75	27,70	0,28	0,28
2	0,473	0,63	0,75	27,70	0,27	0,27
3	0,476	0,63	0,76	27,70	0,26	0,26
4	0,479	0,63	0,76	27,70	0,25	0,25
5	0,482	0,63	0,77	27,70	0,25	0,24
6	0,485	0,63	0,77	27,70	0,24	0,23
7	0,488	0,63	0,78	27,70	0,23	0,22
8	0,491	0,63	0,78	27,70	0,22	0,22
9	0,494	0,63	0,79	27,70	0,21	0,21
10	0,497	0,63	0,79	27,70	0,21	0,20
11	0,502	0,63	0,80	27,70	0,20	0,19
12	0,507	0,63	0,81	27,70	0,18	0,18
13	0,512	0,63	0,82	27,70	0,17	0,17
14	0,519	0,63	0,83	27,70	0,16	0,16
15	0,529	0,63	0,84	27,70	0,14	0,14
16	0,542	0,63	0,86	27,70	0,11	0,12
17	0,558	0,63	0,89	27,70	0,09	0,10
18	0,584	0,63	0,93	27,70	0,05	0,07
19	0,623	0,63	0,99	27,70	0,00	0,05

Interface Shear

Layer	k_c	k_m	k_c/k_m	v_m (cm/sn)	d (Newmark) (cm)	d (Bathurst and Cai) (cm)
1	0,551	0,63	0,88	27,70	0,10	0,11
2	0,550	0,63	0,88	27,70	0,10	0,11
3	0,549	0,63	0,87	27,70	0,10	0,11
4	0,548	0,63	0,87	27,70	0,10	0,11
5	0,547	0,63	0,87	27,70	0,11	0,11
6	0,545	0,63	0,87	27,70	0,11	0,11
7	0,544	0,63	0,87	27,70	0,11	0,12

Table 7.2. Calculation of Displacement for H = 4 m, L = 2,8 m, Spacing = 0,2 m, Lw = 0,2 m, β = 3° (Continued)

8	0,543	0,63	0,86	27,70	0,11	0,12
9	0,541	0,63	0,86	27,70	0,12	0,12
10	0,540	0,63	0,86	27,70	0,12	0,12
11	0,538	0,63	0,86	27,70	0,12	0,12
12	0,536	0,63	0,85	27,70	0,12	0,13
13	0,534	0,63	0,85	27,70	0,13	0,13
14	0,532	0,63	0,85	27,70	0,13	0,13
15	0,529	0,63	0,84	27,70	0,14	0,14
16	0,526	0,63	0,84	27,70	0,14	0,14
17	0,522	0,63	0,83	27,70	0,15	0,15
18	0,517	0,63	0,82	27,70	0,16	0,16
19	0,457	0,63	0,73	27,70	0,32	0,32

Total	d (Newmark) (cm)	d (Bathurst and Cai) (cm)
Base Sliding	0,44	0,47
1	0,72	0,75
2	0,99	1,01
3	1,25	1,27
4	1,51	1,52
5	1,75	1,76
6	1,99	1,99
7	2,22	2,21
8	2,44	2,43
9	2,66	2,64
10	2,86	2,84
11	3,06	3,03
12	3,24	3,21
13	3,42	3,38
14	3,58	3,53
15	3,71	3,67
16	3,86	3,81
17	4,01	3,96
18	4,17	4,12
19	4,49	4,44

- For a constant L/H and L_w/H ratio, the amount of base sliding remains almost constant independent of wall height and reinforcement spacing. Interface shear is independent of L/H ratio. Therefore after the height that interface shear starts to drive, for both L/H = 0.7 and L/H = 1.0 displacements are almost same. The only difference is base sliding and it is so small and can be ignored for big heights. (Table 7.3 – 7.6)

Table 7.3. Calculation of Displacement for H = 2 m, L = 1,4 m, Spacing = 0,2 m, Lw = 0,2 m, β = 3°

External Base Sliding

	k_c	k_m	k_c/k_m	v_m (cm/sn)	d (Newmark) (cm)	d (Bathurst and Cai) (cm)
	0,426	0,63	0,68	27,70	0,44	0,47

Table 7.4. Calculation of Displacement for H = 10m, L = 7 m, Spacing = 0,2 m, Lw = 0,2 m, β = 3°

External Base Sliding

	k_c	k_m	k_c/k_m	v_m (cm/sn)	d (Newmark) (cm)	d (Bathurst and Cai) (cm)
	0,426	0,63	0,68	27,70	0,44	0,47

Table 7.5. Calculation of Displacement for H = 4 m, L = 2,8 m, Spacing = 0,2 m, Lw = 0,4 m, β = 3°

External Base Sliding

	k_c	k_m	k_c/k_m	v_m (cm/sn)	d (Newmark) (cm)	d (Bathurst and Cai) (cm)
	0,429	0,63	0,68	27,70	0,42	0,45

Internal Sliding

Layer	k_c	k_m	k_c/k_m	v_m (cm/sn)	d (Newmark) (cm)	d (Bathurst and Cai) (cm)
1	0,470	0,63	0,75	27,70	0,28	0,28
2	0,473	0,63	0,75	27,70	0,27	0,27
3	0,476	0,63	0,76	27,70	0,26	0,26
4	0,479	0,63	0,76	27,70	0,25	0,25
5	0,482	0,63	0,77	27,70	0,25	0,24
6	0,485	0,63	0,77	27,70	0,24	0,23
7	0,488	0,63	0,78	27,70	0,23	0,22
8	0,491	0,63	0,78	27,70	0,22	0,22
9	0,494	0,63	0,79	27,70	0,21	0,21
10	0,497	0,63	0,79	27,70	0,21	0,20
11	0,502	0,63	0,80	27,70	0,20	0,19
12	0,507	0,63	0,81	27,70	0,18	0,18
13	0,512	0,63	0,82	27,70	0,17	0,17
14	0,519	0,63	0,83	27,70	0,16	0,16
15	0,529	0,63	0,84	27,70	0,14	0,14
16	0,542	0,63	0,86	27,70	0,11	0,12
17	0,558	0,63	0,89	27,70	0,09	0,10
18	0,584	0,63	0,93	27,70	0,05	0,07
19	0,623	0,63	0,99	27,70	0,00	0,05

Interface Shear

Layer	k_c	k_m	k_c/k_m	v_m (cm/sn)	d (Newmark) (cm)	d (Bathurst and Cai) (cm)
1	0,581	0,63	0,93	27,70	0,05	0,07
2	0,580	0,63	0,92	27,70	0,06	0,08
3	0,579	0,63	0,92	27,70	0,06	0,08
4	0,577	0,63	0,92	27,70	0,06	0,08
5	0,576	0,63	0,92	27,70	0,06	0,08
6	0,574	0,63	0,91	27,70	0,06	0,08

Table 7.5. Calculation of Displacement for H = 4 m, L = 2,8 m, Spacing = 0,2 m, Lw = 0,4 m, β = 3° (Continued)

7	0,572	0,63	0,91	27,70	0,07	0,08
8	0,570	0,63	0,91	27,70	0,07	0,09
9	0,568	0,63	0,90	27,70	0,07	0,09
10	0,566	0,63	0,90	27,70	0,08	0,09
11	0,564	0,63	0,90	27,70	0,08	0,09
12	0,561	0,63	0,89	27,70	0,08	0,09
13	0,558	0,63	0,89	27,70	0,09	0,10
14	0,554	0,63	0,88	27,70	0,09	0,10
15	0,550	0,63	0,88	27,70	0,10	0,11
16	0,545	0,63	0,87	27,70	0,11	0,11
17	0,538	0,63	0,86	27,70	0,12	0,12
18	0,529	0,63	0,84	27,70	0,14	0,14
19	0,462	0,63	0,74	27,70	0,30	0,30

Total	d (Newmark) (cm)	d (Bathurst and Cai) (cm)
Base Sliding	0,42	0,45
1	0,70	0,73
2	0,97	0,99
3	1,24	1,25
4	1,49	1,50
5	1,74	1,74
6	1,97	1,97
7	2,20	2,19
8	2,43	2,41
9	2,64	2,62
10	2,85	2,82
11	3,04	3,01
12	3,23	3,18
13	3,40	3,35
14	3,56	3,51
15	3,70	3,65
16	3,81	3,76
17	3,93	3,89
18	4,07	4,02
19	4,37	4,33

Table 7.6. Calculation of Displacement for H = 4 m, L = 4 m, Spacing = 0,2 m, Lw = 0,4 m, β = 3°

External Base Sliding

	k_c	k_m	k_c/k_m	v_m (cm/sn)	d (Newmark) (cm)	d (Bathurst and Cai) (cm)
	0,562	0,63	0,89	27,70	0,08	0,09

Internal Sliding

Layer	k_c	k_m	k_c/k_m	v_m (cm/sn)	d (Newmark) (cm)	d (Bathurst and Cai) (cm)
1	0,600	0,63	0,96	27,70	0,03	0,06
2	0,600	0,63	0,96	27,70	0,03	0,06
3	0,600	0,63	0,96	27,70	0,03	0,06
4	0,600	0,63	0,96	27,70	0,03	0,06
5	0,600	0,63	0,96	27,70	0,03	0,06
6	0,600	0,63	0,96	27,70	0,03	0,06
7	0,600	0,63	0,96	27,70	0,03	0,06
8	0,600	0,63	0,96	27,70	0,03	0,06
9	0,600	0,63	0,96	27,70	0,03	0,06
10	0,600	0,63	0,96	27,70	0,03	0,06
11	0,602	0,63	0,96	27,70	0,03	0,06
12	0,602	0,63	0,96	27,70	0,03	0,06
13	0,604	0,63	0,96	27,70	0,03	0,06
14	0,606	0,63	0,96	27,70	0,02	0,06
15	0,609	0,63	0,97	27,70	0,02	0,05
16	0,612	0,63	0,97	27,70	0,02	0,05
17	0,618	0,63	0,98	27,70	0,01	0,05
18	0,624	0,63	0,99	27,70	0,00	0,05
19	0,625	0,63	1,00	27,70	0,00	0,05

Interface Shear

Layer	k_c	k_m	k_c/k_m	v_m (cm/sn)	d (Newmark) (cm)	d (Bathurst and Cai) (cm)
1	0,581	0,63	0,93	27,70	0,05	0,07
2	0,580	0,63	0,92	27,70	0,06	0,08
3	0,579	0,63	0,92	27,70	0,06	0,08
4	0,577	0,63	0,92	27,70	0,06	0,08
5	0,576	0,63	0,92	27,70	0,06	0,08
6	0,574	0,63	0,91	27,70	0,06	0,08
7	0,572	0,63	0,91	27,70	0,07	0,08

8	0,570	0,63	0,91	27,70	0,07	0,09
9	0,568	0,63	0,90	27,70	0,07	0,09
10	0,566	0,63	0,90	27,70	0,08	0,09
11	0,564	0,63	0,90	27,70	0,08	0,09
12	0,561	0,63	0,89	27,70	0,08	0,09
13	0,558	0,63	0,89	27,70	0,09	0,10
14	0,554	0,63	0,88	27,70	0,09	0,10
15	0,550	0,63	0,88	27,70	0,10	0,11
16	0,545	0,63	0,87	27,70	0,11	0,11
17	0,538	0,63	0,86	27,70	0,12	0,12
18	0,529	0,63	0,84	27,70	0,14	0,14
19	0,462	0,63	0,74	27,70	0,30	0,30

Total	d (Newmark) (cm)	d (Bathurst and Cai) (cm)
Base Sliding	0,08	0,09
1	0,14	0,17
2	0,19	0,24
3	0,25	0,32
4	0,31	0,40
5	0,37	0,48
6	0,44	0,56
7	0,50	0,65
8	0,57	0,73
9	0,64	0,82
10	0,72	0,91
11	0,80	1,00
12	0,88	1,09
13	0,97	1,19
14	1,06	1,30
15	1,17	1,40
16	1,27	1,52
17	1,40	1,64
18	1,53	1,78
19	1,84	2,08

- When all of the parameters are same and only L_w is increased, base sliding and internal sliding doesn't change but interface shear decreases. (Table 7.7 – 7.8)

Table 7.7. Calculation of Displacement for H = 4 m, L = 2,8 m, Spacing = 0,2 m, Lw = 0,2 m, β = 3°

External Base Sliding

	k_c	k_m	k_c/k_m	v_m (cm/sn)	d (Newmark) (cm)	d (Bathurst and Cai) (cm)
	0,425	0,63	0,68	27,70	0,44	0,47

Internal Sliding

Layer	k_c	k_m	k_c/k_m	v_m (cm/sn)	d (Newmark) (cm)	d (Bathurst and Cai) (cm)
1	0,470	0,63	0,75	27,70	0,28	0,28
2	0,473	0,63	0,75	27,70	0,27	0,27
3	0,476	0,63	0,76	27,70	0,26	0,26
4	0,479	0,63	0,76	27,70	0,25	0,25
5	0,482	0,63	0,77	27,70	0,25	0,24
6	0,485	0,63	0,77	27,70	0,24	0,23
7	0,488	0,63	0,78	27,70	0,23	0,22
8	0,491	0,63	0,78	27,70	0,22	0,22
9	0,494	0,63	0,79	27,70	0,21	0,21
10	0,497	0,63	0,79	27,70	0,21	0,20
11	0,502	0,63	0,80	27,70	0,20	0,19
12	0,507	0,63	0,81	27,70	0,18	0,18
13	0,512	0,63	0,82	27,70	0,17	0,17
14	0,519	0,63	0,83	27,70	0,16	0,16
15	0,529	0,63	0,84	27,70	0,14	0,14
16	0,542	0,63	0,86	27,70	0,11	0,12
17	0,558	0,63	0,89	27,70	0,09	0,10
18	0,584	0,63	0,93	27,70	0,05	0,07
19	0,623	0,63	0,99	27,70	0,00	0,05

Interface Shear

Layer	k_c	k_m	k_c/k_m	v_m (cm/sn)	d (Newmark) (cm)	d (Bathurst and Cai) (cm)
1	0,551	0,63	0,88	27,70	0,10	0,11
2	0,550	0,63	0,88	27,70	0,10	0,11
3	0,549	0,63	0,87	27,70	0,10	0,11
4	0,548	0,63	0,87	27,70	0,10	0,11
5	0,547	0,63	0,87	27,70	0,11	0,11

Table 7.7. Calculation of Displacement for H = 4 m, L = 2,8 m, Spacing = 0,2 m, Lw = 0,2 m, β = 3° (Continued)

6	0,545	0,63	0,87	27,70	0,11	0,11
7	0,544	0,63	0,87	27,70	0,11	0,12
8	0,543	0,63	0,86	27,70	0,11	0,12
9	0,541	0,63	0,86	27,70	0,12	0,12
10	0,540	0,63	0,86	27,70	0,12	0,12
11	0,538	0,63	0,86	27,70	0,12	0,12
12	0,536	0,63	0,85	27,70	0,12	0,13
13	0,534	0,63	0,85	27,70	0,13	0,13
14	0,532	0,63	0,85	27,70	0,13	0,13
15	0,529	0,63	0,84	27,70	0,14	0,14
16	0,526	0,63	0,84	27,70	0,14	0,14
17	0,522	0,63	0,83	27,70	0,15	0,15
18	0,517	0,63	0,82	27,70	0,16	0,16
19	0,457	0,63	0,73	27,70	0,32	0,32

Total	d (Newmark) (cm)	d (Bathurst and Cai) (cm)
Base Sliding	0,44	0,47
1	0,72	0,75
2	0,99	1,01
3	1,25	1,27
4	1,51	1,52
5	1,75	1,76
6	1,99	1,99
7	2,22	2,21
8	2,44	2,43
9	2,66	2,64
10	2,86	2,84
11	3,06	3,03
12	3,24	3,21
13	3,42	3,38
14	3,58	3,53
15	3,71	3,67
16	3,86	3,81
17	4,01	3,96
18	4,17	4,12
19	4,49	4,44

Table 7.8. Calculation of Displacement for H = 4 m, L = 2,8 m, Spacing = 0,2 m, Lw = 0,4 m, β = 3°

External Base Sliding

	k_c	k_m	k_c/k_m	v_m (cm/sn)	d (Newmark) (cm)	d (Bathurst and Cai) (cm)
	0,429	0,63	0,68	27,70	0,42	0,45

Internal Sliding

Layer	k_c	k_m	k_c/k_m	v_m (cm/sn)	d (Newmark) (cm)	d (Bathurst and Cai) (cm)
1	0,470	0,63	0,75	27,70	0,28	0,28
2	0,473	0,63	0,75	27,70	0,27	0,27
3	0,476	0,63	0,76	27,70	0,26	0,26
4	0,479	0,63	0,76	27,70	0,25	0,25
5	0,482	0,63	0,77	27,70	0,25	0,24
6	0,485	0,63	0,77	27,70	0,24	0,23
7	0,488	0,63	0,78	27,70	0,23	0,22
8	0,491	0,63	0,78	27,70	0,22	0,22
9	0,494	0,63	0,79	27,70	0,21	0,21
10	0,497	0,63	0,79	27,70	0,21	0,20
11	0,502	0,63	0,80	27,70	0,20	0,19
12	0,507	0,63	0,81	27,70	0,18	0,18
13	0,512	0,63	0,82	27,70	0,17	0,17
14	0,519	0,63	0,83	27,70	0,16	0,16
15	0,529	0,63	0,84	27,70	0,14	0,14
16	0,542	0,63	0,86	27,70	0,11	0,12
17	0,558	0,63	0,89	27,70	0,09	0,10
18	0,584	0,63	0,93	27,70	0,05	0,07
19	0,623	0,63	0,99	27,70	0,00	0,05

Interface Shear

Layer	k_c	k_m	k_c/k_m	v_m (cm/sn)	d (Newmark) (cm)	d (Bathurst and Cai) (cm)
1	0,581	0,63	0,93	27,70	0,05	0,07
2	0,580	0,63	0,92	27,70	0,06	0,08
3	0,579	0,63	0,92	27,70	0,06	0,08
4	0,577	0,63	0,92	27,70	0,06	0,08
5	0,576	0,63	0,92	27,70	0,06	0,08

Table 7.8. Calculation of Displacement for H = 4 m, L = 2,8 m, Spacing = 0,2 m, Lw = 0,4 m, β = 3° (Continued)

6	0,574	0,63	0,91	27,70	0,06	0,08
7	0,572	0,63	0,91	27,70	0,07	0,08
8	0,570	0,63	0,91	27,70	0,07	0,09
9	0,568	0,63	0,90	27,70	0,07	0,09
10	0,566	0,63	0,90	27,70	0,08	0,09
11	0,564	0,63	0,90	27,70	0,08	0,09
12	0,561	0,63	0,89	27,70	0,08	0,09
13	0,558	0,63	0,89	27,70	0,09	0,10
14	0,554	0,63	0,88	27,70	0,09	0,10
15	0,550	0,63	0,88	27,70	0,10	0,11
16	0,545	0,63	0,87	27,70	0,11	0,11
17	0,538	0,63	0,86	27,70	0,12	0,12
18	0,529	0,63	0,84	27,70	0,14	0,14
19	0,462	0,63	0,74	27,70	0,30	0,30

Total	d (Newmark) (cm)	d (Bathurst and Cai) (cm)
Base Sliding	0,42	0,45
1	0,70	0,73
2	0,97	0,99
3	1,24	1,25
4	1,49	1,50
5	1,74	1,74
6	1,97	1,97
7	2,20	2,19
8	2,43	2,41
9	2,64	2,62
10	2,85	2,82
11	3,04	3,01
12	3,23	3,18
13	3,40	3,35
14	3,56	3,51
15	3,70	3,65
16	3,81	3,76
17	3,93	3,89
18	4,07	4,02
19	4,37	4,33

- When spacing between reinforcement layers decrease, reinforced soil gets more strength and when the spacing between the reinforcements decrease to half value, base sliding value doesn't differ, but internal sliding and interface shear almost decrease their half value. Therefore total permanent displacement almost decreases by half value. (Figure 5.33 – 5.48)

- Wall inclination angle doesn't have a significant influence on total permanent displacement. Base Sliding value remains same and Internal Sliding and Interface Shear have almost the same value. (Figure 5.49 – 5.64)

- As verification, Valencia Wall is calculated and 7.6 mm and 8.2 mm displacement values are found. The actual wall had 6 mm surface cracks therefore this methodology gave similar results with the actual displacement. (Table 6.3)

REFERENCES

Allen, T. M. (I993). Issues regarding design and specification of segmental block-faced geosynhetic walls *Transportation Research Record,* 1414 6-11.

AASHTO(1993), *Interims: Standard specifications far highway bridges.* American Association of State Highway and Transportation Official, Washington, DC. USA

ASTM (I996). Designation D4595: Standard test method for tensile properties of geotextiles by the wide-width strip method. *1996 Annual Book of ASTM Standards,* Section 4. Construction, (4.09), American Society for Testing and Materials West Canshohocken, Pennsylvania, USA.

Bachus R. C., Fragaszy, R. J., Jaber M., Olen. K. L., Yuan, Z. and Jewell, R (1993). *Dynamic response of reinforced soil systems.* Engineering Research Division, US Department of the Air Force Civil Engineering Support Agency. March 1993, 1&.2, Report ESL-TR-92-47

Bathurst R.J. (1994). *Reinforced soil slopes and embankments.* Technical Notes for Computer Programs GEOSLOPE and GEOPLOT.

Bathurst. R. J. (1998). NCMA *segmental retaining wall seismic design procedure—supplement to design manual for segmental retaining walls.* National Concrete Masonry Association,. Herdon, Virginia, USA

Bathurst. R. J. and Alfaro M. C. (1996). Review of seismic design, analysis and performance of geosynthetic reinforced walls, slopes and embankments. *Proceedings of the Earth Reinforcement — International Symposium on Earth Reinforcement.* Fukuoka Kyushu, Japan, pp. 887-918.

Bathurst, R. J. and Cai, Z. (I994). In-isolation cyclic load-extension behavior of two geogrids. *Geosynthetics International,* **1**, No. 1,3-17

Bathurst R.J. and Cai. Z. (1995). Pseudo-static seismic analysis reinforced segmental retaining walls. *Geosynthetics Internatinal*, **2**, No. 5, 787-830.

Bathurst, R. J., Cai, *Z.* and Pelletier M. J. (1996). Seismic design and performance of geosynthetic reinforced segmental retaining walls. *Proceedings of the 10th Annual Symposium of the Vancouver Geotechnical Society* Vancouver, British Columbia, Canada.

Bathurst R. J., Cai Z. and Simac, M. R. (1997). Seismic performance charts for reinforced segmental retaining walls. *Proceedings of the geosynthetic: '97.* Long Beach, California, USA, pp. 1001-1014.

Bathurst R. J. and Hatami, K. (1998a). Influence or reinforcement length and base condition on seismic response of geosynthetic reinforced retaining walls. *Proceedings of the 6th International Conference on Geosynthetics*. Atlanta Georgia, USA, pp. 613-616.

Bathurst, R. J. and Hatami, K. (1998b). Seismic response analysis of a reinforced Soil retaining wall *Geosynthetics International* (special issue on Earthquake Engineering. Industrial Fabrics Association International (IFAI)), USA, **5***,* Nos. 1-2, 127-166.

Bathurst, R.J., and Hatami, K. (1998c). Influence of reinforcement properties on seismic response and design of reinforced-soil retaining walls. *Proceedings of the 51st Canadian Geotechnical Conference.* Edmonton, Alberta, Canada, pp. 479-486.

Bathurst, R. J. and Simac, M. R. (1993). Laboratory testing of modular unit-geogrid facing connections. *STF 1I90 Geosynthetic Soil Reinforcement Testing Procedures* (ed. S. C. J. Cheng), American Society for Testing and Materials (Special Technical Publication), pp. 32-48.

Bathurst, R. J. and Simac, M. R. (1994). Geosynthetic reinforced retaining wall structures in North America. Keynote Paper *Proceedings of the 5th International Conference on Geotextiles, Geomembranes and Related Products.* Singapore, pp. 1275-1295.

Bonaparte, R., Schmertmann, G. R. and Williams, N. D. (I986). Seismic slopes reinforced with geogrids and geotextiles. *Proceedings of the International Conference on Geotextiles.* Vienna, Austria, pp. 273-278.

Cai, Z. and Bathurst, R. J. (1995). Seismic response analysis of geosynthetic reinforced soil segmental retaining walls by finite element method. *Computers and Geotchnics,* **17**. No. 4, 523-546.

Cai, Z. and Bathutst, R. J. (1996a). Seismic-induced permanent displacement of geosynthetic reinforced segmental retaining walls. *Canadian Geotechnical Journal,* 31,937-955.

Cai, Z. and Bathurst, R. J. (1996b). Deterministic sliding block methods for estimating seismic displacements of earth structures, *Soil Dynamics and Earthquake Engineering,* 15, 255-268.

Canadian Foundation Engineering Manual (CFEM) (1993). 3rd edition, Canadian Geotechnical Society. BiTech Publishers Ltd Richmond, British Columbia, Canada.

Chida. S., Minami, K. and Adachi, K. (I985). *Test de stabilité de remblais en Terre Armée* (unpublished report translated from Japanese.

Christopher, B. R, Gill, S. A., Giroud. J. P., Juran, I., Schlosser. F., Mitchell J. K., and Dunnicliff, J. (1989). *Reinforced soil structures: Volume I. Design and construction guidelines.* Federal Highway Administration, Washington, DC, USA, Report No. FHWA-RD-89-043.

Ebeling, R. M. and Morrison. E. E. (1993). *The seismic design of waterfront retaining structures.* Naval Civil Engineering Laboratory Technical Report ITL-92-11 NCEL TR-939, Port Huenene, California, USA.

Eliahu. U. and Watt, S. (1991). Geogrid-reinforced wall withstands earthquake. *Geotechnical Fabrics Repot,* IFAI, St Paul Minnesota, USA, **9**, No. 2, 8-13.

Elms, D. G. and Richards, R. (1990). Seismic design of retaining walls ASCE Specially Conference Design and Performance of Earth Retaining Structures, Cornell University, Ithaca, New York, USA, pp. 854-871, ASCE Geotecnical Special Publication No. 25.

Federal Highway Administration (FHWA) (1996). *Mechanically stabilized earth wails and reinforced soil slopes design and construction guidelines.* FHWA Demonstration Project 82 (V. Elias and B. R. Christopher), Washington, DC. USA.

Franklin, A. G. and Chang. F. K. (1977). *Permanent displacement of earth embankments by Newmark sliding block analysis.* Misc. Paper S-71-17, Soil and Pavements Laboratory, US Army Eng. Waterways Expt. Station., Vicksburg, Mississippi, USA.

Hatami K. and Bathurst R. J. (1999a). Frequency response analysis of reinforced-soil retaining walls. *Proceedings of the 8th Canadian Conference on Earthquake Engineering (8CCEE).* Vancouver, British Columbia, Canada, pp. 341-346.

Hatami, K. and Bathurst. R J. (1999b). Dynamic response of reinforced-soil retaining walls to ground motion. Part II: parametric analysis. *Proceedings of the 17th Canadian Congress of Applied Mechanics, CANCAM 99.* McMaster University, Hamilton, Ontario. Canada, pp 89-90.

Hatami K. and Bathurst R. J. (2000). Effect of structural design on fundamental frequency of reinforced-soil retaining wails. *Soil Dynamics and Earthquake Engineering,* **19**, No, 3. 137-157.

Kramer S. L. (1996a). *Geotechnical earthquake engineering.* Prentice-HalI, New Jersey, USA.

Leshchinsky, D. (l995). *Design procedure for geosynthetic reinforced steep slopes.* Waterways Experiment Station, US Army Corps of Engineers, Vicksburg, Mississippi, USA. Technical Report REMR-GT-120 (Temporary Number).

Leshchinsky, D., Ling, H. I. and Hants, G. A. (1995). Unified design approach to geosynthetic reinforced slopes and segmental walls. *Geosynthetics International,* **2**, No. 5, 845-881.

Ling. H. I., Wu. J. T. H. and Tatsuoka, F. (1992). Short-term strength and deformation characteristics of geotextiles under typical operational conditions. *Geotextiles and Geomembranes,* **11**, No. 2, 185—219.

Ling H. I., Leshchinsky, D. and Perry, E. B. (1996). A new concept on seismic design of geosynthetic reinforced soil structures: permanent-displacement limit. *Earth Reinforcement: Proceedings of the International Symposium on Earth Reinforcement, IS-Kyushu '96.* Fukuoka, Kyushu, Japan. pp, 117-122.

Ling H. I., Leschinsky, D. and Perry, E. B. (1997). Seismic design and performance of geosynthetic reinforced soil structures. *G éotechnique,* **47**, No. 5, 933-952.

Ling H. I., Mohri Y. and Kawabata, T. (1998). Tensile properties of geogrids under cyclic loadings, *Journal of Geotecnical and Geoenviromental Engineering,* ACSE, **124**, No. 8, 782-787.

Ling H. I., Leschinsky, D., (1998) Effects of vertical acceleration on seismic design of geosynthetic - reinforced soil Structures. *Géotechnique,* **48**, No. 3, 347-373.

Mononbe N. and Matsuo. K. (1929). On the determination of earth pressure during earthquake. *Proceedings of the World Engineering Congress.* Tokyo. Japan, pp. 177—185.

Newmark N. M. (1965). Effect of earthquakes on dams and embankments. *Géotechnique,* **15,** No. 2, 139-159.

Okabe S. (1924). General theory on earth pressure and seismic stability of retaining wall and dam. Doboku Gakkai. *Journal of the Japan Society of Civil Engineers,* **10,** No. 6, 1277-1323.

Pelletier M. J. (1996). *Investigation of the seismic resistance of reinforced walls using small-scale shaking table testing.* M Eng Thesis, Department of Civil Engineering. Royal Military College of Canada, Kingston, Ontario, Canada.

Richards, R. and Elms, D. G. (1979). Seismic behavior of gravity retaining walls. *Journal of the Geotechnical Engineering Division, ASCE.* **105**, (GT4), 449-464.

Sandri, D. (1994), Retaining walls stand up to the Northridge earthquake. *Geotechnical Fabrics Report* (IFAI, St. Paul, Minnesota, USA), **12**, No. 4, 30-31 (and personal communication).

Sarma S. K. (1975). Seismic stability of earth dams and embankments. *Géotechique*, **25,** No. 4, 473-761.

Seed. H. B. and Whitman. R V. (1970). Design of earth remaining structures for dynamic loads. *Proceedings of the ASCE Specialty Conference. Lateral Stresses in the Ground and Design of Earth Retaining Structures*. Ithaca, New York, pp. 103-147.

Segrestin, P. and Bastick. M. J. (1988). Seismic design of reinforced earth retaining walls — the contribution of finite element analysis. *Theory and Practice of Earth Reinforcement: Proceedings of the International Geotechnical Symposium on*

Theory and Practice of Earth Reinforcement. IS-Kyushu '88. Fukuoka, Japan, Balkema, Rotterdam, pp. 577-582.

Simac, M. R., Bathust. R J., Berg, R. R. and Lothspeich, S. E. (1993). *National Concrete Masonry Association segmental retaining wail design manual*. Earth Improvement Technologies.

Steedman, R S. and Zeng, X. (1990). The influence of phase on the calculation of pseudo-static earth pressure on a retaining wall. *Géotechnique*, **40**, No. 1, 101-112.

Stewart, J. P., Bray, J. D., Seed, R B. and Sitar, N. (1994). Preliminary Report on the Principal Geotechnical Aspects of the January 17, 1994 Northridge Earthquake Engineering Research Centre, University of California at Berkeley, California, USA, June 1994, Report No. UCB/EERC-94/08.

Whitman, R. V. (1990). Seismic design and behavior of gravity retaining walls. *ASCE Specialty Conference: Design and Performance of Earth Retaining Structures, ASCE Geotechnical Special Publication No. 25,* Cornell University. Ithaca, New York, USA. pp. 817-842.

Wolfe, W. E., Lee, K. L., Rea, D. and Yourman, A. M, (1978). The effect of vertical motion on the seismic stability of reinforced earth walls. *Proceedings of the ASCE Symposium on Earth Reinforcement.* Pittsburgh, Pennsylvania, USA, pp. 856-879.

Yogendrakumar, M., Bathurst, R. J. and Finn, W. D. L. (1991). Response of the reinforced soil slopes to earthquake loadings. *Proceedings of the 6th Canadian Conference on Earthquake Engineering.* Toronto. Ontario, Canada, pp. 445-452.

Yogendrakumar, M., Bathurst, R. J. and Finn, W. D. L. (1992). Dynamic response analysis of a reinforced soil retaining wall. *Journal of Geotechnical Engineering, ASCE.* **118**, No. 8, 1158 -1167.

Zarrabi K. (1979). *Sliding of gravity retaining wail duing earthquakes considering vertical acceleration and changing inclination of failure surface.* MSc thesis. Department of Civil Engineering, Massachusetts Institute of Technology, Cambridge, Massachusetts, USA.